The Structures of Cu_A and Cytochrome *a* in Cytochrome *c* Oxidase

Thesis by

Craig Timothy Martin

In Partial Fulfillment of the Requirements

for the Degree of

Doctor of Philosophy

California Institute of Technology

Pasadena, California

1985

(Submitted August 17, 1984)

To my parents for their constant support

and

to my wife, Lynmarie, para las sonrisas.

Acknowledgements

I would like to thank all of the past, present, and unofficial members of the Chan group for putting up with me during the past several years. It has been a pleasure to work with them and I have learned a great deal from them. I would also like to thank my advisor, Sunney Chan, for his guidance and advice. It is he who has taught me always to keep in mind "the big picture."

This work represents the collaborative efforts of many people. Specifically, I would like to thank Professor Charles Scholes for his expertise in ENDOR and for the unrestricted use of his spectrometer. I would also like to thank Drs. Savely Goldin and Kryzstof Falkowski for their assistance with the ENDOR measurements. For assistance in obtaining the NMESE measurements, I thank Professor Larry Dalton and Ho Kim. At Caltech, I have benefited greatly from the open environment of the departments. The experiments with yeast were greatly aided by assistance from Drs. Judy Campbell and Carl Parker, and their respective groups. I also acknowledge Dr. Stu Scherer for his generous gift of yeast auxotrophs and for advice on yeast genetics. I am grateful to Dr. Ron Pace for the suggestion of a protein helix model for Cu_A coordination. Finally, I would like to thank Professor Bob Birge for a collaborative attempt at understanding the electronic structure of Cu_A, and Profs. Bo Malmstrom and Harry Gray for a collaboration studying the laccases early in my stay at Caltech.

Within the Chan group I would like to thank specifically Tom Stevens, Dave Blair, Jeff Gelles, Gary Brudvig, Randy Morse, and Hsin Wang for their advice, criticisms, and friendship. I would also like to extend warm appreciation to Joey, Steve, Joel, Tim, Utpal, Bernie, Larry, and other members of the group for adding to my life at Caltech.

I am especially grateful to my good friends Bob and Denise, and to my family for providing love and constant encouragement throughout my life. Finally, a very special thanks to Lynmarie, who has made it all worthwhile. I look forward to a life with her filled with happiness.

ABSTRACT

Cytochrome c oxidase contains four metal centers, two heme irons and two copper centers. The two low-potential centers, Cu_A and cytochrome a, function in the transfer of electrons from cytochrome c to the oxygen binding site within cytochrome oxidase. Although almost nothing is currently known about the mechanism of proton pumping in cytochrome oxidase, it is very likely that at least one of these low-potential metal centers is directly involved in the translocation of protons across the inner mitochondrial membrane. Essential to a complete understanding of the mechanisms of electron transfer and proton pumping in cytochrome oxidase is a knowledge of the structures of the involved metal centers.

In this work, the spectroscopic tool of electron nuclear double resonance (ENDOR) is used in conjunction with the direct incorporation of isotopically substituted amino acids into the yeast protein to determine the identities of ligands to Cu_A and cytochrome a in cytochrome oxidase. For cytochrome a, the incorporation of [1,3-$^{15}N_2$]histidine into the yeast protein results in the appearance of an ENDOR signal associated with hyperfine coupling to the histidine ring ^{15}N, thereby unambiguously identifying histidine as an axial ligand to cytochrome a. Comparison of this result with similar results in the native and ^{15}N-substituted bis-imidazole model compounds metmyoglobin-imidazole and bis-imidazole tetraphenyl porphyrin, provides strong evidence that cytochrome a is coordinated by two axial histidine ligands.

Similar studies on the effect of the incorporation of [1,3-$^{15}N_2$]histidine into yeast cytochrome oxidase demonstrate that histidine is a ligand to Cu_A. The incorporation of [β,β-$^2H_2$]cysteine into the protein reveals that the two strongly coupled protons previously observed in the ENDOR spectrum of Cu_A (H. L. Van Camp, et al. (1978) Biochim. Biophys. Acta 537, 238) can be assigned to the methylene protons on cysteine, proving conclusively that cysteine is a ligand to

[β-^{13}C]cysteine-substituted protein. These results, combined with the resolution in the native enzyme of a new hyperfine coupling to a third strongly coupled proton for Cu_A, provide strong evidence for the coordination of two cysteine ligands to Cu_A.

Armed with the identification of one histidine and two cysteine ligands to Cu_A, we present a model for the physical and electronic structure of the oxidized Cu_A center. This model is characterized by the delocalization of a substantial amount of unpaired spin density away from the copper atom and into an orbital between the two cysteine sulfur ligands. This model satisfactorily explains many of the unusual spectroscopic features of Cu_A and should prove to be of use in future studies of the nature of the Cu_A site.

With the positive identification of ligands to cytochrome a and Cu_A, we have analyzed the available protein sequence data for the subunits of cytochrome oxidase from a wide variety of organisms, and are able to reach some conclusions regarding the physical location of these metal centers in the subunit structure of the protein. The cysteine ligand(s) to Cu_A most certainly derive from the two conserved cysteine residues in subunit II. Furthermore, it is predicted that all of the metal centers in cytochrome oxidase cannot be located in subunit II, and are quite likely shared with subunit I. Finally, we present a model for the protein coordination of Cu_A in which the two cysteine sulfur ligands to Cu_A originate in two cysteine residues which are physically adjacent on the face of an α-helix in subunit II.

TABLE OF CONTENTS

LIST OF TABLES AND FIGURES

CHAPTER I

CHAPTER II

CHAPTER III

CHAPTER IV

CHAPTER I

INTRODUCTION

Cytochrome c oxidase catalyzes the four-electron reduction of molecular oxygen to water in the final step of cellular respiration in all higher forms of life. When cytochrome c oxidase (also known as cytochrome aa_3) was first discovered over 40 years ago, little was understood about the active sites within the protein (1). Although the involvement of iron in oxygen reduction (2) was determined as early as 10 years prior to the discovery of cytochrome oxidase, it was only within the last 20 years that the direct involvement of copper was shown (3). It is now well known that the functioning enzyme contains four metal centers, two heme iron groups and two copper centers (4,5). The oxygen binding site is made up of one heme iron (cytochrome a_3) and one of the copper atoms (Cu_B). Together these two metals form an exchange coupled EPR-silent site in the oxidized protein. The other two metal centers, cytochrome a and Cu_A, function in the transfer of electrons from the external electron donor cytochrome c to the oxygen binding site within cytochrome oxidase. These two metal centers may also be involved in the recently demonstrated (6,7) proton pumping function of the enzyme.

The electrons necessary for the reduction of dioxygen are accepted from the small, water soluble protein cytochrome c. This protein can carry only one electron at a time, so that the complete reaction is given by

(1) 4 cytochrome c^{+2} + 4 H^+ + O_2 $\longrightarrow$ 4 cytochrome c^{+3} + 2 H_2O.

The electrons enter cytochrome oxidase from the cytosolic (outward) side of the mitochondrial membrane, while the protons are consumed from the mitochondrial matrix (inside). In addition, at least four protons are translocated across the mitochondrial membrane from the matrix to the cytosol. Both the consumption of protons from the inside and the pumping of protons across the membrane contribute to the electrochemical membrane potential essential to energy conser-

vation in cellular respiration. The energy required by cytochrome oxidase to pump protons against a potential gradient arises from the difference in reduction potentials between cytochrome $\underline{c}^{+2}$ and dioxygen. At physiological substrate concentrations, this difference has been estimated to be 460 mV, or about 21 kcal per 2 electrons transferred (6). The energy available from this reaction is sufficient to drive the translocation of protons against a potential gradient. However, almost nothing is known about the mechanism by which cytochrome oxidase couples this source of potential energy to the physical translocation of protons across the membrane.

Cytochrome oxidase generally exists as a dimer and is known to span the inner mitochondrial membrane in an asymmetric fashion. Electron microscopy imaging studies have yielded a crude picture of the enzyme as it sits in the membrane (8). This transmembranous orientation, shown in Fig. 1, is essential to the above energy conservation; however, little is known about the location of the metal centers within this structure or what roles any of them might play in proton pumping. In fact, little experimental evidence exists to directly implicate any one of the four metal centers in proton pumping by cytochrome oxidase.

An important first step in the understanding of the mechanisms of both dioxygen reduction and proton pumping in cytochrome oxidase is the determination of the coordination structure and the electronic properties of each of the four metal centers. As mentioned previously, the two iron centers are known to exist in the protein as heme iron. Of these, only cytochrome $\underline{a}_3$ (at the oxygen binding site) can bind externally added ligands. For some time people have studied the oxygen binding site and have determined the effect of the addition of various exogenous ligands on its spectroscopic properties (9,10). In particular, electron paramagnetic resonance (EPR) spectroscopy has been used to measure hyperfine couplings between ligand nuclei and the unpaired spin at the site. Isotopic substitution of specific atomic constituents in an externally added ligand molecule, and the measurement

Figure 1

The physical structure and orientation of a cytochrome c oxidase dimer embedded in the mitochondrial inner membrane as determined by electron microscopic imaging studies (8).

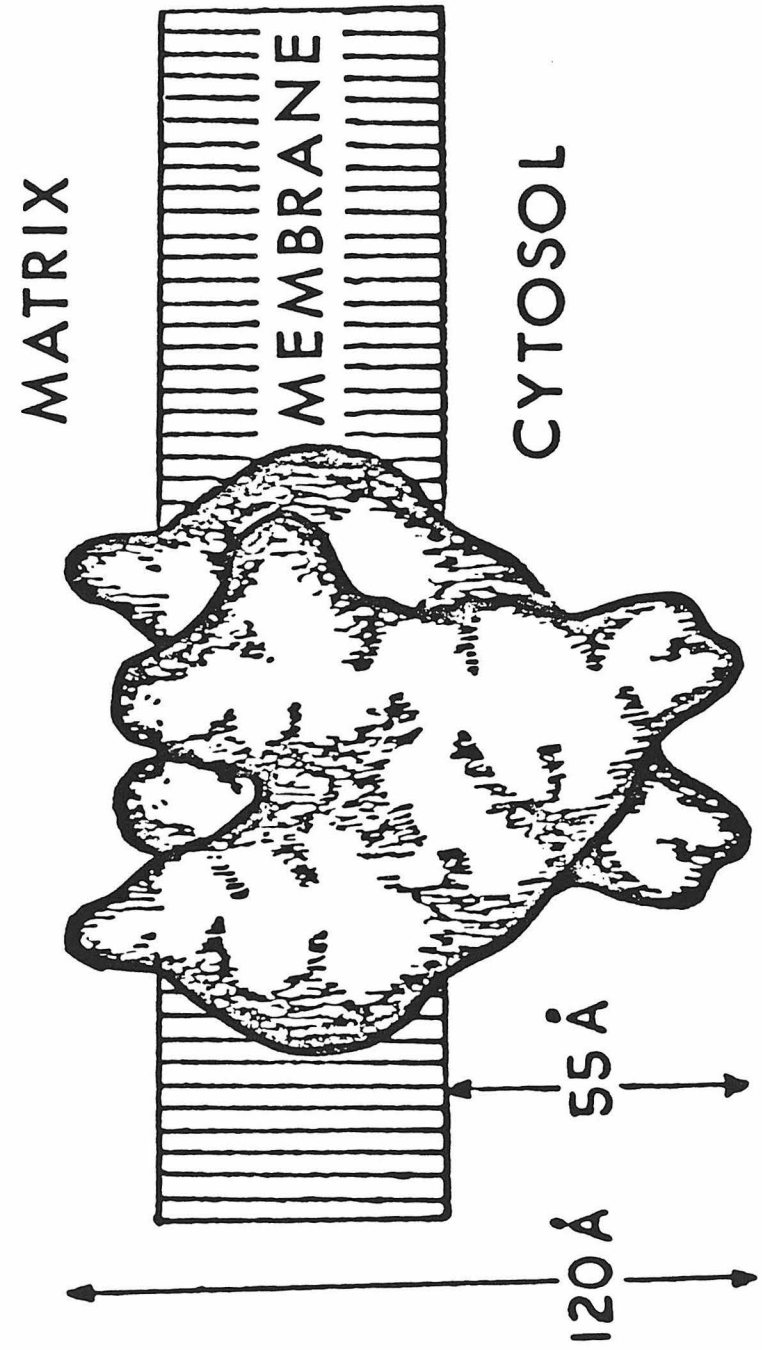
MATRIX
MEMBRANE
CYTOSOL
100 Å
55 Å
120 Å

(by EPR spectroscopy) of the resulting changes in the hyperfine couplings, has allowed the unambiguous determination of ligand binding to the metal center (11). Recently, the axial protein (endogenous) coordination of the oxygen binding site iron, cytochrome $\underline{a}_3$, was determined via the effect of the specific incorporation of isotopically substituted histidine into the protein on the EPR spectrum of cytochrome $\underline{a}_3$ (12). This constitutes the first positive identification of an amino acid ligand to any of the metal centers in cytochrome oxidase.

The observation of changes in ligand hyperfine interactions following the substitution of specific nuclear isotopes in the coordinating ligands of paramagnetic metal centers is a simple yet powerful method of determining the coordination environment of the metal sites. EPR spectroscopy, in particular, allows one to measure changes at a particular metal center, even in complex metalloproteins such as cytochrome oxidase. However, many hyperfine couplings are too small (relative to EPR linewidths) to be resolvable by EPR and other techniques are required to measure them. Prominent among these techniques is electron nuclear double resonance (ENDOR) spectroscopy which combines the sensitivity and selectivity of EPR spectroscopy with the narrow linewidths of nuclear magnetic resonance (NMR) spectroscopy (13,14). In the ENDOR experiment one monitors a partially saturated EPR transition while sweeping the radio frequency field over a frequency range corresponding to the energy of NMR transitions. When the NMR transition of an interacting nucleus is induced, more energy states are accessible to the EPR transition and the saturation is partially relieved. This manifests itself in an increased EPR absorption. The technique of ENDOR spectroscopy is quite specific in that one monitors only the nuclear transitions of atoms which interact directly (through hyperfine coupling) with the particular paramagnetic center being studied. The resultant ENDOR signal observed is that of the EPR transition being monitored, but the linewidth of the signal is the small linewidth characteristic of the

NMR transition. Hence ENDOR is particularly useful in detecting small hyperfine couplings in systems with relatively large EPR linewidths.

The determination of hyperfine couplings in metal centers within a protein provides some information on the number and type of ligand nuclei at the site. For example, ENDOR studies of Cu_A in oxidized cytochrome oxidase have previously determined the involvement of two protons and one nitrogen in the coordination environment of the Cu_A center (15). Unfortunately, the chemical identity of the involved ligands cannot be determined from these data alone.

We have recently developed a system for the direct incorporation into the yeast protein of amino acids which are specifically substituted with non-naturally abundant nuclear isotopes (16). Yeast strains which are auxotrophic for a particular amino acid are grown in a medium containing that amino acid synthesized with specific isotopic substituents. The yeast then incorporates the substituted amino acid into all of its proteins, and cytochrome oxidase containing this isotopic substitution may then be isolated from the yeast. The substituted protein is unperturbed with respect to structure and activity; however, as discussed above, the resultant change in the hyperfine couplings to the metal centers may be measured by EPR and/or ENDOR spectroscopies.

In this thesis, we utilize the techniques of ENDOR spectroscopy and isotopic substitution to uniquely identify amino acids coordinated to two of the metal centers in cytochrome oxidase. From the strengths of the observed hyperfine couplings we can draw conclusions about the overall structures and electronic distributions at the metal sites. Moreover, the identification of amino acid ligands to the metal centers can be used, along with comparison of evolutionary sequence conservation data for cytochrome oxidase, to provide some information on the probable locations of the metal centers in the primary sequence of the protein. From these data, models for both the physical and electronic structure of Cu_A are presented which explain many of the unique spectroscopic features of Cu_A. The information presented here

regarding the structures of Cu_A and cytochrome *a* will no doubt be of great utility in the further study of the mechanisms by which cytochrome *c* oxidase carries out its unique biochemical functions.

REFERENCES

1. Keilin, D., and Hartree, E. F. (1939) Proc. R. Soc. London, Ser. B 127, 167-191.

2. Keilin, D. (1925) Proc. R. Soc. London, Ser. B 98, 312-339.

3. Beinert, H., Griffiths, D. E., Wharton, D. C., and Sands, R. H. (1962) J. Biol. Chem. 237, 2337-2346.

4. Wikstrom, M., Krab, K., and Saraste, M. (1981) Cytochrome Oxidase: A Synthesis, Academic Press, London.

5. Malmstrom, B. G. (1980) in Metal Ion Activation of Dioxygen, Spiro, Thomas G., ed., John Wiley and Sons, New York, 181-207.

6. Wikstrom, M., and Krab, K. (1979) Biochim. Biophys. Acta 549, 177-222.

7. Wikstrom, M. (1984) Nature (London) 308, 558-560.

8. Fuller, S., Capaldi, R. A., and Henderson, R. (1979) J. Mol. Biol. 134, 305-327.

9. Wilson, D. F., and Erecinska, M. (1978) Meth. Enzymol. 53, 191-201.

10. Stevens, T. H., Brudvig, G. W., Bocian, D. F., and Chan, S. I., (1979) Proc. Natl. Acad. Sci., U.S.A. 76, 3320-3324.

11. Stevens, T. H., Bocian, D. F., and Chan, S. I. (1979) FEBS Lett. 97, 314-316.

12. Stevens, T. H., and Chan, S. I. (1981) J. Biol. Chem. 256, 1069-1071.

13. Kevan, L., and Kispert, L. D. (1976) Electron Spin Double Resonance Spectroscopy, John Wiley and Sons.

14. Scholes, C. P. (1979) in Multiple Electron Resonance Spectroscopy, Dorio, M. M., and Freed, J. H., eds., Plenum Press, New York, 297-329.

15. Van Camp, H. L., Wei, Y. H., Scholes, C. P., and King, T. E. (1978) Biochim. Biophys. Acta 537, 238-246.

16. Stevens, T. H. (1981) Ph.D. Thesis, California Institute of Technology, Pasadena.

CHAPTER II

THE STRUCTURE OF Cu_A

INTRODUCTION

The spectroscopic properties of Cu_A in oxidized cytochrome *c* oxidase have long been considered unusual for an isolated Cu(II) center. The copper hyperfine interactions are quite small and isotropic and the largest component of the copper hyperfine does not coincide with the largest g-value (1). Furthermore, the low-field g-value of oxidized Cu_A is smaller than that found in more typical Cu(II) complexes and the high-field g-value is below that of the free electron (2,3). X-ray edge absorption studies have shown that the electronic distribution at copper changes little upon change in oxidation state; in fact, the copper edge in the oxidized protein appears to reflect either a very covalent Cu(II) or a copper which is formally Cu(I) (4). These and other data have prompted a proposal that the unpaired spin resides primarily on an associated (cysteine) sulfur ligand and that the copper in oxidized Cu_A is formally Cu(I) (5-7).

Cu_A also shows an intense (ε = 3000 M^{-1} cm^{-1}) optical absorption band at 830 nm. For this reason it has sometimes been compared to the blue copper proteins which are characterized by the presence of a ligand (cysteine sulfur) to metal charge transfer band near 600 nm (8). These copper centers, whose sole function appears to be electron transfer, contain a single cysteine ligand and two histidine ligands in a very distorted tetrahedral environment. The coordination geometry is midway between the square planar geometry found in normal, or Type 2, oxidized copper centers and the tetrahedral environment preferred by reduced copper centers. It is known that the physical coordination sphere in the blue coppers changes little upon reduction of Cu(II) to Cu(I), thereby minimizing the rearrangement energy associated with electron transfer (9). The covalency conferred by the ligation of a "soft" cysteine sulfur results in the blue copper centers' having a fairly small copper hyperfine coupling, ranging from

35-80 G (10). This copper hyperfine coupling is somewhat larger than that observed for Cu_A (1), but is less than the couplings typically observed in Type 2 copper centers.

Although some of the spectroscopic properties of Cu_A appear similar to those of the blue coppers, many spectroscopic features of Cu_A are quite different from those of the blue copper centers. As will be discussed later in this chapter, the linear electric field effect (LEFE) and magnetic circular dichroism (MCD) data of Cu_A are particularly unusual. The differences in structure and chemical properties of Cu_A versus the blue coppers may reflect a difference in function between the two types of copper centers.

The proposal that the unpaired electron in Cu_A resides primarily on a Cys sulfur radical (5,6) has gained considerable support from the observation of nuclear hyperfine interactions from two strongly coupled protons in the electron nuclear double resonance (ENDOR) spectrum of oxidized Cu_A (11). It has been proposed that these two protons are the protons on methylene carbon adjacent to the sulfur of the aforementioned cysteine radical. This would be in agreement with a significant localization of unpaired spin on sulfur. Furthermore, the ENDOR spectrum of Cu_A shows a moderately weak hyperfine coupling to a nitrogen nucleus. This coupling is about one-half as strong as that observed for the coupling of a histidine nitrogen nucleus in the blue coppers (12). The unusually small nitrogen hyperfine coupling in Cu_A might be expected if it involves spin polarization from unpaired spin centered primarily on a sulfur radical, mediated by orbitals on the copper. Both of these assignments have remained untested, however, since the ENDOR spectrum yields only the identity of the coupled nucleus and contains no information regarding its molecular origin.

We have recently developed a system for the incorporation of isotopically substituted amino acids into cytochrome oxidase and have used this system to identify ligands to several of the metal centers in the protein (13,14). This technique allows the unambiguous

assignment of an observed nuclear hyperfine interaction to a particular amino acid type. We present here results proving the coordination of one histidine and at least one cysteine as ligands to Cu_A. Evidence is also presented which strongly implicates a second cysteine ligand in the coordination of this site. In the light of these results, we present a model for the Cu_A center which explains many of the unusual spectroscopic features of this unique copper center.

MATERIALS AND METHODS

Chemicals used in the protein purifications were of enzyme grade when available; otherwise they were reagent grade. Amino acids and antibiotics were the highest grades available from Sigma. Ammonium sulfate in the growth medium was reagent grade from Baker. Vitamins and media for selection and crossing of yeast strains were obtained from Difco. The [1,3-$^{15}N_2$]histidine used for yeast growth was 95% ^{15}N in both histidine ring positions and was obtained from Veb Berlin-Chemie, Berlin-Aldershof. The [β-^{13}C]cysteine was 95% ^{13}C and was obtained from Cambridge Isotopes, Boston.

Preparation and Characterization of Yeast Strains

Wild Type Strain. The wild type Saccharomyces cerevisiae haploid strain D273-10B (mating type α) was used in the growth of yeast for the isolation of unsubstituted (native) protein. This strain has been shown to respire efficiently on the non-repressive carbon source galactose (ie., it contains the GAL^+ trait) and produces good quantities of mitochondria.

Histidine Auxotrophs. For the preparation of the [^{15}N]His-substituted protein, the S. cerevisiae auxotroph haploid strains designated SS328 (α ura_3-52, GAL, SUC2, ∂his 3, D200, lys2-801^o, ade2-101^o) and SS330 (a ura_3-52, GAL, SUC2, ∂his 3, D200, tyr1, ade2-101^o) were obtained from Drs. Stu Scherer and Carl Parker (Caltech). These two haploid strains were crossed just before use so that subsequent growth was predominantly in the diploid form. These strains were found to be ideally suited for the preparation of [^{15}N]His-substituted protein in that the histidine mutation in these strains is a gene deletion rather than a single base substitution; consequently, revertant levels were always well below the detection

limit (less than 0.001%). The large-scale growth of yeast cells was as previously described (14), except that, in place of unsubstituted histidine, 4.0 g of DL-[1,3-$^{15}N_2$]histidine·HCl were added to the media to prepare the substituted protein.

Cysteine Auxotrophs. The cysteine auxotroph yeast strain used in the preparation of [^{2}H]Cys-substituted cytochrome oxidase has been described previously (14). In an attempt to improve the yield for the growth of [^{13}C]Cys-substituted protein, a new cysteine auxotroph strain was prepared. The S. cerevisiae cysteine auxotroph haploid strain JW1-2C (a Cys2-1a, CUP1) (15) was obtained from the Yeast Genetic Stock Center, Berkeley, California. This strain is unable to utilize galactose as a carbon source (ie., it is GAL$^-$) and is therefore unsuitable for the respiratory growth of yeast.

To correct this respiratory deficiency, the JW1-2C strain was crossed with the wild type D273-10B strain according to standard procedures (16). The flow chart in Fig. 1 outlines the steps taken to isolate a GAL$^+$, Cys$^-$ strain from a cross of the above haploid strains. Since the D273-10B strain contains no simple marker to allow its selective removal in later steps, a large excess of JW1-2C cells was crossed with a small amount of D273-10B cells and allowed to grow on standard rich (YEPD) medium for 1 day. These were then replica plated onto minimal medium containing galactose as the sugar and incubated for 1 day. This served the purpose of removing any remaining JW1-2C haploids. At this point, only crossed diploids and a small amount of D273-10B haploids remained. These were then plated onto nitrogen-poor medium and allowed to sporulate for 2 days, thereby producing ascospores containing four haploid crosses encased in an ascus. These ascospores were then treated with the digestive enzyme glusulase to remove the ascus and sonicated to separate the spores. Brief treatment with ether killed any remaining diploids. At this step, the only remaining cells were crossed haploids and a small amount of the original D273-10B haploids. The final selection for the

Figure 1

Flow chart describing the crossing of two different haploid yeast strains: wild type D273-10B (mating type α) contains the GAL^+ trait and the mutant strain JW1-2C (mating type a) contains the Cys^- trait. The resultant cross contains the desired traits from each of the two starting strains; ie., it is a GAL^+, Cys^- cysteine auxotroph.

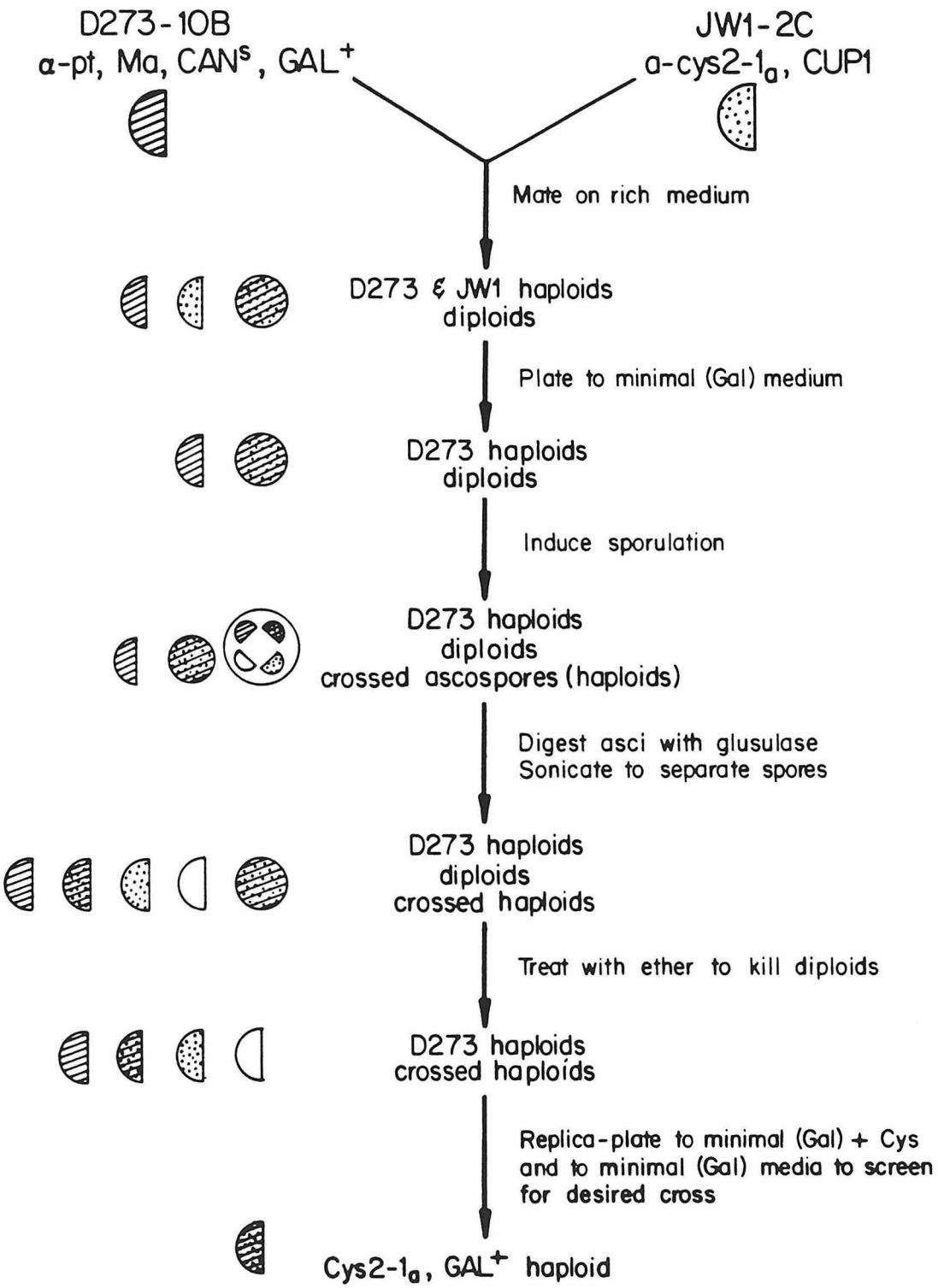
D273-10B
α-pt, Ma, CAN^s, GAL$^+$
JW1-2C
a-cys2-1$_a$, CUP1
Mate on rich medium
D273 & JW1 haploids
diploids
Plate to minimal (Gal) medium
D273 haploids
diploids
Induce sporulation
D273 haploids
diploids
crossed ascospores (haploids)
Digest asci with glusulase
Sonicate to separate spores
D273 haploids
diploids
crossed haploids
Treat with ether to kill diploids
D273 haploids
crossed haploids
Replica-plate to minimal (Gal) + Cys
and to minimal (Gal) media to screen
for desired cross
Cys2-1$_a$, GAL$^+$ haploid

desired GAL^+, Cys^- cross was achieved by plating onto minimal (galactose) medium supplemented with cysteine and allowing the cells to grow for 2 days. These plates containing single colonies, each derived from a single cell, were then replica plated to minimal (galactose) medium with and without added cysteine. After 2 days, colonies were selected that grew well on media with cysteine but not on the media lacking added cysteine. The resultant GAL^+, Cys^- haploid yeast strains were then checked for growth on petite medium to determine respiration sufficiency (to insure favorable production of mitochondria). Strains were then stored according to standard procedures and were routinely rechecked for reversion. The strain designated CY1-2-1 showed a low rate of reversion and was used in this study for the large-scale growth of [^{13}C]Cys-substituted yeast.

Large Scale Growth of Yeast

The growth of cells for the isolation of [^{2}H]Cys-substituted protein was carried out in a 360 liter fermentor, and has been described previously (17). The yeast cysteine auxotrophs for the growth of [^{13}C]Cys-substituted protein were grown as described previously (14), except that the media contained the following specifically added amino acids: 5 g each of His, Ser, Met, Thr, Trp, Tyr, Phe, Asn, Glu, Arg; 20 g of Gly; 50 g of Lys; and 4.0 g of DL-[β-^{13}C]cysteine·HCl (95% ^{13}C). Cells were allowed to grow to a density of 5.5×10^7 cells/ml at which time the revertant level was measured and found to be less than 0.001%.

The large scale growth of [^{15}N]His-substituted yeast cells was similar to that of the [^{13}C]Cys-substituted cells, except that 5 g of Cys were added and unsubstituted His was absent. Also added were 25 g each of adenine sulfate and uracil. The medium contained 4.0 g of DL-[1,3-$^{15}N_2$]histidine·HCl (95% ^{15}N at both imidazole ring positions). Cells were allowed to grow to a density of 2.9×10^7 cells/ml. At harvest, the cell density of revertants was below the level of detection (0.001%).

Preparation of Protein

Yeast mitochondria were isolated according to the procedure of George-Nascimento et al. (18), except that the buffer used during the Dyno-Mill cell disruption was 0.4 M in sucrose. This procedure resulted in the breakage of at least 80% of the yeast cells. Yeast cytochrome oxidase was isolated from the mitochondria and purified as described previously (14). The final protein was suspended in 0.5% Tween 20, 20 mM Tris, pH 7.4. Protein concentration was typically 0.1 mM in 0.2 to 0.3 ml sample volumes.

Cytochrome oxidase from beef heart was prepared by the method of Yu et al. (19), and was suspended in 0.5% cholate, 50 mM potassium phosphate, pH 7.4. In one experiment, beef heart protein was prepared by the method of Hartzell and Beinert (20). The beef heart protein was 0.1-0.3 mM in cytochrome oxidase, and was suspended in 0.5% Tween 20, 50 mM Tris, pH 7.4. Sample volumes were 0.3 mls for the Hartzell preparation, but 1.5 mls for that prepared according to Yu et al.

Spectroscopic Techniques

NMR Spectroscopy. The ^{1}H NMR spectra of unsubstituted cysteine and [^{13}C]cysteine were recorded on a Bruker WM500 NMR spectrometer at the Southern California Regional NMR Facility. Spectra were recorded using D_2O as an internal lock. No spin decoupling was used.

EPR Spectroscopy. EPR spectra were recorded on a Varian E-Line Century Series X-band spectrometer equipped with an Air Products Heli-Trans low temperature controller. Data were collected and stored on a PDP8/A (Digital Equipment Corp.) microcomputer interfaced to the spectrometer. Instrumental conditions are given in the figures. The microwave power was always maintained below the level of saturation for the Cu_A signal (and therefore also below that for cytochrome *a*).

ENDOR Spectroscopy. ENDOR spectra were recorded at the State University of New York at Albany in collaboration with Prof. Charles P. Scholes, as described previously (11). Specific conditions are given in the legends to the figures. Although the sample tubes were designed to hold 1.5 mls of solution, samples were generally ca. 0.3 mls in volume and were placed in smaller quartz tubes mounted concentrically inside the larger ENDOR tube. This served to keep the sample near the maximum in the microwave field and resulted in an optimal cavity filling factor.

It is important to point out that in order to obtain optimal signal intensities, spectra were recorded under conditions of rapid passage (21) so that the signals appear shifted somewhat in the direction of the sweep from their true positions. To measure the true positions of ENDOR signals, two spectra were recorded under identical conditions, but in opposite sweep directions. The true peak position was then estimated as the average of the positions in these two sweeps.

NMESE Spectroscopy. NMESE spectra were recorded at the University of Southern California in collaboration with Prof. Larry Dalton, on a spectrometer described previously (22). The two-pulse spin echoes (23) were obtained using microwave pulses of 20 and 40 nanosecond pulsewidths, respectively. The delay time (τ) between pulses (and before data aquisition) was varied from 200 nanoseconds in 10 nanosecond intervals up to 2 microseconds. The data were analyzed using the maximum entropy method of resolution enhancement (24) followed by an apodization method of Fourier transform to convert to the frequency domain (25).

RESULTS

Characterization of Labeled Amino Acids

[^{15}N]Histidine. To verify the extent of ^{15}N substitution in the [1,3-$^{15}N_2$]histidine, the natural abundance ^{13}C NMR spectrum was recorded prior to the growth of the substituted yeast. The proton decoupled spectrum, part of which is shown in Fig. 2, shows clearly the incorporation of ^{15}N into the amino acid. The triplet centered at 32.2 ppm is assigned to the single imidazole ring carbon (6-C) situated between the two substituted nitrogens. Consequently, in the proton decoupled spectrum, this ^{13}C resonance is split only by the two (^{15}N) nitrogens. The two nitrogens have the same spin-spin couplings to the (6-C) carbon so that the resultant NMR signal for this carbon is a (1:2:1) triplet (assuming 100% ^{15}N substitution). Integration of the peaks within the triplet confirms greater than 95% incorporation of ^{15}N at both imidazole ring nitrogen positions.

[^{2}H]Cysteine. The [β,β-$^{2}H_2$]cysteine used in the growth of [^{2}H]Cys-substituted yeast has been characterized previously (17). To verify the extent of substitution at the methylene carbon (β-CH_2) position, the natural abundance ^{13}C NMR spectrum of the [$^{2}H_2$]cysteine was recorded. Analysis of the proton couplings to the methylene carbon confirmed greater than 90% substitution of the methylene protons by deuterium.

[^{13}C]Cysteine. In order to confirm the extent of ^{13}C substitution in [β-^{13}C]cysteine, the ^{1}H NMR spectrum of the methylene protons was examined. The 500 MHz ^{1}H NMR spectra of native cysteine·HCl and [β-^{13}C]cysteine in D_2O are compared in Fig. 3. The signal centered at 3.02 ppm in the spectrum of cysteine·HCl corresponds to the methylene protons. Since the methylene carbon is

Figure 2

^{13}C NMR spectrum of 500 mM [1,3-$^{15}N_2$]histidine in D_2O. Conditions: ^{13}C resonance frequency, 22.6 MHz; temperature, 304 K; broadband ^{1}H decoupled.

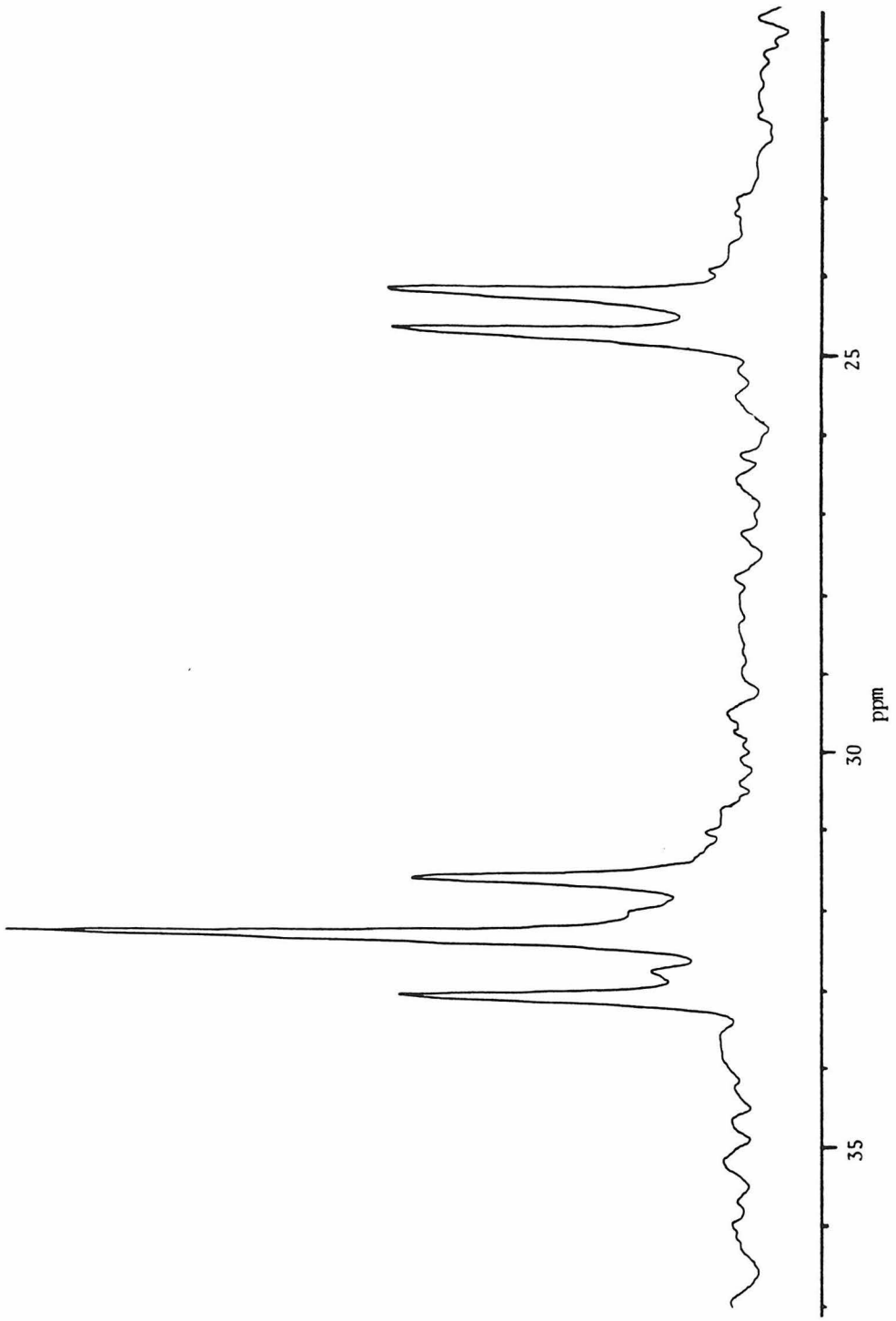
25
30
35
ppm

Figure 3

Natural abundance ^{1}H NMR spectra of 100 mM native cysteine·HCl and [β-^{13}C]cysteine in D_2O. Samples were not adjusted for pH. Conditions: ^{1}H resonance frequency, 500 MHz; temperature, 298 K; line broadening, 0.2 Hz.

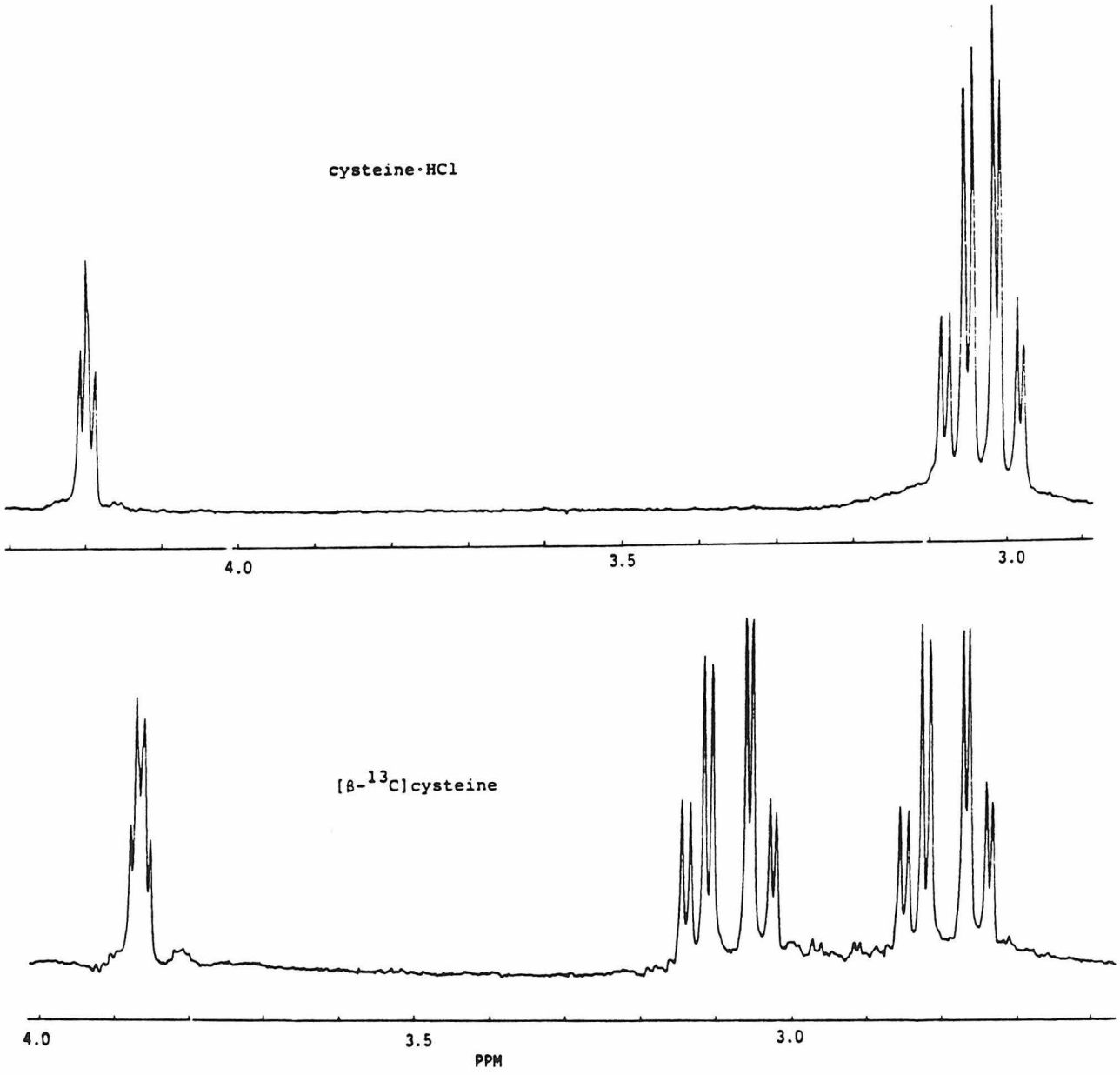
cysteine·HCl
4.0
3.5
3.0
[β-13C]cysteine
4.0
3.5
3.0
PPM

attached to an asymmetric center (the α-carbon), the two methylene protons are magnetically inequivalent, and in fact show slightly different chemical shifts at this field. Due to this chemical shift inequivalence, the two protons further split each other into two sets of doublets. Finally, they are each split by the single proton attached to the α-carbon, resulting in the multiplet shown in Fig. 3A. The spectrum of [β-^{13}C]cysteine (Fig. 3B) clearly shows a splitting (J = 145 Hz) of this multiplet into two sets by the enriched ^{13}C (note that since the samples were dissolved in D_2O without pH adjustment; the chemical shift corresponding to the center of the ^{1}H signals is slightly different in cysteine and cysteine·HCl). Integration of the signals in the spectrum of the substituted sample verifies greater than 95% enrichment of ^{13}C at the methylene carbon.

EPR Spectral Comparisons of Native and Substituted Yeast Proteins

The EPR spectrum of Cu_A in [^{2}H]Cys-substituted yeast cytochrome oxidase has been published previously (14). The spectrum of Cu_A in this preparation showed some narrowing in linewidth relative to that in the unsubstituted yeast protein, suggesting a decrease in unresolved hyperfine couplings in the substituted protein. This was assumed to be due to the disappearance of hyperfine coupling to the methylene protons of cysteine. In other respects, the spectrum was quite similar to that of the native yeast protein.

The EPR spectra of oxidized Cu_A in cytochrome oxidase isolated from wild type yeast and yeast substituted with [^{13}C]Cys and [^{15}N]His are compared in Fig. 4. The three spectra display no significant differences, and are all quite similar to the spectrum of oxidized Cu_A from the beef heart protein (not shown). The spectra of the substituted proteins demonstrate that incorporation of [^{13}C]Cys and [^{15}N]His into the Cu_A site results in no large change (greater than about 30 MHz) in the hyperfine couplings to Cu_A.

Figure 4

EPR spectra of Cu_A in (A) native, (B) [^{13}C]Cys-substituted, and (C) [^{15}N]His-substituted yeast cytochrome oxidase. Conditions: temperature, 15 K; microwave power, 10 microwatts; field modulation,

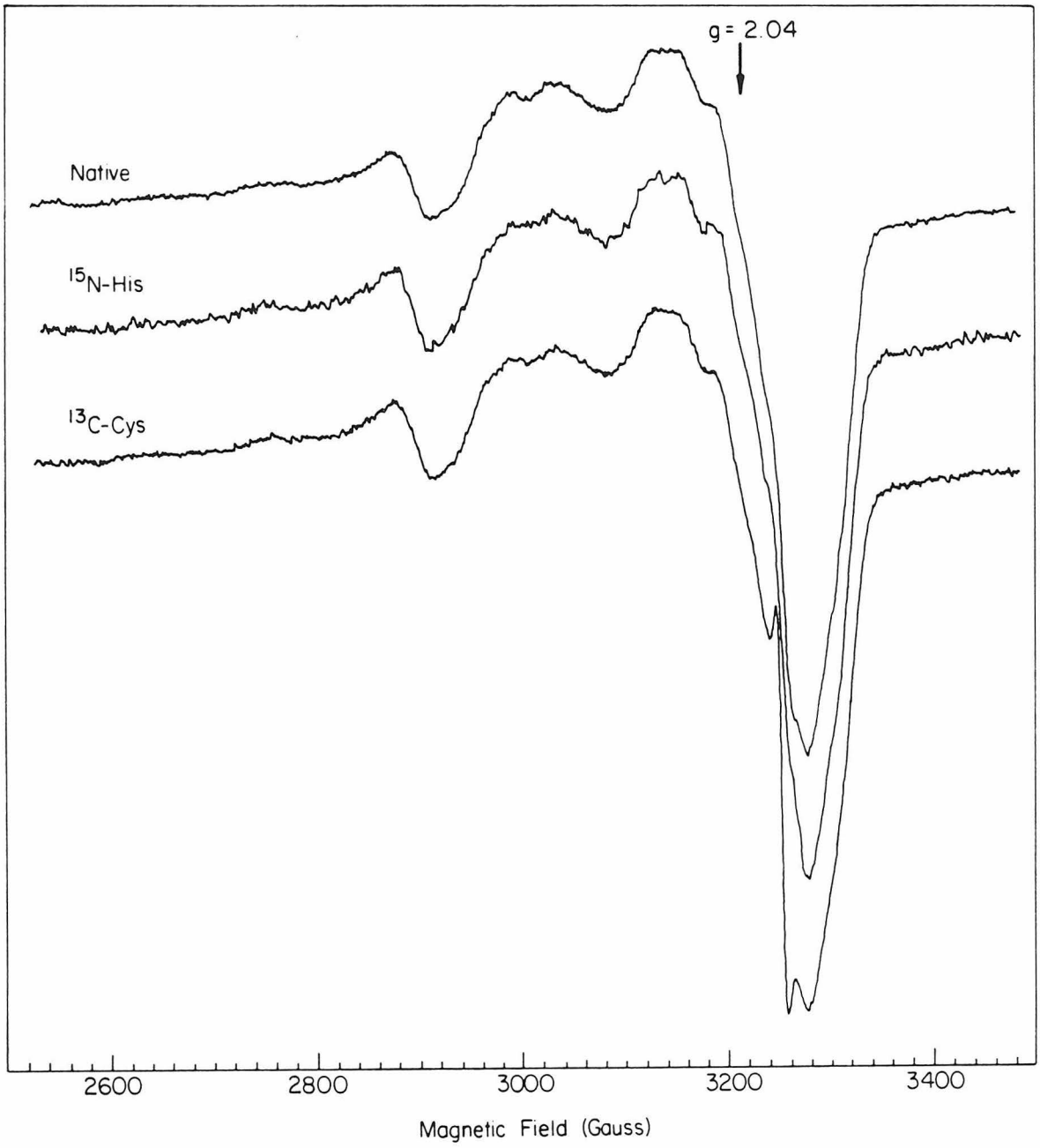
g = 2.04
Native
^{15}N-His
^{13}C-Cys
2600
2800
3000
3200
3400
Magnetic Field (Gauss)

Comparison of ENDOR Spectra of Cu_A in Native and Substituted Proteins

ENDOR spectroscopy is much better suited to the measuring of small hyperfine couplings than is EPR spectroscopy. In order to resolve small changes in hyperfine couplings resulting from the incorporation of isotopically substituted amino acids into the coordination sphere of Cu_A, we now examine the ENDOR spectra of Cu_A in the native and isotopically substituted yeast proteins.

Unsubstituted Yeast Cytochrome Oxidase. The ENDOR spectrum of Cu_A in native yeast cytochrome oxidase is shown in Fig. 5. By analogy to the previously characterized ENDOR spectrum of Cu_A in beef heart cytochrome oxidase (11), we briefly point out the important spectral in this region. At low frequency, the two signals observed at 8.9 and 6.9 MHz have been assigned to a non-proton nucleus (most likely nitrogen). This was shown for the beef heart protein by the effect of a change in the microwave resonant frequency (and therefore resonant field position for the same g-value). Due to the uniquely large magnetic moment of the proton, a change in magnetic field strength affects the positions of signals due to protons much more than it affects other nuclei (see later in this section).

The symmetrical signals centered at 13 MHz in the ENDOR spectrum of the native protein arise from unresolved weakly coupled protons (each proton contributes two signals centered about the nuclear Zeeman frequency - in this case, $(^1H) = 13.5$ MHz). The two large resolved signals in the 18-24 MHz region of the spectrum have been assigned (from the field dependence of proton ENDOR signals) to two strongly coupled protons.

[^{15}N]His-Substituted Cytochrome Oxidase. In order to determine whether the ENDOR signals observed near 8 MHz in the native protein arise from coupling to a histidine nitrogen, we prepared cytochrome oxidase in which ^{15}N was substituted for (naturally abundant) ^{14}N at

Figure 5

ENDOR spectrum of Cu_A (observed at g = 2.04) in native yeast cytochrome oxidase. Conditions: temperature, 2.1 K; microwave power, 10 microwatts; microwave frequency, 9.03 GHz; field modulation, 4.0 G; sweep rate, 5.2 MHz/sec; instrumental time constant, 0.02 sec.

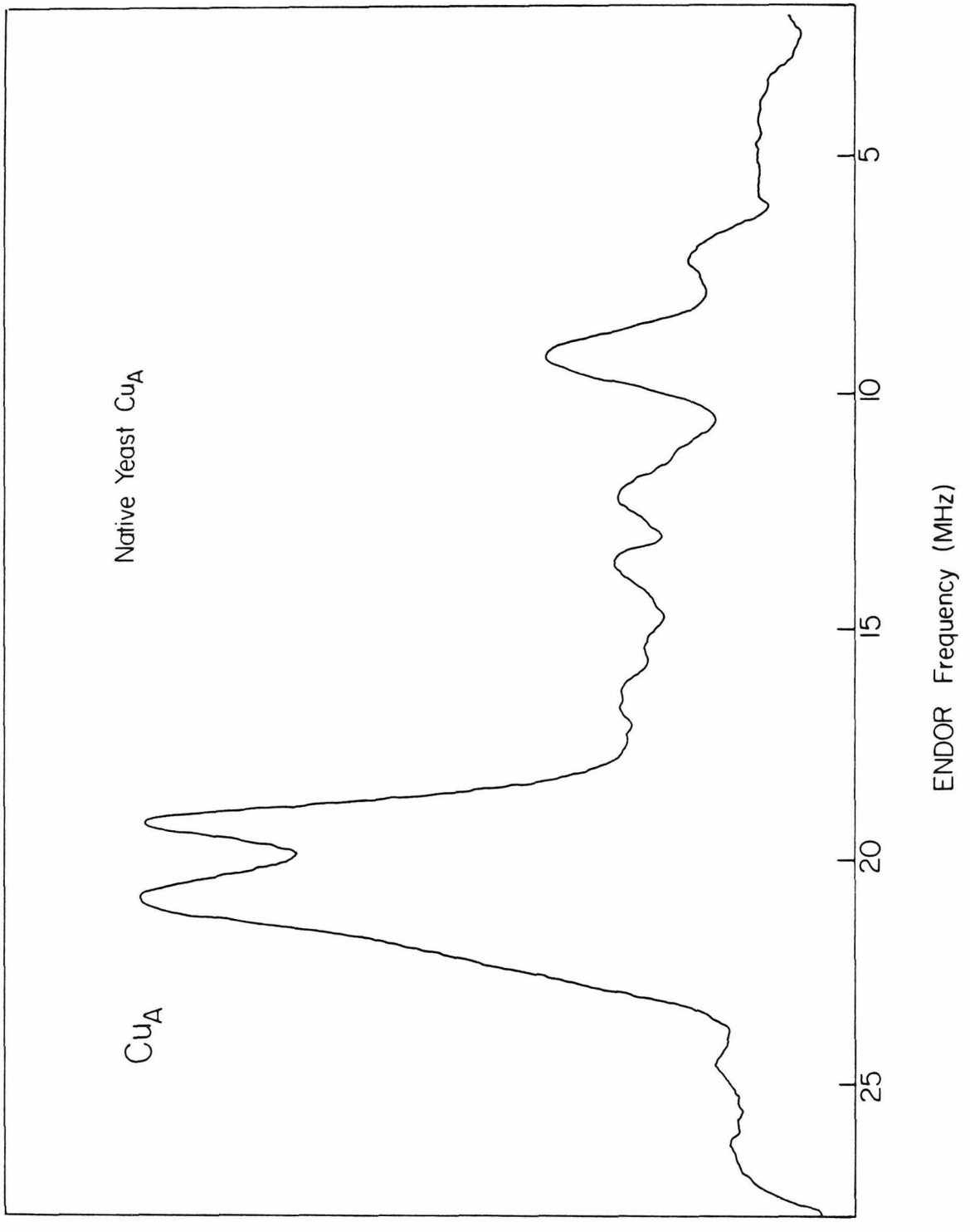
Native Yeast Cu_A
Cu_A
5
10
15
20
25
ENDOR Frequency (MHz)

both histidine ring nitrogen positions. Comparison of the [^{15}N]His and native protein ENDOR spectra (Fig. 6), reveals that the intensities of the ^{14}N ENDOR signals at 7 and 9 MHz are substantially reduced in the spectrum of the [^{15}N]His protein relative to that of the native protein. Due to the difference in the nuclear magnetic moments between the two nitrogen isotopes, substitution of the ^{14}N nucleus by ^{15}N would replace the ^{14}N ENDOR signals at 7 and 9 MHz by ^{15}N ENDOR signals at 10 and 13 MHz, respectively. We do, in fact, observe increased intensity in the weakly coupled proton region of the ENDOR spectrum for the [^{15}N]His protein, consistent with the appearance of new resonances at 10 and 13 MHz. From these observations, it is clear that there is at least one histidine ligand to Cu_A in cytochrome c oxidase.

The spectra reported in Fig. 6 also allow us to determine whether there exist any new signals attributable to histidine nitrogen which have not been previously resolved. Digital subtraction of the two spectra, shown in Fig. 6C, verifies the decrease in the [^{14}N]His nitrogen signals at 7 and 9 MHz and the appearance of new signals near 12 MHz. The rest of the spectrum from 31-1 MHz, however, shows no substantial differences between the native and [^{15}N]His-substituted proteins, particularly in the region of 18-24 MHz where the large proton signals might preclude direct resolution of smaller signals.

[^{2}H]Cys-Substituted Cytochrome Oxidase. To test the hypothesis that the strongly coupled protons observed in ENDOR spectra of the native protein arise from hyperfine interactions with the methylene protons on one or more cysteine ligands to Cu_A, we compare in Fig. 7 the ENDOR spectra of Cu_A in [^{2}H]Cys-substituted and native cytochrome oxidase. The [^{2}H]Cys-substituted protein sample was particularly dilute and therefore required considerable signal averaging and optimization of aquisition parameters in order to obtain the best possible ratio of signal to noise. To show that the changes observed between the samples are not due to anomalous effects of the field

Figure 6

ENDOR spectra of Cu_A (observed at g = 2.04) in (A) native and (B) [^{15}N]His-substituted yeast cytochrome oxidase. The difference spectrum (A-B) is shown below. Conditions: temperature, 2.1 K; microwave power, 10 microwatts; microwave frequency, (A) 9.03 GHz and (B) 9.08 GHz; field modulation, 4.0 G; sweep rate, 5.2 MHz/sec; instrumental time constant, 0.02 sec.

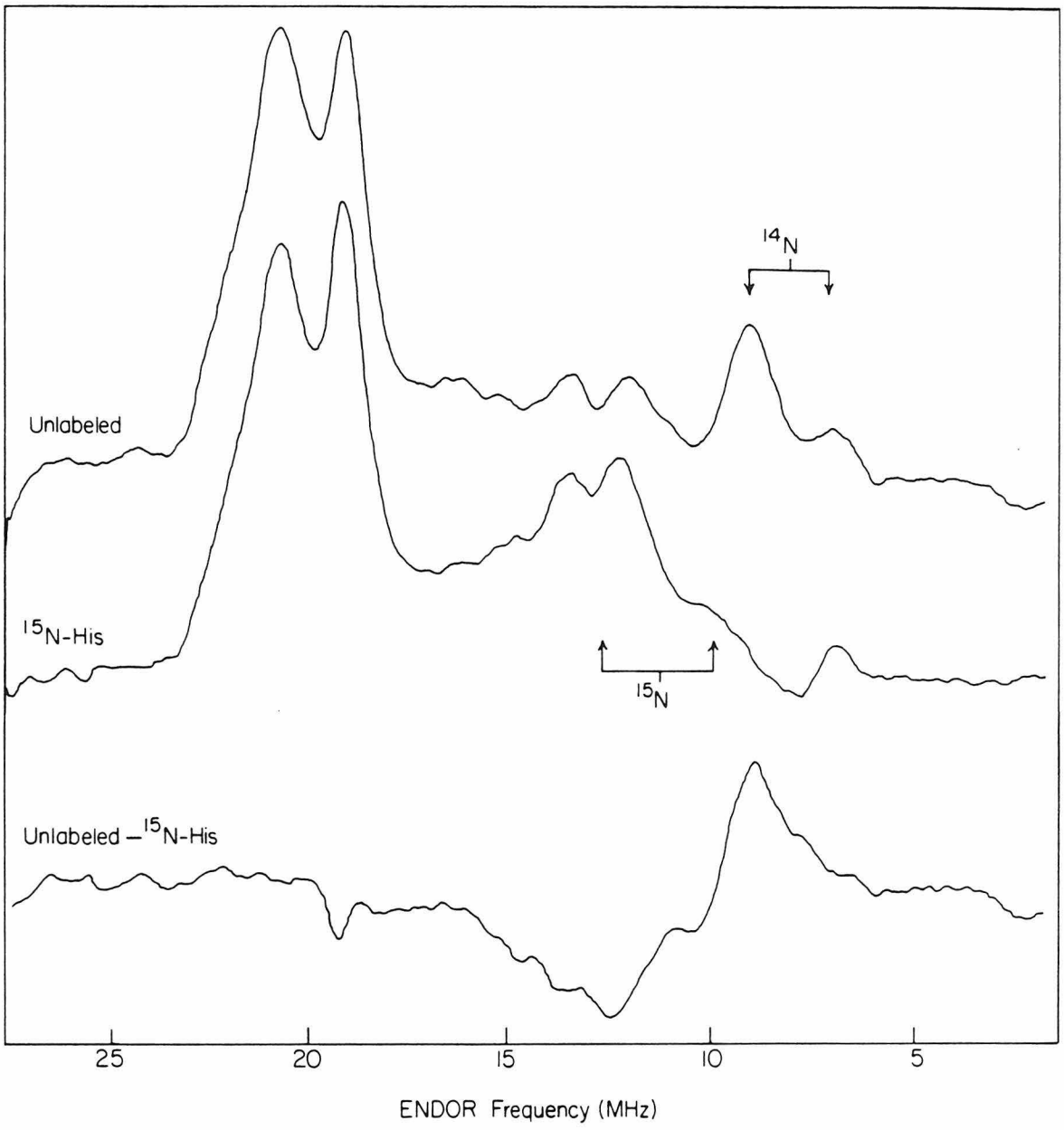
^{14}N
Unlabeled
^{15}N-His
^{15}N
Unlabeled – ^{15}N-His
25
20
15
10
5
ENDOR Frequency (MHz)

modulation under the conditions of rapid passage used in these experiments, two different field modulation amplitudes were used (compare Figs. 7A and 7B). Comparison of the ENDOR spectra of native and [^{2}H]Cys-substituted Cu_A reveals a significant change in the 18-24 MHz region of the spectrum of the [^{2}H]Cys sample, which is independent of field modulation amplitude. As approximate indicators of intensity for changes in this region, we have used internal comparisons with the ^{14}N ENDOR resonance at 9 MHz and with the weakly coupled proton ENDOR resonances near 14 MHz. Both methods indicate that the intensity of the signals in the 18-24 MHz region decreases by more than 50% on substitution of [^{2}H]Cys for native cysteine in the yeast protein.

The apparent incomplete disappearance of signals in this region may be due to the presence of non-deuterated cysteine in the protein. This could occur either by the incorporation of native cysteine into the yeast protein by revertant yeast strains, or by some (unknown) enzymatically catalyzed proton exchange process. The important result for this study is that some cysteine has been substituted. The large decrease in intensity in the 18-24 MHz region of the ENDOR spectrum of the ^{2}H-substituted protein verifies successful incorporation of [^{2}H]Cys into the protein. One might expect to observe the appearance of <u>new</u> ENDOR signals associated with the (I=1) deuterium nucleus. Unfortunately, the small deuteron nuclear magnetic moment precludes direct observation of the deuterium ENDOR, which is predicted to appear in the 1-3 MHz region of the spectrum. In any case, these ENDOR results together with the EPR data reported previously (14,17), demonstrate unambiguously that there is at least one cysteine ligand associated with Cu_A.

In order to ascertain whether there are weaker proton hyperfine interactions from cysteines associated with Cu_A, we have compared in Fig. 8 the ENDOR spectra of Cu_A in native and [^{2}H]Cys-substituted cytochrome oxidase in the region of the weakly coupled protons. Although the signal to noise does not allow us to completely rule out spectral changes in this region, it appears that there are no

Figure 7

ENDOR spectra of Cu_A (observed at g = 2.04) in native and [^{2}H]Cys-substituted yeast cytochrome oxidase observed at two different field modulations: A, 4.0 G; B, 6.4 G. Other conditions: temperature, 2.1 K; microwave power, 10 microwatts; microwave frequency, 9.12 GHz; sweep rate, 3.1 MHz/sec. The instrumental time constants for the native and [^{2}H]Cys samples were 0.05 and 0.15 sec, respectively; and in B it was 0.10 sec throughout.

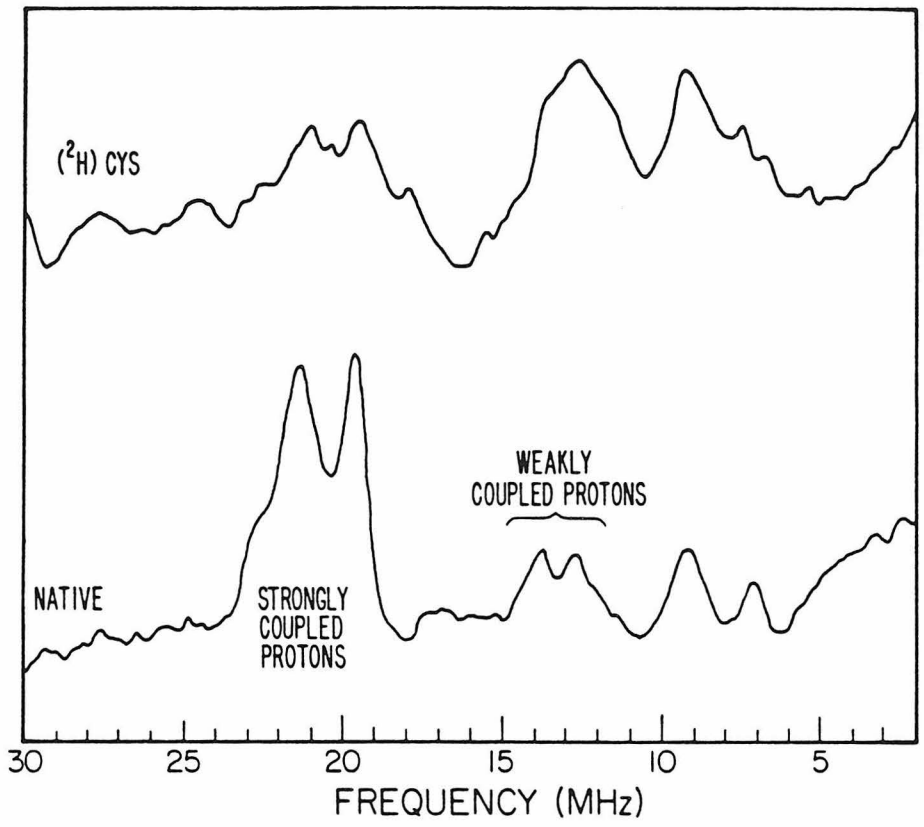
(^{2}H) CYS
WEAKLY
COUPLED PROTONS
NATIVE
STRONGLY
COUPLED
PROTONS
30
25
20
15
10
5
FREQUENCY (MHz)

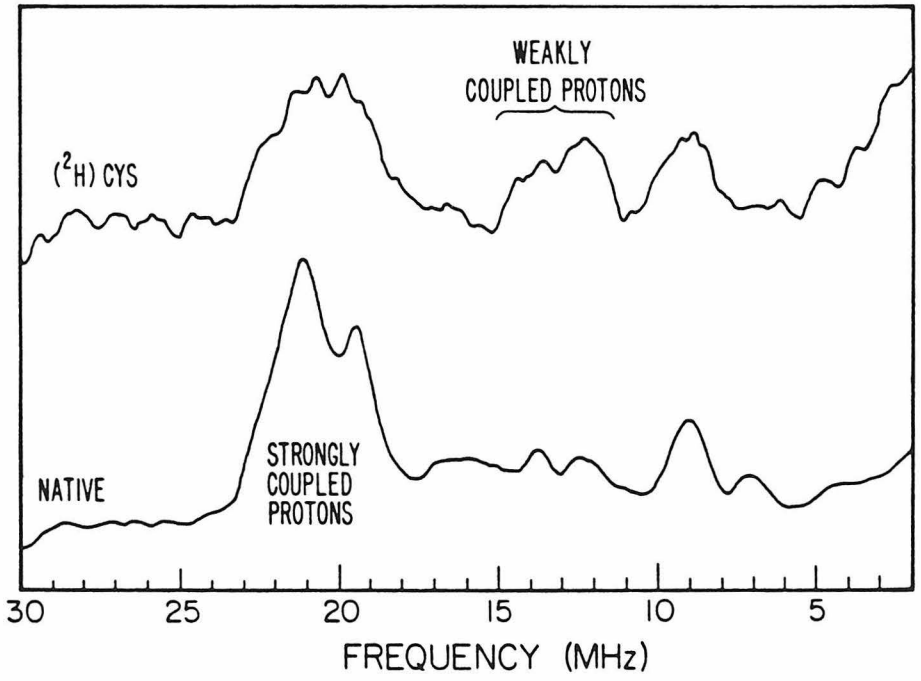
WEAKLY
COUPLED PROTONS
(^{2}H) CYS
NATIVE
STRONGLY
COUPLED
PROTONS
30
25
20
15
10
5
FREQUENCY (MHz)

Figure 8

ENDOR spectra showing the weakly coupled proton region of Cu_A (observed at g = 2.00) in native and [^{2}H]Cys yeast cytochrome oxidase. Conditions: temperature, 2.1 K; microwave power, 10 microwatts; microwave frequency, 9.12 GHz; field modulation, 0.5 G; sweep rate, 0.4 MHz/sec; instrumental time constants were 0.05 and 0.10 sec for the native and [^{2}H]Cys proteins, respectively.

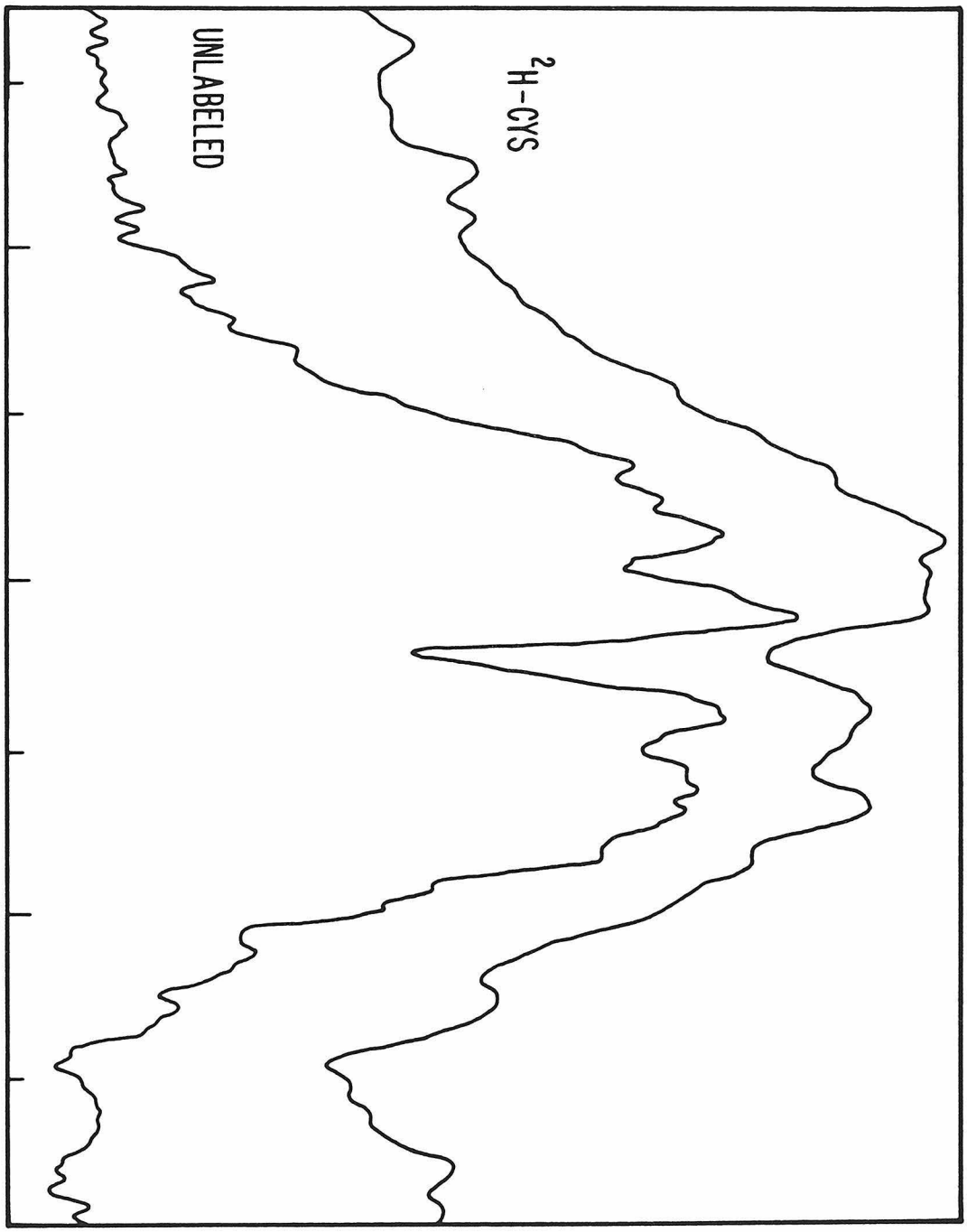
^{2}H-CYS
UNLABELED
15
14
13
FREQUENCY (MHz)

significant differences in this region between the spectra of the native and [^{2}H]Cys-substituted proteins.

[^{13}C]Cys-Substituted Cytochrome Oxidase. To confirm the identification of cysteine as a ligand to Cu_A and to attempt to determine whether there are more than one cysteine sulfurs coordinated to Cu_A, we prepared a sample of cytochrome oxidase incorporating cysteine substituted with ^{13}C at the methylene carbon. At frequencies above 7 MHz, the ENDOR spectra of oxidized Cu_A in the native and ^{13}C-substituted yeast proteins possess no significant differences, as shown in Fig. 9. However careful examination of the low frequency region (1-10 MHz) reveals a new ENDOR signal near 5 MHz in the spectrum of the ^{13}C-substituted protein. Scanning only this region and optimizing ENDOR conditions for this signal, we see in Fig. 10 that there is clearly a new signal at 5.0 MHz which is not present in the native protein. This signal can only be due to a coupling to ^{13}C of a cysteine ligand, and we predict a Zeeman partner for this signal at either 1.6 or 11.8 MHz. Examination of spectra such as those in Fig. 9 reveals no new features near 12 MHz. Unfortunately the baseline drift at frequencies below 2 MHz does not allow us to verify the existence of a Zeeman partner at 1.6 MHz, however this assignment seems most likely. Averaging narrow sweeps in both directions yields a true peak position of 5.2 MHz for the new signal, corresponding to a ^{13}C coupling of 3.6 MHz for the cysteine methylene carbon.

Weakly coupled ^{13}C hyperfine signals should occur centered at the ^{13}C nuclear Zeeman frequency. Under the conditions used in Fig. 10, such signals will appear centered at 3.4 MHz. The lack of such signals in the ENDOR spectrum of the [^{13}C]Cys-substituted protein suggests that there are no very weakly coupled ^{13}C nuclei at the Cu_A site. Note, however, that since the strength of the interaction would be quite weak, the intensity of these signals would probably be quite low and hence they may not be resolved from the background noise.

Figure 9

ENDOR spectra of Cu_A (observed at g = 2.04) in (A) native and (B) [^{13}C]Cys-substituted yeast cytochrome oxidase. Conditions: temperature, 2.1 K; microwave power, 10 microwatts; microwave frequency, (A) 9.03 GHz and (B) 9.07 GHz; field modulation, 4.0 G; sweep rate, 5.2 MHz/sec; instrumental time constant, 0.02 sec.

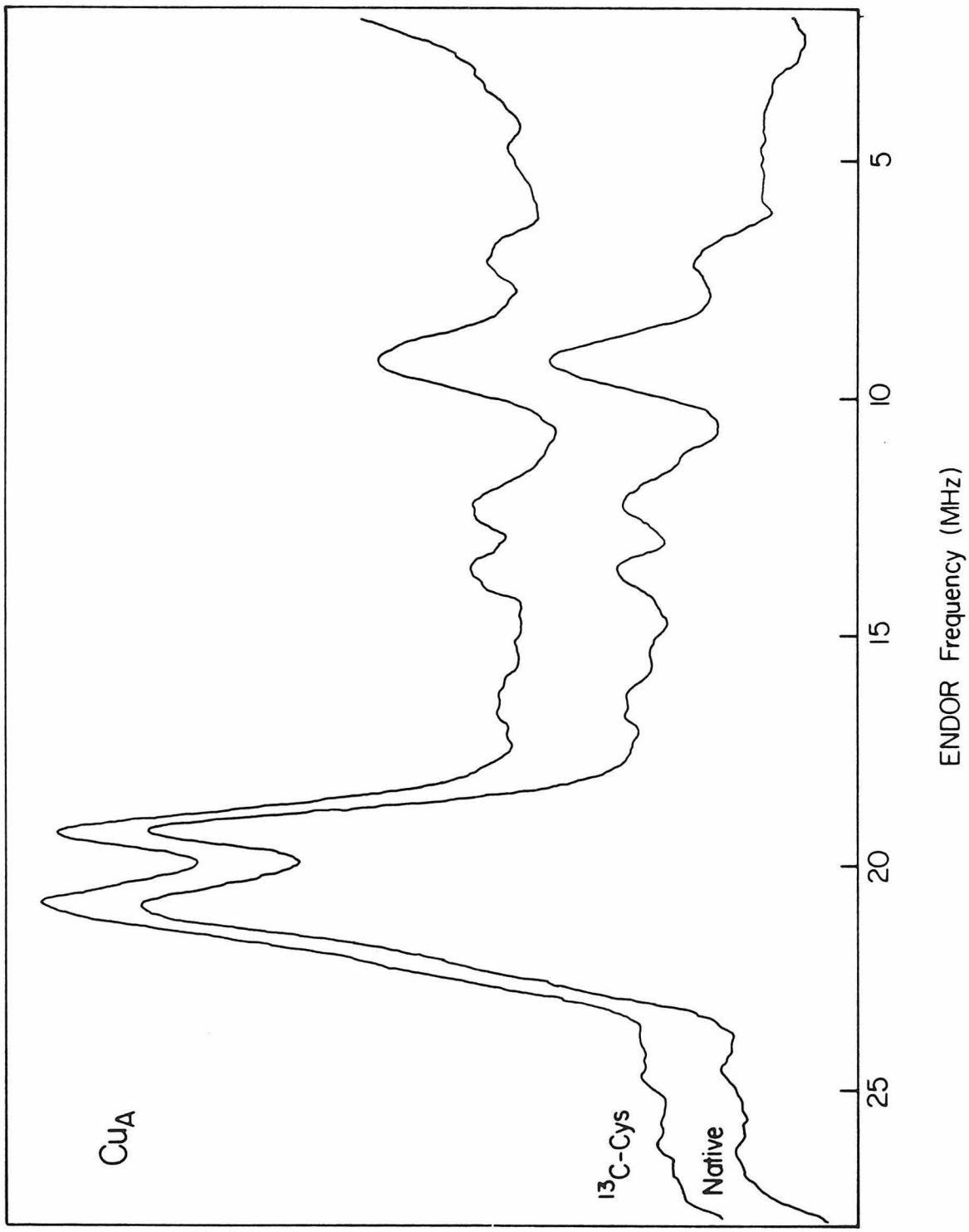
Cu_A
^{13}C-Cys
Native
5
10
15
20
25
ENDOR Frequency (MHz)

Figure 10

ENDOR spectra of Cu_A (observed at g = 2.04) in (A) native and (B) [^{13}C]Cys-substituted yeast cytochrome oxidase showing the new signal arising from ^{13}C incorporation. Conditions: temperature, 2.1 K; microwave power, 3.2 microwatts; microwave frequency, (A) 9.03 GHz and (B) 9.07 GHz; field modulation, 2.0 G; sweep rate, 2.0 MHz/sec; instrumental time constant, 0.05 sec.

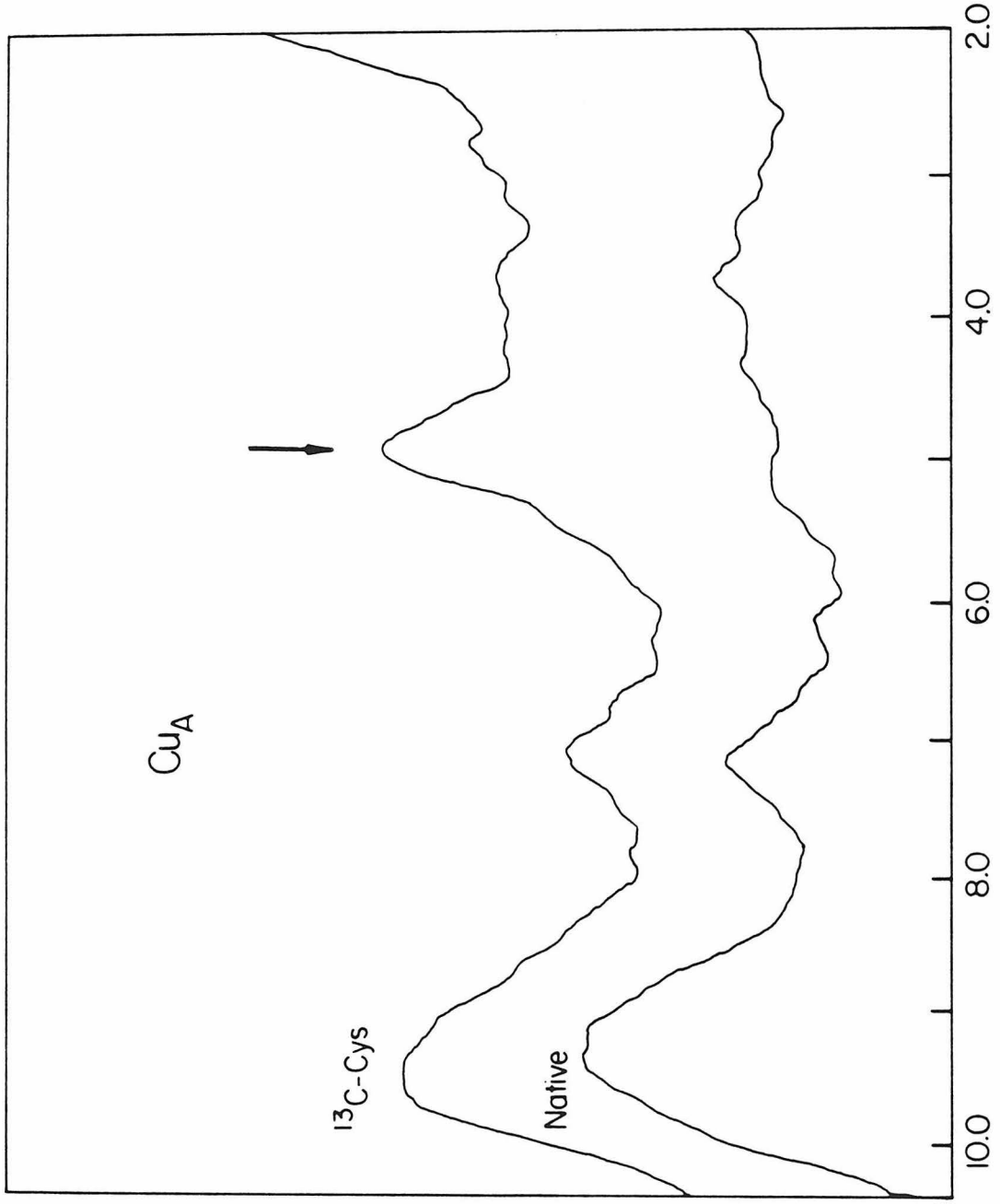
Cu_A
^{13}C-Cys
Native
10.0
8.0
6.0
4.0
2.0
ENDOR Frequency (MHz)

Comparison of ENDOR Spectra of Cu_A in the Yeast and Beef Proteins

The ENDOR spectra of Cu_A from the yeast and beef heart proteins are qualitatively the same, although the exact magnitudes of some of the couplings are not identical. The assignment of previously reported ENDOR signals (in the beef heart protein) to specific amino acid ligands prompts us to reexamine the spectrum of Cu_A from the beef heart protein. The availability of larger and more concentrated beef heart protein samples, and improved facilities for the signal averaging of spectra, have allowed a substantial improvement in resolution over the original ENDOR data (11). The general features of the new beef heart ENDOR spectrum in the 31-1 MHz region, shown in Fig. 11, are similar to those in the original spectrum from beef heart and are also similar to data reported here for the yeast protein.

Assigned Hyperfine Couplings in Cu_A. The histidine nitrogen ENDOR signals at 9.5 and 7.6 MHz are quite well resolved in the spectrum of the beef heart protein. Averaging signal positions obtained from frequency sweeps in opposite directions (not shown), we obtain a nitrogen hyperfine coupling of 17.9 MHz for this ^{14}N Zeeman pair.

The two strongly coupled cysteine methylene proton signals are observed in the spectrum of the beef heart protein at 18.7 and 22.3 MHz. These signals correspond to (corrected) proton hyperfine couplings of 11.0 and 18.6 MHz. The spectrum in Fig. 11 also shows a newly resolved signal at about 4.2 MHz. Using the measured proton nuclear Zeeman frequency of 13.60 MHz, and after correcting for rapid passage effects (see Materials and Methods section), calculations predict that this signal is the Zeeman partner of the strongly coupled cysteine methylene proton at 22.3 MHz. Similar calculations predict that the partner for the strongly coupled proton at 18.7 MHz should appear at 8.5 MHz. This signal position is identical to that of one of the histidine nitrogen ENDOR transitions, so that it is not

Figure 11

ENDOR spectrum of Cu_A (observed at g = 2.04) in beef heart cytochrome oxidase. Conditions: temperature, 2.1 K; microwave power, 10 microwatts; microwave frequency, 9.09 GHz; field modulation, 4.0 G; sweep rate, 5.2 MHz/sec; instrumental time constant, 0.01 sec.

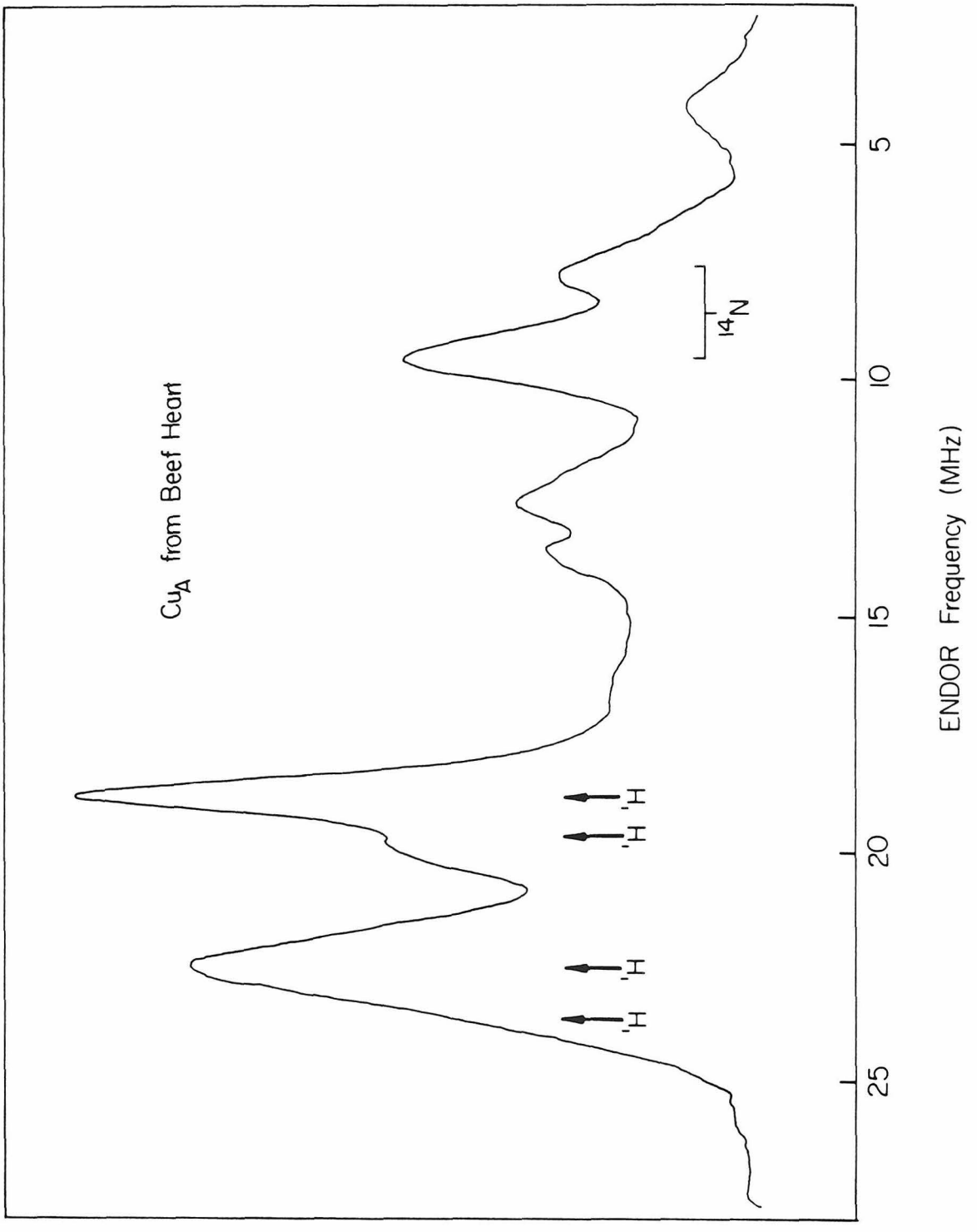
Cu$_A$ from Beef Heart
^{14}N
H
H
H
H
5
10
15
20
25
ENDOR Frequency (MHz)

expected to be resolved. The weak intensities of these low-frequency proton signals relative to their partners at higher frequencies is predicted by the ENDOR enhancement effect (26), which states that the intensity of a signal within a Zeeman pair is proportional to the square of the resonant frequency of the transition.

Resolution of New Signal(s) in the 18-24 MHz Region. Another feature not previously reported for ENDOR spectra of Cu_A in the beef heart protein is the resolution of a new signal at 19.9 MHz. This signal appears in Fig. 11 as a distinct peak adjacent to the proton resonance at 18.6 MHz. This new signal may be due to a second nitrogen coupling to Cu_A. Alternatively, this signal may arise from a strongly coupled proton, either from a subset of molecules possessing a slightly different conformation at the copper site, or from a third entirely new proton in close interaction with the Cu_A site. This last alternative raises the possibility of a second cysteine ligand to Cu_A with at least one strongly coupled methylene proton.

The Issue of One Vs. Two Cysteine Ligands to Cu_A

The resolution of a new strongly coupled proton signal in the ENDOR spectrum of Cu_A raises the interesting question of whether the signals in the 18-24 MHz region can be totally accounted for by the presence of only one cysteine ligand to Cu_A. It is quite possible that there are three or four distinct cysteine methylene protons interacting with copper to yield three or four ENDOR signals in this region of the spectrum. This would indicate a unique coordination for Cu_A in which two cysteine ligands are strongly coordinated to the copper center. We now present spectroscopic results directed at selecting between coordination schemes involving one or two cysteine ligands.

NMESE Study of [^{13}C]Cys-Substituted Cytochrome Oxidase. The sample of [^{13}C]Cys-substituted cytochrome oxidase allows us to investigate the possibility of a second cysteine ligand to Cu_A. Although only one new signal is resolved in the ENDOR spectrum of Cu_A in the [^{13}C]Cys-substituted protein, it is possible that smaller couplings to a second ^{13}C nucleus are not resolved by ENDOR. In particular, very weak interactions will have very low intensity and may not be discernible from the noise. In an attempt to determine the presence of any very weakly coordinated cysteine ligands to Cu_A, we have examined the nuclear modulation of electron spin echo (NMESE) spectra of native and [^{13}C]Cys-substituted yeast cytochrome oxidase. NMESE spectroscopy (23) is particularly useful for determining hyperfine couplings which are often too small to detect by ENDOR spectroscopy.

The two-pulse echo decay envelopes presented in Fig. 12, compare the echo modulation patterns for native and ^{13}C-substituted Cu_A. The Fourier transforms of these data, presented in Fig. 13, show that the modulation pattern in each spectrum is dominated by a ^{1}H modulation frequency of 13.3 MHz. This corresponds to the nuclear Zeeman frequency of very weakly coupled protons for this field position and is common in spectra of copper centers in proteins. The peak in the Fourier transform at 26.6 MHz is due to an overtone of this Zeeman resonance frequency. One significant difference between the ^{13}C-substituted and native protein spectra is the presence of a modulation at approximately 5 MHz in the [^{13}C]Cys sample which is absent in the native sample. This new modulation must be due to a coupling of ^{13}C to the Cu_A center. Under the conditions of this experiment, the ^{13}C nuclear Zeeman frequency is 3.4 MHz. Since the modulation frequencies observed in NMESE occur at the same frequencies as ENDOR transitions, we can calculate the ^{13}C hyperfine coupling to be approximately 4.5-5.5 MHz. This signal is quite likely from the same ^{13}C hyperfine interaction observed in the ENDOR spectra of these samples, and does not represent a new ^{13}C hyperfine coupling.

Figure 12

Electron spin echo decay envelopes (observed at g = 2.06) of Cu_A in native and [^{13}C]Cys yeast cytochrome oxidase. Echo intensities were measured using a two-pulse technique with pulse widths of 20 and 40 nanoseconds, respectively. The delay between pulses (τ) was moved in 10 nanosecond increments, starting at 200 nanoseconds. Conditions: microwave frequency, 9.06 GHz; temperature, 4.2 K, other conditions as described in reference (22).

Electron Spin Echo Decay

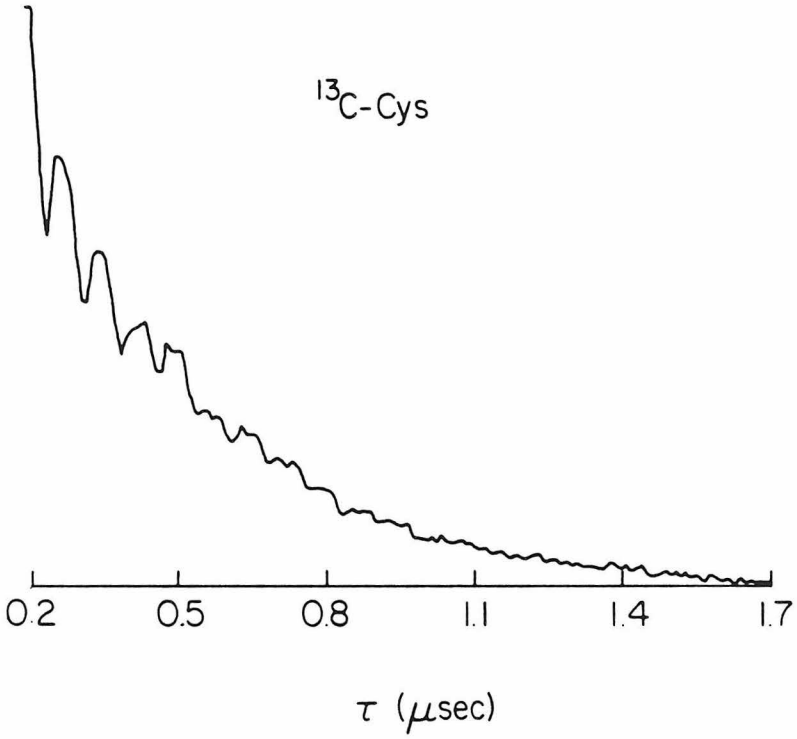

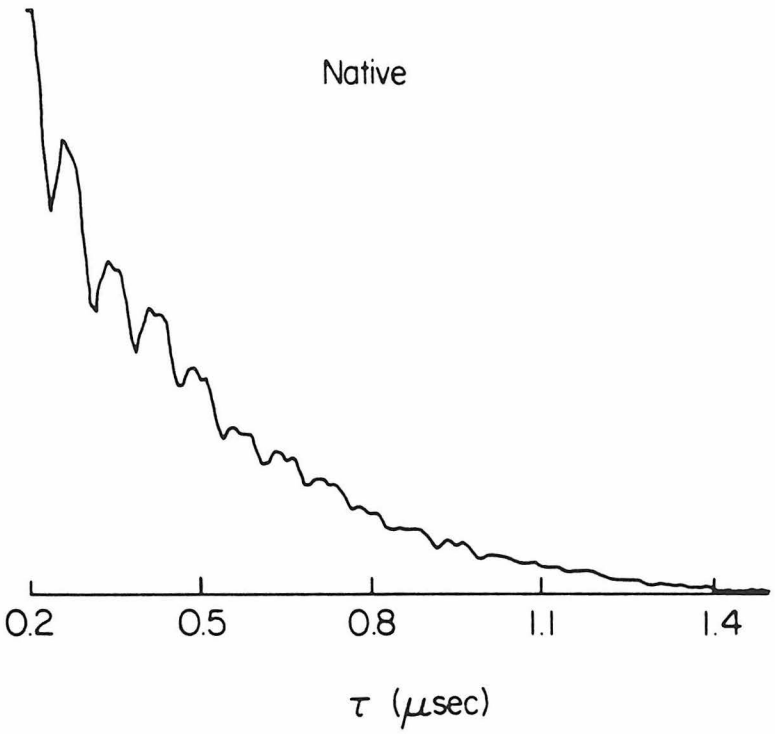

Figure 13

Fourier transforms of the data in figure 12, showing the nuclear modulation of electron spin echo (NMESE) frequencies for Cu_A in native and [^{13}C]Cys yeast cytochrome oxidase. An apodization method was used as described in the text.

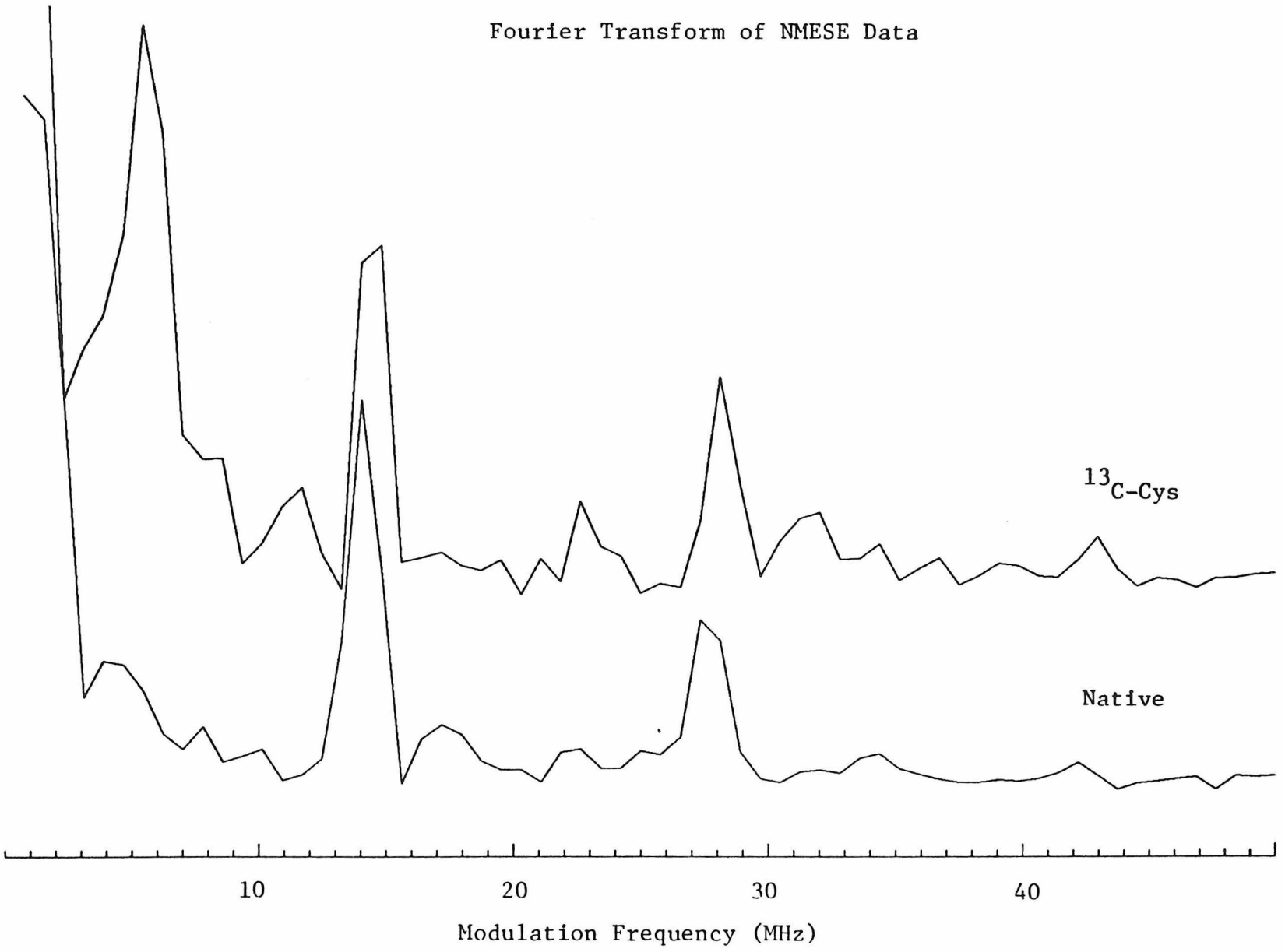
Fourier Transform of NMESE Data
^{13}C-Cys
Native
10
20
30
40
Modulation Frequency (MHz)

ENDOR Spectra of Cu_A at Two Different Microwave Frequencies. In order to determine whether the newly resolved signal near 19.9 MHz in the spectrum of the beef heart protein is due to a strongly coupled proton, we have made use of the difference in nuclear magnetic moments of the various nuclei. The nuclear Zeeman interaction is linearly proportional to the involved nuclear magnetic moment. For protons, the nuclear magnetic moment is quite large, so that the nuclear Zeeman interaction is normally greater than or comparable to the hyperfine interaction, even in strongly coupled systems such as exist here. Since the nuclear Zeeman interaction, but not the hyperfine component, is sensitive to the field strength, the application of a higher microwave frequency (and hence a higher magnetic field for constant g-value) will cause a much greater shift in signals arising from protons than for signals of other nuclei. The ENDOR spectra of Cu_A in beef heart cytochrome oxidase at two different electronic frequencies are compared in Fig. 14. A large field-dependent shift is observed in these spectra not only for the signals at 18.7 and 22.3 MHz, but also for the newly resolved signal at 19.9 MHz. Furthermore, the general shape of the entire spectrum in the 18-24 MHz region shows little change, consistent with a concerted shift of all signals in this region and minor, if any, contributions from non-proton nuclei.

ENDOR Spectra of Cu_A in Two Different Beef Heart Preparations. In order to help determine the nature of the newly resolved proton signals in the 18-24 MHz region of the Cu_A ENDOR spectrum, we examined the ENDOR spectra of oxidized Cu_A in two different preparations of beef heart cytochrome oxidase. ENDOR spectra of Cu_A from beef heart cytochrome oxidase isolated according to the procedures of King, et al. (19) and Hartzell, et al. (20) are compared in Fig. 15. This comparison clearly shows that if conformational heterogeneity causes different methylene proton couplings within a sample, the nature and extent of this conformational heterogeneity are independent of the nature of the preparation.

Figure 14

ENDOR spectra of Cu_A in beef heart cytochrome oxidase at two different microwave frequencies: 9.08 and 9.34 GHz. (A) a wide sweep range showing both the region of the strongly coupled protons and the histidine nitrogens; and (B) an enlarged view showing only the region of the strongly coupled protons. Other conditions: temperature, 2.1 K; microwave power, 10 microwatts; field modulation, 4.0 G; sweep rate, 5.2 MHz/sec; instrumental time constant, 0.02 sec.

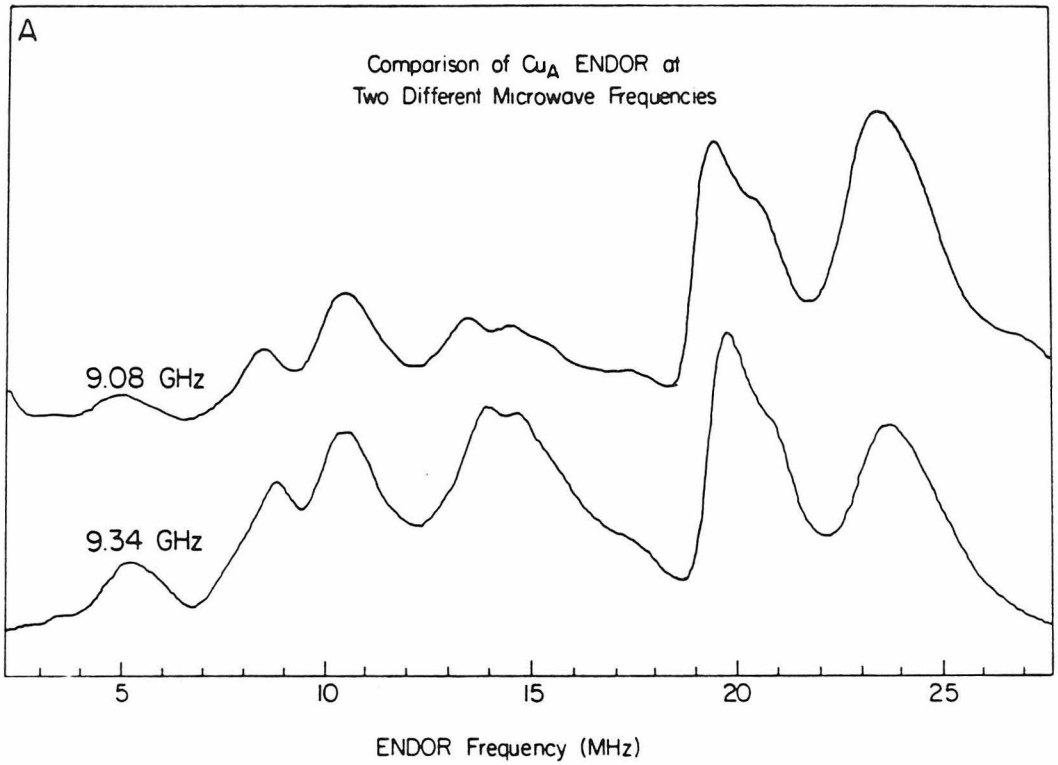
A
Comparison of Cu_A ENDOR at
Two Different Microwave Frequencies
9.08 GHz
9.34 GHz
5
10
15
20
25
ENDOR Frequency (MHz)

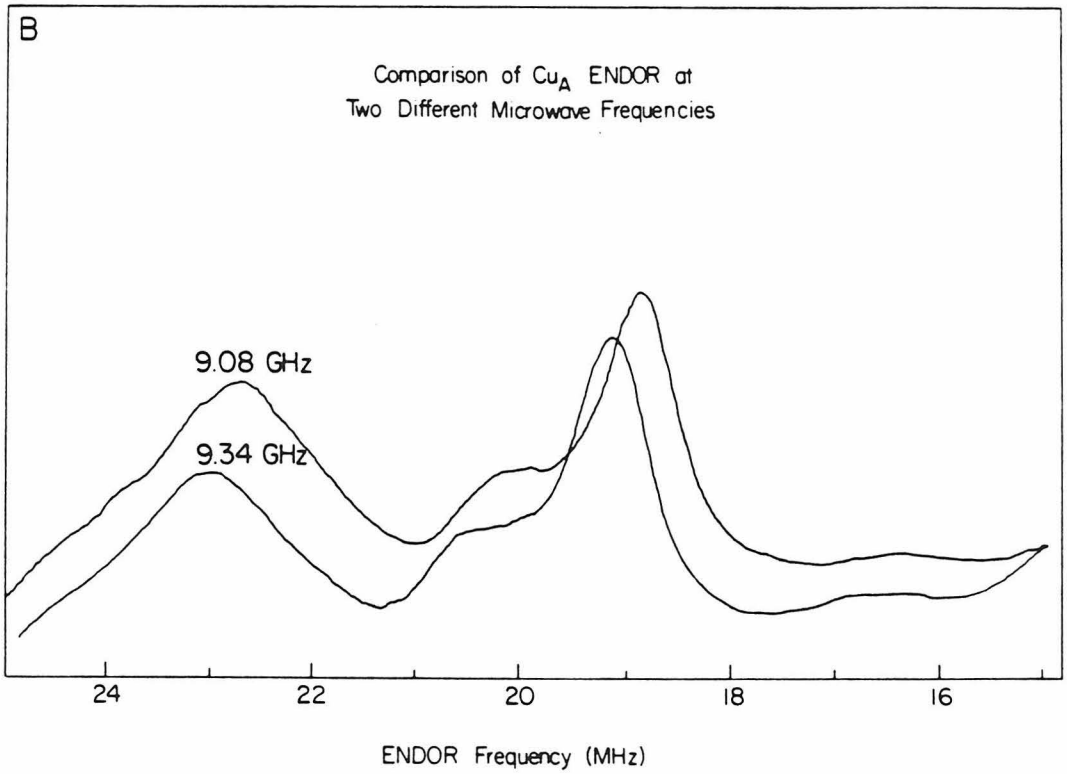
B
Comparison of Cu_A ENDOR at
Two Different Microwave Frequencies
9.08 GHz
9.34 GHz
24
22
20
18
16
ENDOR Frequency (MHz)

Figure 15

ENDOR spectra of Cu_A in two different preparations of beef heart cytochrome oxidase: (A) protein purified according to the procedure of Yu, et al. (19); and (B) prepared according to the procedure of Hartzell, et al. (20). Conditions: temperature, 2.1 K; microwave power, 10 microwatts; microwave frequency, (A) 9.08 and (B) 9.11 GHz; field modulation, 4.0 G; sweep rate, 5.2 MHz/sec; instrumental time constant, 0.01 sec.

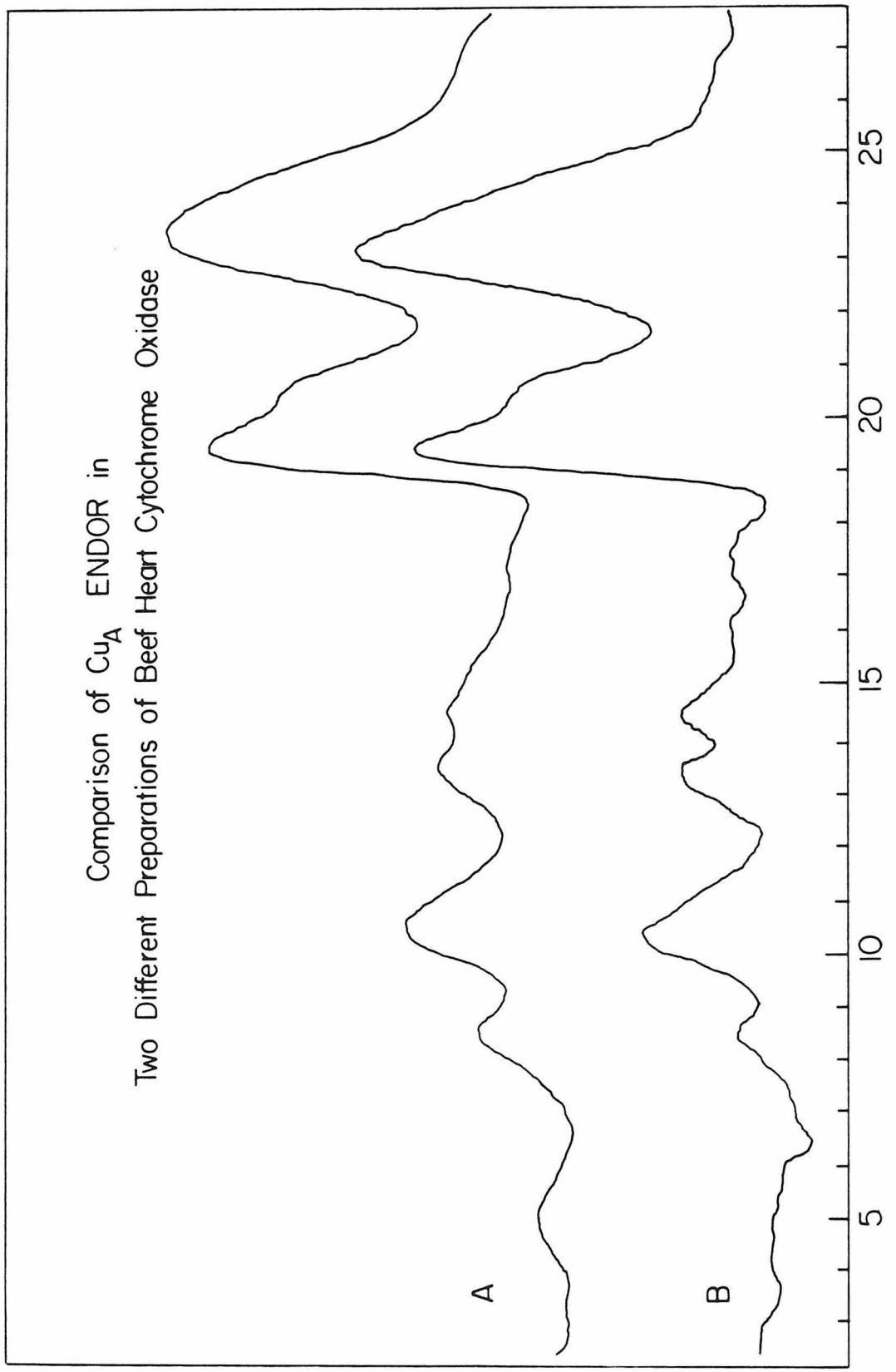
Comparison of Cu_A ENDOR in
Two Different Preparations of Beef Heart Cytochrome Oxidase
A
B
5
10
15
20
25
ENDOR Frequency (MHz)

DISCUSSION

Cytochrome c oxidase isolated from the yeast Saccharomyces has spectroscopic properties very similar to those of the beef heart protein (14,17). As will be shown in chapter IV, there is also extensive evolutionary sequence homology between cytochrome oxidase from these and other eukaryotic species. Based on these considerations, it is certain that the active sites in yeast and beef heart cytochrome oxidase are very nearly identical. Certainly the identity of the ligands to Cu_A must be the same between these species; the spectroscopy of the site is quite unusual and is unlikely to be so similar for different coordination spheres.

Identification of Ligands to Cu_A

Inasmuch as the yeast system can be manipulated to allow direct incorporation of isotopically substituted amino acids into the protein, we have used this system to probe the structure of Cu_A by preparing [^{2}H]Cys-, [^{13}C]Cys-, and [^{15}N]His-substituted cytochrome oxidases. These studies, together with those described in a recent report (13), represent the first concrete information regarding the identity of endogenous ligands to the metal centers in cytochrome c oxidase.

Histidine is a Ligand to Cu_A. The assignment of a 16 MHz hyperfine coupling to ^{14}N of a histidine ligand in the native protein is confirmed by the observed changes in the 7-15 MHz region of the Cu_A ENDOR spectrum on substitution of [1,3-$^{15}N_2$]His for native (^{14}N) histidine in cytochrome oxidase. Two observations are unambiguous: 1) the strong peak at 9 MHz is no longer present in the spectrum of the [^{15}N]His protein; and 2) the changes in intensity and line shape of the 10-15 MHz region are consistent with two new signals (from a

Zeeman pair) arising from ^{15}N substitution. There appear to be no other ENDOR signals that might be ascribed to histidine ring nitrogens. Digital subtraction of the two spectra shows, in particular, that there are no histidine nitrogen couplings in the 19–24 MHz region of the native protein spectrum.

It is interesting to note that a hyperfine coupling of 16–17 MHz is unusually small for a histidine nitrogen ligand to Cu(II) (12,27). However, as will be discussed later in this section, it is not unexpected for a system in which the unpaired spin is substantially delocalized away from copper.

Cysteine is a Ligand to Cu_A. The existence of at least one cysteine as a ligand to Cu_A is demonstrated by the ENDOR studies of [β,β-$^2H_2$]Cys-substituted cytochrome oxidase. The two resonances seen at 19.7 and 21.7 MHz in the native yeast protein spectrum decrease in intensity by more than 50% on substitution of [^{2}H]Cys for native cysteine. The incomplete elimination of intensity in this region can be rationalized in several ways. It is possible that some proton exchange may have occurred at the methylene carbon during the biosynthesis of the enzyme. Also, although revertant levels appeared to be low throughout the growth of the yeast (17), the particular strain used for the growth of this sample (different from that used in the growth of [^{13}C]Cys-substituted yeast) had a moderately high reversion rate. Since the mutant yeast strain is at a significant disadvantage relative to revertants, it is possible that during the final hours of growth, the revertant strains had begun to become a moderate fraction of the total cell density in the fermentor. In this case, the revertants could synthesize and incorporate (unlabeled) cysteine, resulting in a fraction of the isolated protein being of normal isotopic composition.

The measurement of a hyperfine coupling to ^{13}C in Cu_A isolated from [β-^{13}C]Cys-substituted yeast unambiguously confirms the assignment of at least one cysteine ligand to Cu_A. The lack of any

other couplings to ^{13}C in either the ENDOR or NMESE spectra indicates that either: 1) there is only one cysteine ligand to Cu_A, 2) there is a second cysteine ligand with a negligible hyperfine interaction, or 3) there are two cysteine ligands to Cu_A with almost identical hyperfine couplings to the methylene ^{13}C, such that the two ENDOR signals appear as one. These possibilities will be discussed below in the context of other ENDOR findings and information on the overall structure of the site.

The Possibility of a Second Cysteine Ligand to Cu_A

The newly resolved signal near 20 MHz in the Cu_A ENDOR spectrum of beef heart cytochrome oxidase may be explained in more than one way. First, it may be that there exists some structural heterogeneity in the Cu_A centers which causes a subset of them to have slightly different methylene proton hyperfine couplings. As will be discussed in a later section, this change in hyperfine coupling could easily occur by a slight rotation of the β-CH_2 group relative to the π-orbital on sulfur containing the unpaired spin density. Although small rotations of this sort are not unexpected in a protein, this interpretation would require two distinct populations of Cu_A centers within the isolated protein with very precise, yet different, rotational orientations. Moreover, it would require this heterogeneity to be a property of the oxidized protein independent of the method of preparation. Although conformational heterogeneity has been observed for the coordination at the oxygen binding site in cytochrome oxidase, it is not only dependent on the method of isolation, but also varies from preparation to preparation within samples of beef heart protein prepared by the same procedure (28). The heterogeneity observed at the oxygen binding site is probably due to different modes of coordination of exogenous ligands. Cu_A binds no exogenous ligands and is unlikely to show similar effects.

A second interpretation is that the signal seen at 19.9 MHz is due to hyperfine coupling to a (^{14}N) nitrogen ligand. However ENDOR spectra recorded at two different microwave frequencies (Fig. 14) rule out this possibility. The new signal shifts with a change in the field position in the manner expected for a proton. Due to the uniquely large magnitude of the proton nuclear magnetic moment relative to all other nuclei, this signal can be unambiguously assigned to a proton hyperfine coupling.

Finally, the signal seen at 19.9 MHz may be due to a third methylene proton on a second cysteine ligand to Cu_A. In this case, the other proton on this second cysteine could give rise to one of the strongly coupled proton signals or it may be at an angle (see the following section) relative to the orbital containing the unpaired spin such that its coupling is very small. Regardless, although the assignment of individual peaks in the spectrum to specific methylene proton pairs is not possible with the available data, this interpretation would predict a fourth methylene proton coupling. Careful analysis of the beef heart protein Cu_A ENDOR spectrum in the region near 23-24 MHz reveals a shoulder on one side of the major signal at 23 MHz, consistent with the presence of an underlying signal near 24 MHz. ENDOR spectra taken in opposite sweep directions (not shown) demonstrate that this distortion is not caused by rapid passage or similar effects. This shoulder at high frequency is even more pronounced in the ENDOR spectra of the yeast protein (the new signal being centered at about 22.5 MHz). For these reasons, we feel that there is good cause to suspect four different strongly coupled proton signals in the 19-24 MHz region of the Cu_A ENDOR spectra, and that these signals originate from two sets of methylene protons from two different cysteine ligands to Cu_A. The fact that only one ^{13}C hyperfine coupling has been measured in the ENDOR spectrum of the [^{13}C]Cys-substituted protein would indicate that the two sulfur atoms have very similar spin densities so that the resonances from the two methylene ^{13}C-carbons are coincident.

The new finding of more than two strongly coupled protons to Cu_A in the beef heart protein (and presumably also in the yeast protein) is evidence that there are <u>two</u> cysteine ligands to Cu_A. The comparable magnitude of these couplings, combined with the apparent measurement of only one resonance for ^{13}C hyperfine interaction(s) in the [^{13}C]Cys sample, shows that if there are two cysteine ligands to Cu_A, each has very similar unpaired spin density.

<u>Estimation of the Unpaired Spin Density on Cysteine Sulfur</u>

We now examine the observed methylene proton hyperfine couplings in an attempt to estimate the extent of delocalization of unpaired spin density from copper onto the cysteine sulfur ligand(s). Although precise solutions require a knowledge of which signals arise from couplings to protons on the same cysteine ligand, the qualitative arguments are the same for all protons with resonances in the 19–24 MHz region of the ENDOR spectra. To illustrate the approach, the following analysis will initially assume that the protons with couplings of 11.0 and 18.6 MHz in the beef heart protein arise from methylene protons on the same cysteine.

<u>The McConnell Relation and Hyperconjugation</u>. Hyperfine interactions from methylene protons adjacent to a π-type sulfur radical have been found to arise primarily from hyperconjugation (29,30). The coupling from such a methylene proton is expected to be isotropic and its magnitude depends on the dihedral angle $\emptyset$ between the C–H bond and the sulfur 3p orbital containing the unpaired electron (see Fig. 16) according to the following equation:

$$A = A_o \rho_s^{\pi} \cos^2\emptyset. \qquad (1)$$

In this equation A_o is a constant, typically 86 MHz for various sulfur radicals (see Gordy (30) for a recent review), and ρ_s^{π} is the π-spin

Figure 16

Geometry of a sulfur 3p orbital (containing unpaired spin density) with respect to the adjacent methylene protons. The diagram is drawn such that the methylene carbon lies directly behind the sulfur.

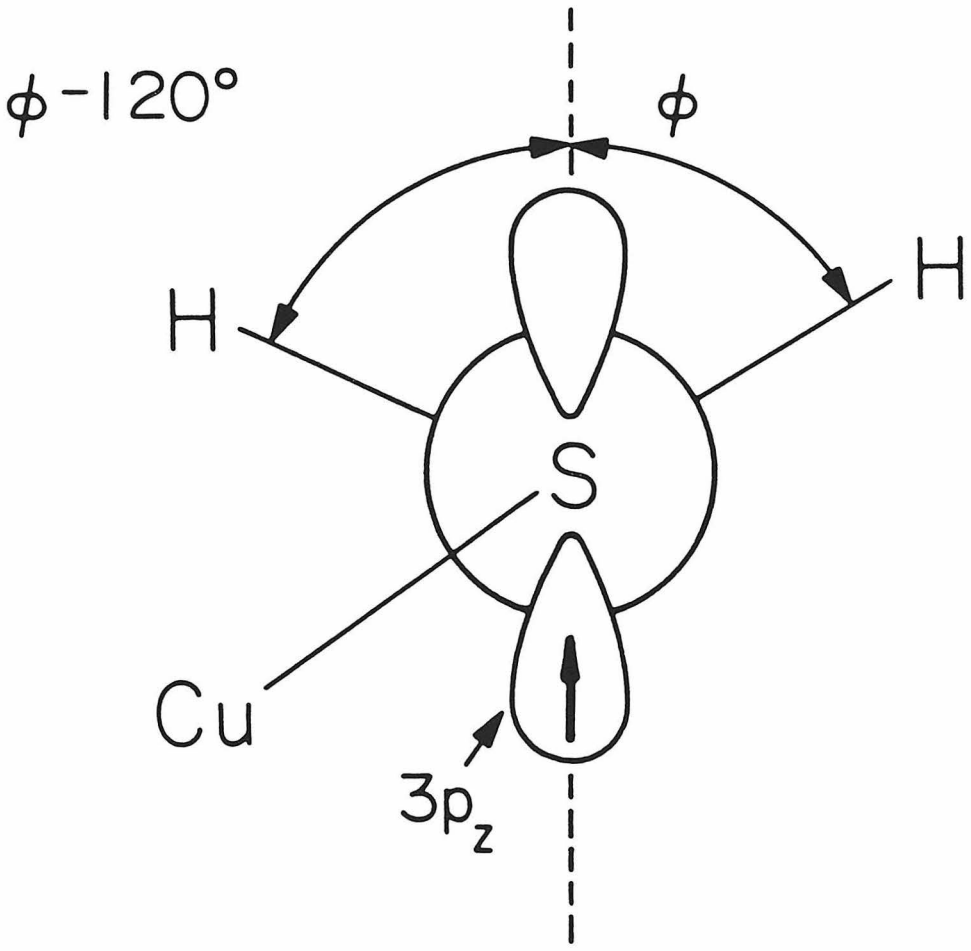
ϕ-120°
ϕ
H
H
S
Cu
3p$_z$

density centered on sulfur (specifically, the p-orbital contribution). Assuming a dihedral angle of 120° between the two protons and using the measured proton hyperfine couplings, one can solve for ρ_s^π and the proton dihedral angles for a sulfur radical like those found in irradiated cysteine (31). Due to the cosine nature of the above equation two distinct sets of solutions are found. For the Cu_A center with proton hyperfine couplings of 11.0 and 18.6 MHz, one solution of equation (1) results in a situation in which about 25% of the unpaired electron spin resides in a π-type orbital on sulfur, whereas the second solution places about 70% of the unpaired spin on sulfur.

For either of these two solutions to equation (1), the dihedral angles of the methylene protons are in a region of the function wherein the predicted hyperfine couplings are very sensitive to the dihedral angle. As an example, for the solution predicting the localization of 25% of the unpaired spin on sulfur, the dihedral angle for the proton giving rise to the 11.0 MHz proton hyperfine coupling is calculated to be 43°. The slope of the function at this point is such that a rotation of only 0.7° will result in a 1 MHz change in the hyperfine coupling (or a 0.5 MHz change in the observed signal position). Given the relatively narrow linewidths of the strongly coupled proton signals for Cu_A (approximately 0.5 to 1 MHz), we can predict that at low temperatures the distribution of dihedral angles for each of the methylene protons is quite narrow, ie. that the cysteine sulfur ligands have very little rotational freedom. This interesting structural result must be explained by future models for the site.

Factors Affecting the Quantitation of Unpaired Spin Density. The use of equation (1) to fit the observed hyperfine couplings of the strongly coupled protons provides valuable information regarding both the physical structure and the electronic distribution at the Cu_A site. However, two different considerations can lead to deviations from the ideal situation assumed by the equation. First, the

treatment above assumes hyperconjugation as the only contribution to unpaired spin at the methylene protons. Another mechanism which can contribute to the observed hyperfine interaction is spin polarization (32). This mechanism of unpaired spin transfer is independent of angle, but it cannot be predicted without detailed molecular orbital calculations on the entire system. If this mechanism contributes to the observed hyperfine interaction, the spin densities on sulfur calculated by equation (1) will be overestimated. However, spin polarization drops off substantially as it propagates from bond to bond and so should represent a minor contribution to the unpaired spin density on methylene protons two bonds removed. In model studies of sulfur-centered radicals equation (1) has proven adequate to explain the measured hyperfine couplings, and contributions from spin polarization have been found to be negligible (30). We expect that it is negligible in this system as well.

Experimental verification of the proposal that hyperfine coupling to the methylene protons in Cu_A arises purely from hyperconjugation is provided by the measurement of hyperfine coupling to ^{13}C substituted at the methylene carbon of cysteine. Although the methylene carbon is presumably of tetrahedral geometry, and therefore possesses a significant amount of s-orbital character through sp^3 hybridization, the measured ^{13}C hyperfine coupling of 3.6 MHz is quite small. By comparison, the $CF_3^{\cdot}$ radical is close to tetrahedral in geometry (with an estimated s-orbital spin density of 0.20), and contains a ^{13}C hyperfine coupling of 760 MHz (33). By comparison, the unpaired spin density in the s-orbital of the cysteine methylene carbon(s) at Cu_A must be quite small, indicating very little spin polarization to carbon from unpaired spin localized on sulfur. The contribution from spin polarization to the hyperfine interaction at the methylene protons one bond removed must certainly be negligible.

A second consideration with respect to the use of equation (1) in determining the extent of delocalization onto sulfur is that the form of the equation assumes that the unpaired spin is localized in a

simple 3p orbital on sulfur. It is possible that in order to provide better overlap with copper, or with other nearby atomic centers, the orbital containing the unpaired spin will be partially sp-hybridized. To the extent that admixture of other orbitals on sulfur is involved, the analysis using equation (1) will underestimate the total unpaired spin density on sulfur.

The above considerations lead to the conclusion that the use of equation (1) and the measured methylene proton hyperfine coupling constants for Cu_A to predict the unpaired spin density at the sulfur of a cysteine ligand will, at worst, underestimate the total unpaired spin density localized on sulfur. Therefore, we are led to the solution of equation (1) which estimates at least 25% unpaired spin density in an orbital on sulfur. If, as evidence suggests, there are four different strongly coupled methylene protons interacting with Cu_A, then the total unpaired spin density delocalized away from the copper orbitals is greater than 50%, indicating a very unusual oxidized copper site.

Considerations of the Unpaired Spin Density on Cu_A

The observation of a ^{13}C hyperfine interaction for the cysteine methylene carbon(s) and the determination of at least two (and possibly as many as four) strongly coupled cysteine methylene protons allows us to conclude that there is substantial delocalization of unpaired spin density away from copper and onto one or more cysteine sulfurs. This proposal for the coordination of Cu_A explains many of the unusual spectroscopic features of the site; in particular, the relatively small and isotropic copper hyperfine interaction is now readily explained.

As mentioned previously, Cu_A is spectroscopically unique in several respects. Prominent among these is the unusually small and isotropic nature of the copper hyperfine interaction (1). One simple explanation of this result is that a substantial amount of the

unpaired spin in Cu_A is delocalized onto orbitals away from the copper atom (5,6). This interpretation is consistent with the localization of a substantial amount of unpaired spin on sulfur ligand orbital(s). An alternative explanation for the anomalously small and isotropic copper hyperfine in Cu_A is that the unpaired electron is not in a pure Cu(3d) orbital, but in one which contains a significant amount of Cu(4p) character (1,34). We now examine this latter proposal as it applies to Cu_A and to other copper protein systems.

The Admixture of Cu(4p) Character in Tetrahedral Complexes. Admixture of Cu(4p) orbital character into the Cu(3d) orbitals is often invoked to explain the small copper hyperfine couplings in the blue copper proteins (35,36) and has also been proposed to explain the small couplings in Cu_A (1,34). Admixture of a large amount of 4p character into a 3d orbital whose orbital plane is perpendicular to it can indeed result in an orbital with more spherical shape and therefore a more isotropic interaction with the copper nucleus. Furthermore the contribution from a 4p orbital to the hyperfine coupling with copper is opposite in sign to the contribution from a 3d orbital, resulting in an overall decrease in the measured hyperfine couplings.

Such an admixture of 4p and 3d character can occur in systems of tetrahedral symmetry which require equal overlap with all four ligands. For example, the mixing of 4pz character into the 3dxy orbital has the effect of pointing the lobes of the 3dxy orbital out of the plane towards the corners of a tetrahedron and increasing the angle between any two lobes. The same reasoning can explain admixture of the 4px and 4py orbitals with the 3dyz and 3dxz orbitals, respectively. Thus, for tetrahedral centers, such as the copper in Cs_2CuCl_4, redirection of the orbital lobes results in better overlap between the metal 3d orbital and the four ligand orbitals so that the energy cost of mixing in the higher lying 4p orbital is offset by improved interactions with the ligands. In tetrahedral symmetry,

hybridization is necessary to optimize equal overlap with all four equivalent ligand orbitals.

In many cases, however, a so-called tetrahedral Cu(II) complex may have different ligand types with different ligand field strengths, so that interaction with one ligand type is more energetically favored. Thus, although the copper hyperfine coupling in the tetrahedral complex Cs_2CuCl_4 is quite small (25×10^{-4} cm^{-1}), indicating significant admixture of 4pz character into the 3dxy orbital, the hyperfine coupling in $Cu(phen)Cl_2$ (CuN_2Cl_2), which also has a tetrahedral geometry, is 123×10^{-4} cm^{-1} (37,38). In this case, owing to the very different ligand character of the phenanthroline nitrogen and Cl^-, equal overlap with all four ligands is not energetically preferred. This result illustrates the argument that admixture of 4pz character into the 3dxy orbital is less favorable for tetrahedral (geometry) coordination in mixed ligand complexes. The argument becomes still stronger as the ligand coordination is moved towards a flattened tetrahedral geometry. In this case, the smaller ligand-metal-ligand angles become less than 109^o, approaching the 90^o angle found between the lobes of a pure 3dxy orbital. Considering that for Cu(II) the $3d^84p$ configuration lies about 125,000 cm^{-1} above the $3d^9$ configuration (39), the energy benefit of improved orbital overlap must be substantial before significant 4pz admixture can lower the overall energy of the system. These results show that in tetrahedral copper coordination complexes with mixed ligand types, admixture of 4p character into the 3d orbitals may not always be invoked to explain a decreased copper hyperfine interaction.

The Extent of Cu(4p) Admixture in Cu_A. The coordination symmetry of Cu_A (and of the blue coppers as well) is certainly not tetrahedral. Even if the coordination at these sites were roughly tetrahedral in geometry, the true symmetry at the copper is not tetrahedral and equal overlap with all four ligands is not necessarily desired. For example, assuming that Cu_A is coordinated by two

cysteine sulfurs and one or two histidine imidazole (or other) nitrogens in a flattened tetrahedral geometry, a copper orbital such as 3dxy would achieve stabilizing orbital overlap with the two sulfur sigma orbitals with very little 4pz admixture. This would of course be at the expense of poor overlap with nitrogen sigma orbitals; however, imidazole nitrogen σ-orbitals are relatively hard and thus do not stabilize Cu(II) as well as the more soft sulfur ligand orbitals. In fact, for a histidyl ligand with its imidazole ring plane oriented perpendicular to the S-Cu-S (and therefore 3dxy) plane, overlap between the empty imidazole π^* orbital and the copper 3dxy orbital is favorable, resulting in a stabilizing back-bonding interaction. The relatively weak nitrogen hyperfine measured in this work confirms that the interaction of the imidazole ring nitrogen with the orbital containing the unpaired electron is small.

Owing to the non-tetrahedral symmetry of the Cu_A site and the large energy cost of Cu(4p) admixture, it is likely that the small and isotropic nature of the copper hyperfine interaction in Cu_A arises not from Cu(4p) orbital admixture, but rather from extensive delocalization of unpaired spin from copper onto associated cysteine sulfur ligand(s).

A MODEL FOR THE STRUCTURE OF Cu_A

The positive identification of one histidine and at least one, and very likely two, cysteine ligands to Cu_A is a significant step forward in the understanding of the structure of the Cu_A center in cytochrome oxidase. The coordination of a second cysteine ligand to copper would make Cu_A unique among known metalloproteins. The unusual nature of this metal active site, both structurally and spectroscopically, and its importance in the functioning of cytochrome oxidase, make the understanding of the physical and electronic structures of this site a necessary prerequisite to understanding cytochrome oxidase as a whole.

The Proposed Physical Structure

In order to aid the understanding of the interactions between copper and its ligands in Cu_A, we present in Fig. 17 a possible structure for the Cu_A site. In this model, the copper is coordinated by two cysteine sulfurs and two histidine nitrogens. Superimposed on the structure shown in Fig. 17 is the coordinate axis system used to discuss the involved atomic orbitals on copper and its ligands. We have placed the z-axis along the bisector between the two sulfur atoms and the x-axis in the S-Cu-S plane in order to conform with the conventions used in group character tables. The coordination geometry is assumed to be approximately tetrahedral.

The Proposed Electronic Structure

In the most simple crystal field limit, the symmetry of the center shown in Fig. 17 is tetrahedral, and the initial orbital energy ordering is as shown in Fig. 18. However inequivalence of the four ligands reduces the site symmetry. Assuming two equivalent nitrogen

Figure 17

Structural model for copper coordination by two cysteine sulfurs and two histidine nitrogens showing the coordinate axis system used in the text.

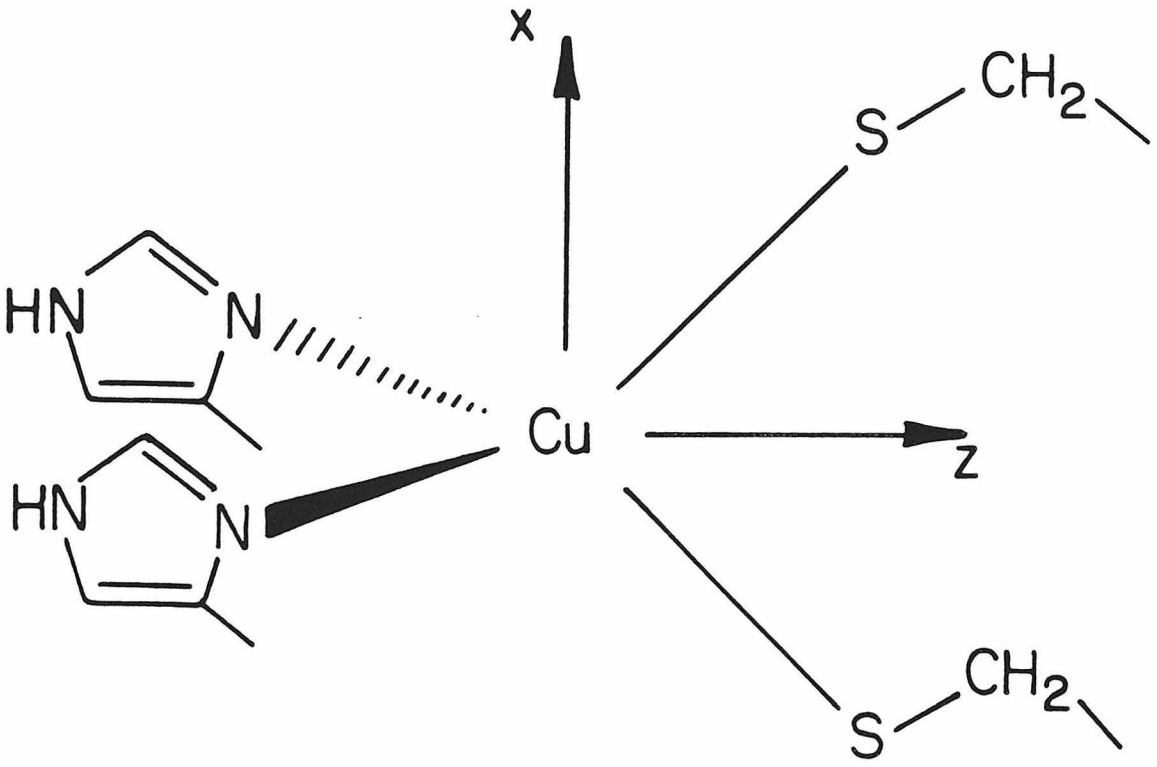
X
CH2
S
HN
N
Cu
Z
HN
N
CH2
S

Figure 18

Orbital energy diagram for the proposed Cu_A model site presented in the text. For comparison, the orbital energies of a typical blue copper center (36) are also shown.

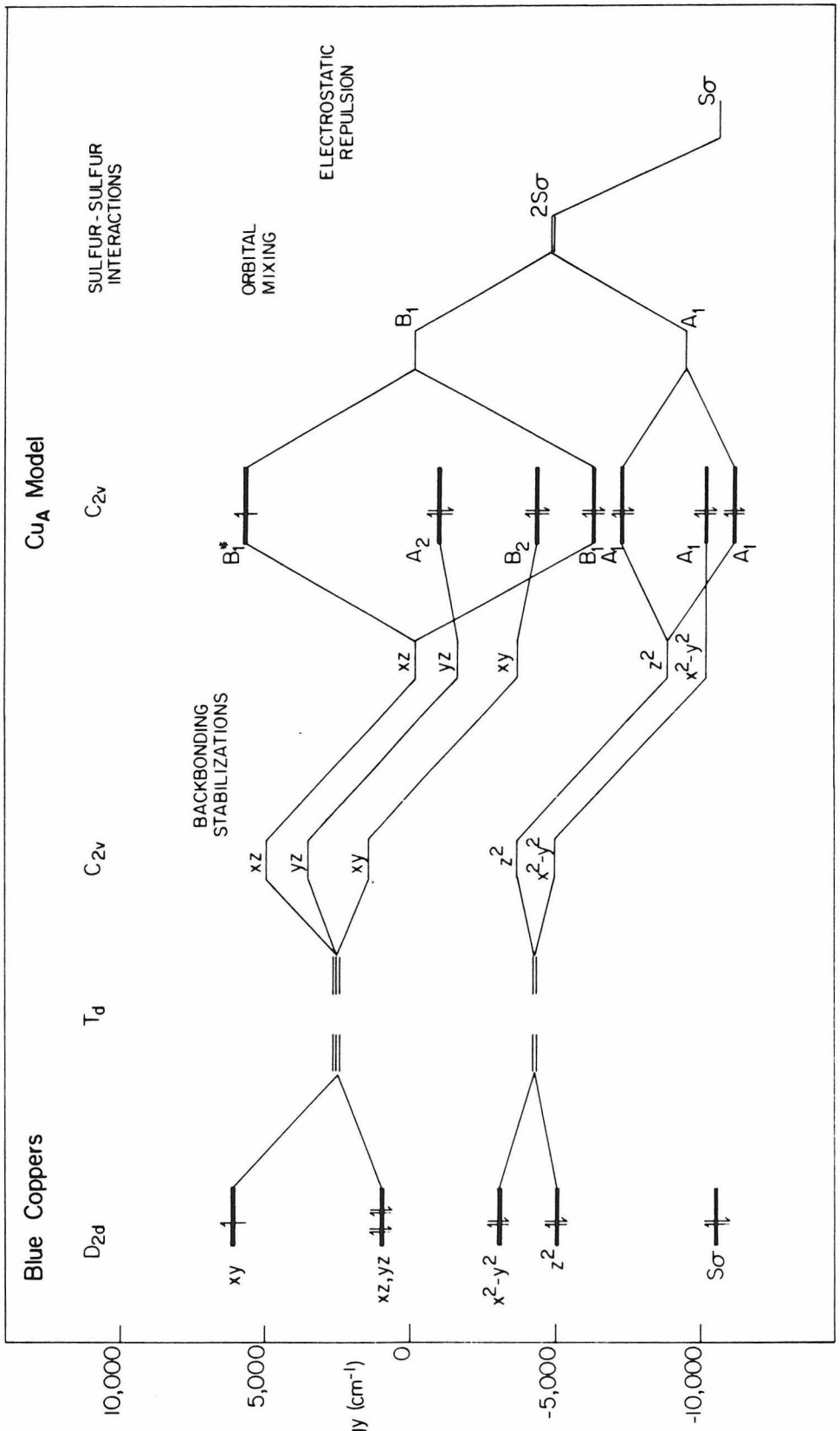
Blue Coppers
Cu_A Model
D_{2d}
T_d
C_{2v}
C_{2v}
SULFUR-SULFUR INTERACTIONS
ORBITAL MIXING
ELECTROSTATIC REPULSION
BACKBONDING STABILIZATIONS
xy
xz,yz
x^2-y^2
z^2
Sσ
xz
yz
xy
z^2
x^2-y^2
B_1^*
A_2
B_2
B_1
A_1
B_1
A_1
A_1
A_1
2Sσ
Sσ
Energy (cm^{-1})
10,000
5,000
0
-5,000
-10,000

ligands and two equivalent sulfurs coordinated in an approximately tetrahedral geometry, the symmetry of the center becomes C_{2v}. The 3dxz (B_1) orbital on copper overlaps directly with the thiolate sulfur orbitals and is raised in energy. The ligand field strength of the thiolate ligand has been estimated to be moderately strong (40), so that the 3dxz orbital on copper will be raised in energy the most by this coordination. The 3dxz orbital will be the highest lying copper 3d orbital and therefore will contain the unpaired electron. Note that due to a different choice of axes, the highest occupied orbital in the blue coppers is typically referred to as 3dxy (36). The degeneracies of the remaining orbitals will be lifted by the reduction in symmetry as shown qualitatively in Fig. 18. However, before discussing the effects of this coordination on the other orbitals of copper it is instructive to examine the electronic features of the two sulfur centers and their interactions with copper.

In addition to the straightforward interaction of the sulfur (sigma) atomic orbitals with the 3dxz orbital on copper, the resulting site symmetry allows <u>direct</u> interaction between the two sulfur atoms. As shown at the far right in Fig. 18, electrostatic repulsion between the two (charged) thiolate sulfur atoms will raise the orbital energies of each. Assuming a S-Cu-S angle of 90° and S-Cu separations of 2.2 Å (consistent with available EXAFS data for Cu_A (41)), the disulfide separation will be 3.1 Å. To a first approximation, we can estimate the energy of the coulombic repulsion as that of two point charges in a medium of dielectric 10, separated by 3.1 Å. Examining the interaction between the sulfurs more closely, however, we see that the lone pair sigma orbitals on each sulfur center can combine to form the symmetric A_1 and antisymmetric B_1 symmetry orbitals, as shown in Fig. 19. These orbitals will be different in energy, the symmetric A_1 ligand orbital being lower in energy relative to the B_1 ligand orbital. To provide an approximate estimate of the energy difference between the A_1 and B_1 ligand orbitals, we note that the bond strength of the S-S bond in cystine is 50 kcal/mole (42) at a bond distance of

Figure 19

Representation of the molecular orbitals originating from the direct interaction between two sulfur ligands to Cu_A.

$S(3p_z)$

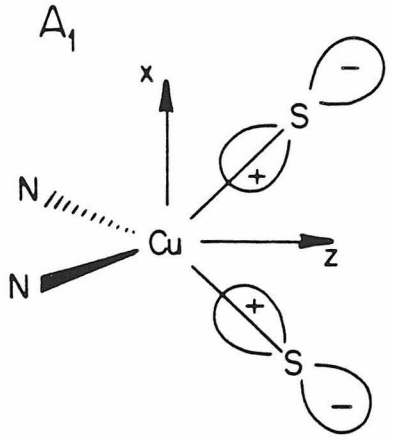

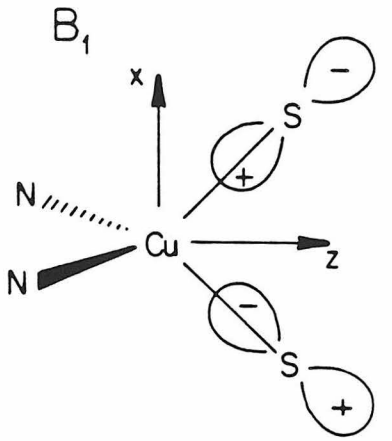

$S(3d_{yz})$

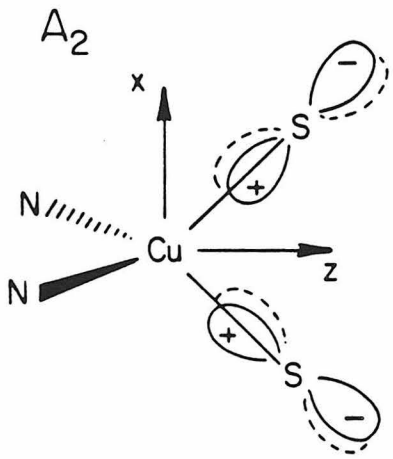

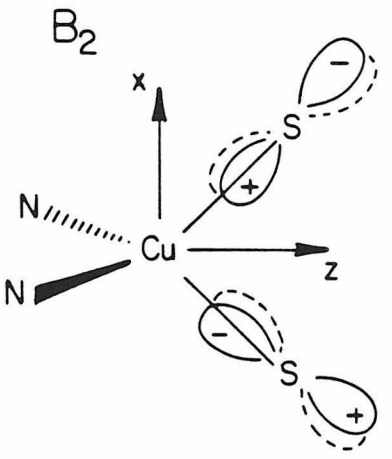

$S(3d_{xz})$

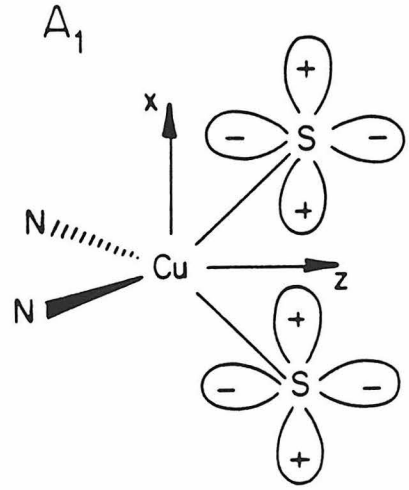

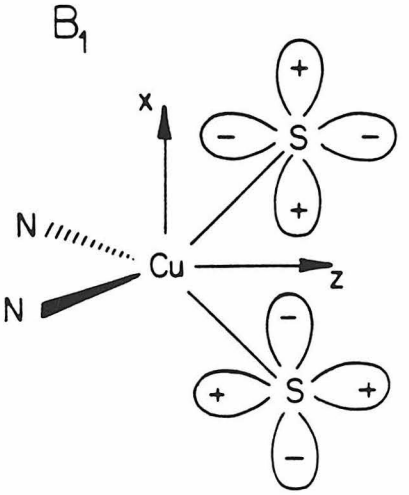

2.04 Å (43). As the equilibrium bond length drops from 2.04 Å, the magnitude of this interaction will also drop; however, the sulfur valence orbitals are rather diffuse and should allow significant overlap at the distance proposed here. We assume for this model that the bonding interaction between the individual sulfur sigma orbitals is half that found in cystine. The electronic effects presented here serve to raise the B_1 ligand orbital energy well above that of the sulfur sigma orbital found in the mono-cysteine blue copper centers, allowing the B_1 orbital energy to approach more closely the energies of the Cu 3d orbitals.

The symmetry of the B_1 sulfur ligand orbital allows it to mix effectively with the Cu(3dxz) orbital to form a bonding (with respect to copper and sulfur) B_1 and an anti-bonding B_1^* orbital. It is this new B_1^* orbital in which the unpaired electron finally resides in this model for Cu_A. The extent to which the sulfur B_1 orbital is raised in energy by the mechanisms discussed above will affect the relative contributions of the sulfur B_1 and copper 3dxz orbitals to the resulting B_1^* molecular orbital. Similarly, depending on the extent to which the copper 3d orbitals (specifically the 3dxz orbital) are lowered in energy by backbonding interactions (see below), the B_1^* molecular orbital will have substantial sulfur radical character.

The molecular orbital energy diagram shown in Fig. 18 illustrates several other stabilizing interactions between copper and its ligands. These interactions are difficult to estimate quantitatively and we will merely point out the qualitative features of this model. First, the unoccupied 3d orbitals of sulfur can combine as shown in Fig. 19 to yield unoccupied ligand molecular orbitals. These ligand orbitals can overlap with the occupied 3dxy and 3dyz orbitals on copper to delocalize charge (but not unpaired spin) onto the relatively soft sulfur ligands. This backbonding interaction not only lowers the energy of the copper 3dxy and 3dyz orbitals specifically, but also lowers the interelectronic repulsion (and therefore orbital energies) of the entire copper 3d shell. The relatively hard (filled) imidazole

nitrogen sigma lone pair destabilizes the Cu(3dyz) orbital with which it overlaps, offsetting somewhat the energy stabilization that the 3dyz orbital gains from backbonding to the empty sulfur 3d orbitals. The unoccupied imidazole π^* orbital, however, can interact with the Cu(3dxz) orbital, to allow a stabilizing back-bonding interaction and to propagate some unpaired spin into the imidazole π^* orbital.

The main features of this model for the Cu_A site in cytochrome oxidase are the raising in energy of the sulfur ligand orbitals and a concomitant lowering in energy of the Cu 3d atomic orbitals relative to a mono-thiolate copper center such as is found in the blue coppers. This allows more complete mixing of the sulfur orbitals with the copper 3d orbital containing the unpaired electron. The end result of these interactions is an oxidized copper center with substantial Cu(I)-sulfur radical character.

Analysis of Spectroscopic Data with Respect to the Proposed Model

With this new model for the Cu_A site, we are now in a position to explain many of the unusual spectroscopic features associated with this unique site.

Nitrogen Hyperfine Coupling. In this model the interaction of an imidazole ligand to Cu_A with the (3dxz) orbital containing the unpaired electron on copper is dominated by π-type overlap, rather than the conventional sigma interaction. This overlap will allow for the propagation of some unpaired spin density onto the imidazole ligand. However, since this unpaired spin density is primarily in a π^*-type orbital of the imidazole ring and the electron spin is further delocalized out of the Cu(3dxz) orbital onto the sulfur ligands, hyperfine coupling between the unpaired electron spin and the imidazole nitrogen nucleus is expected to be weak relative to systems in which sigma bonding to the Cu(3dxz) orbital is involved. As the ENDOR results have shown, the measured hyperfine coupling to the

proximal imidazole ring nitrogen is indeed weak relative to that seen in other copper proteins. This is also confirmed by the nuclear modulation of electron spin echo data for Cu_A (44) which show an unusually shallow ^{14}N modulation, indicating a very weak hyperfine interaction. This is atypical of imidazole coordination in Cu(II) centers, which generally shows a deep ^{14}N modulation pattern from interaction with the distal imidazole ring nitrogen (45,46).

Copper Hyperfine Couplings. As discussed in the preceding section, Cu_A is characterized by a small and isotropic copper hyperfine interaction which cannot be fully explained by the admixture of Cu(4p) orbital character. In the current model, the molecular orbital containing the unpaired spin has substantial contributions from a Cu(I)-cysteine disulfide anion radical. Hence the unusually small and isotropic copper hyperfine observed for Cu_A is explained by the delocalization of unpaired spin onto the two sulfurs. Not only is unpaired spin density moved away from the copper nucleus (decreasing the hyperfine interaction), but it is no longer in a pure Cu(3dxz) orbital, so that its interaction with the copper nucleus is less anisotropic than if it were constrained to that orbital.

EPR g-values. The unusual high-field g-value of 1.99 for Cu_A (3) can also be explained simply by this model. As discussed previously (14), to obtain a g-value less than the free electron g-value of 2.0023, the molecular orbital containing the unpaired spin must possess a contribution from an atomic orbital with a spin-orbit coupling constant opposite to that of the copper $3d^9$ system. Sulfur orbitals meet this requirement. Although the exact g-values will depend strongly on the nature of the composite molecular orbital, it is interesting to note that the g-values for Cu_A (1.99, 2.04, and 2.18) are quite similar to those (1.99, 2.01, and 2.21) for a neutral cysteine disulfide radical produced by UV irradiation of cysteine (30,31).

X-ray Absorption Edge Studies. The x-ray absorption edge data for oxidized Cu_A indicates that the copper is either Cu(I) or a very covalent Cu(II) (4). In the above model, Cu_A is both very covalent and has a high degree of Cu(I) character. Upon reduction, the added electron goes into the B_1^* orbital which contains significant sulfur radical character. That is, the formal oxidation state of the copper remains close to +1 in both the reduced and oxidized forms of the center. This explains the observed result of the x-ray edge study which shows very little shift in the position of the edge upon reduction of the site - the copper is already partially "reduced" in the oxidized state.

Linear Electric Field Effect Studies. The linear electric field effect (LEFE) data for Cu_A (44) also confirm the unusual nature of the coordination at Cu_A. This technique measures the shift in g-value of an EPR resonance in the presence of an applied electric field (47). The form of the observed shift is very sensitive to the symmetry (not just geometry) at the site. The results for Cu_A (44) are quite unlike those found in Type I or Type II Cu(II) complexes (48). The shape, in particular, is unlike that of any copper complex yet studied, and the magnitude of the shift is smaller than that observed for the blue copper centers. Mims and Peisach (44) conclude that the ligand field at Cu_A is not tetrahedral and that it differs radically from that of the square planar (Type II) coppers and the blue coppers. The coordination of a second cysteine sulfur and, in particular, the delocalization of substantial spin density onto the two cysteine sulfurs represent a radical change from the copper centered paramagnetic site which exists in the mono-cysteine sulfur coordinated blue coppers.

Magnetic Circular Dichroism Studies. The magnetic circular dichroism (MCD) spectrum of Cu_A shows a relatively intense negative

MCD band centered at about 785 nm (49,50) which corresponds to the 830 nm optical absorbance. The 830 nm optical transition in Cu_A has been compared to the 600 nm transition of the blue coppers. However, the strength of the MCD band near 800 nm in Cu_A ($\Delta\varepsilon = -2.5\ M^{-1}\ cm^{-1}\ T^{-1}$) is 5 to 10 times stronger than the MCD band associated with the 600 nm absorbance of blue copper centers (51).

Noting the slight blue shift of the Cu_A MCD band at 785 nm relative to the absorption at 830 nm, we are prompted to look for a B-type MCD partner at lower energy. Analysis of near-IR MCD data for reductive titrations of oxidized cytochrome oxidase reveals a positive band at 1550 nm ($\Delta\varepsilon = +0.9\ M^{-1}\ cm^{-1}\ T^{-1}$) which disappears in parallel with the negative MCD band near 800 nm. Results from reductive titrations of cyanide-inhibited oxidized cytochrome oxidase have been used to associate this band with the cytochrome $\underline{a}_3$ center (49). It has been claimed that the single band at 1550 nm in these spectra merely shifts to slightly lower wavelength during the titration. In this interpretation, the band at 1550 nm is assigned wholly to the cytochrome $\underline{a}_3$ center, in both the native oxidized protein and in the cyanide-inhibited mixed-valence species. No explanation is offered as to why the band should occur at approximately the same energy in both the low-spin (oxidized) cytochrome $\underline{a}_3$-CN species and in the native oxidized cytochrome $\underline{a}_3$ (presumably high-spin (52,53)) species. Careful analysis of the MCD results reveals that, in the fully oxidized cyanide-inhibited complex, a <u>new</u> band occurs at slightly lower wavelength, overlapping the original MCD band at 1550 nm. This is evident from the increased intensity in this region upon cyanide binding. We assign this new band to the cytochrome $\underline{a}_3$-CN species and the original band at 1550 nm to oxidized Cu_A. In the fully oxidized mixed-valence state the two bands are not resolved, so that, as the band at 1550 nm disappears during the reductive titration, the composite band <u>appears</u> to shift to lower wavelength.

The assignment of a new MCD band associated with Cu_A can now be interpreted in terms of the above molecular orbital model for the Cu_A site. This new band may well be the positive partner of the negative band near 800 nm in a B-type MCD transition. Note that, to first-order, B-type MCD transition intensities are inversely proportional to the energy separation between the excited states and nearby excited states with which they can be mixed by the magnetic field (54,55). In addition, the states must be of the appropriate symmetry to be mixed by the angular momentum operator of the magnetic field interaction. The fact that no band has been assigned in MCD spectra of the blue coppers which is an obvious partner to the charge transfer band at 600 nm implies that the corresponding partner is far separated in energy from the band near 600 nm and/or is poorly mixed by the magnetic field.

The state diagram shown in Fig. 20 compares the excited state energies of a typical blue copper center with a qualitative state diagram for the current model of Cu_A (taken from the orbital energy diagram presented in Fig. 18). The cysteine sulfur ligand to metal charge transfer band ($S\sigma \leftarrow B_2$) characteristic of blue coppers can be compared with the 830 nm (in this case $B_1 \leftarrow B_1$) transition of Cu_A. Two major differences are apparent which may account for the very different MCD results discussed above. First, both the ground B_1 and the excited B_1 states for Cu_A are mixtures of ligand and metal orbitals. The fact that the excited state contains some Cu(3dxz) character allows it to be mixed with the other metal 3d orbitals by an external magnetic field. The L_x and L_z operators can mix 3dxz with 3dxy and 3dyz, respectively, while the L_y operator can mix 3dxz with both $3dx^2-y^2$ and $3dz^2$. Therefore a magnetic field will mix the excited state B_1 with the nearby A_1, B_2, and A_2 states. The state diagram shown in Fig. 20 predicts that the MCD transition at 1550 nm (6450 cm^{-1}) could be either the $A_2 \leftarrow B_1$ or $B_2 \leftarrow B_1$ transition.

In addition, the extent of mixing between two states is inversely proportional to energy separation between them. Since the lowering of

Figure 20

A state diagram comparing the energies of the ground and excited states for the blue coppers and for the model for Cu_A proposed in the text. The blue copper state energy levels are taken from (36); those of the model are taken from the orbital energy diagram shown in Fig. 18.

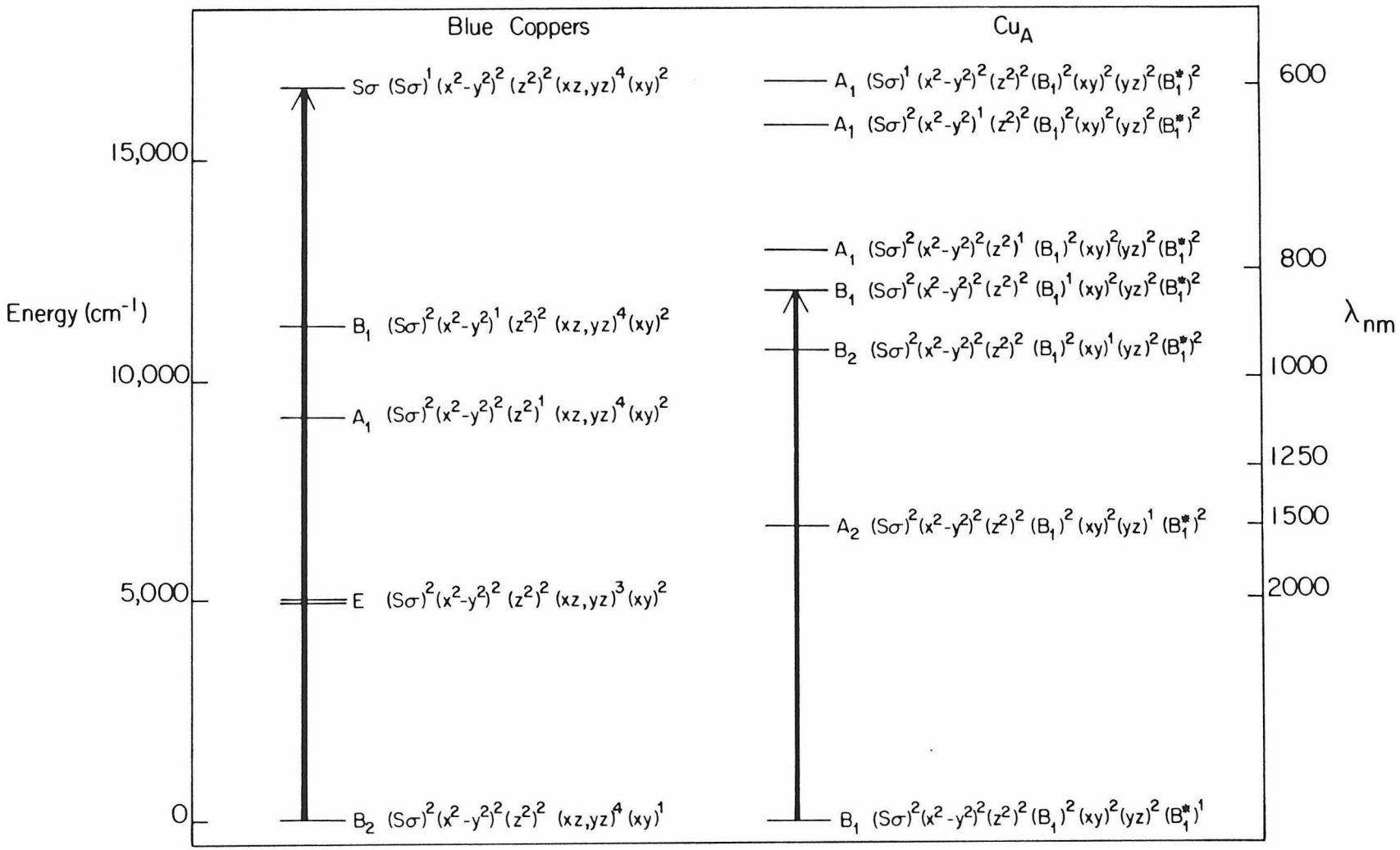
Blue Coppers
Cu$_A$
Energy (cm^{-1})
15,000
10,000
5,000
0
600
800
1000
1250
1500
2000
λ_{nm}
$S\sigma$ $(S\sigma)^1(x^2-y^2)^2(z^2)^2(xz,yz)^4(xy)^2$
B_1 $(S\sigma)^2(x^2-y^2)^1(z^2)^2(xz,yz)^4(xy)^2$
A_1 $(S\sigma)^2(x^2-y^2)^2(z^2)^1(xz,yz)^4(xy)^2$
E $(S\sigma)^2(x^2-y^2)^2(z^2)^2(xz,yz)^3(xy)^2$
B_2 $(S\sigma)^2(x^2-y^2)^2(z^2)^2(xz,yz)^4(xy)^1$
A_1 $(S\sigma)^1(x^2-y^2)^2(z^2)^2(B_1)^2(xy)^2(yz)^2(B_1^*)^2$
A_1 $(S\sigma)^2(x^2-y^2)^1(z^2)^2(B_1)^2(xy)^2(yz)^2(B_1^*)^2$
A_1 $(S\sigma)^2(x^2-y^2)^2(z^2)^1(B_1)^2(xy)^2(yz)^2(B_1^*)^2$
B_1 $(S\sigma)^2(x^2-y^2)^2(z^2)^2(B_1)^1(xy)^2(yz)^2(B_1^*)^2$
B_2 $(S\sigma)^2(x^2-y^2)^2(z^2)^2(B_1)^2(xy)^1(yz)^2(B_1^*)^2$
A_2 $(S\sigma)^2(x^2-y^2)^2(z^2)^2(B_1)^2(xy)^2(yz)^1(B_1^*)^2$
B_1 $(S\sigma)^2(x^2-y^2)^2(z^2)^2(B_1)^2(xy)^2(yz)^2(B_1^*)^1$

the energy of the B_1 excited state discussed above brings this state closer in energy to the states with which it can be mixed, the magnitude of the MCD signal for this transition will be still greater. In the case of the blue coppers, the excited state is more purely ligand-based and further removed in energy from the copper 3d orbitals, so that the magnetic field will not efficiently mix the excited state with the copper orbitals. These considerations satisfactorily explain the anomalous nature of the MCD spectrum for Cu_A.

CONCLUSION

The successful incorporation of isotopically substituted amino acids into yeast cytochrome oxidase has allowed us to unambiguously identify ligands to the Cu_A site in cytochrome oxidase. The ENDOR studies of the [^{15}N]His-substituted protein prove conclusively the coordination of a histidine ring nitrogen to Cu_A. Similar studies of the [^{2}H]Cys- and [^{13}C]Cys-substituted proteins conclusively identify at least one cysteine ligand to Cu_A, and the identification of a new ENDOR resonance from a third strongly coupled cysteine methylene proton in the beef heart protein is good evidence that Cu_A has, in fact, <u>two</u> cysteine sulfur ligands. The strength of these proton hyperfine couplings indicates that the unpaired spin in the oxidized Cu_A center is extensively delocalized away from copper and onto the cysteine sulfurs. The coordination of two cysteine sulfurs to copper and the resulting electronic distribution at the site make Cu_A center unique among copper proteins.

The determination of an unusual coordination environment for Cu_A allows us to explain many of the spectroscopic properties of the center, and we have developed a model for the site to aid in the interpretation of these data. The unique feature of this model is the strong interaction of two thiolate sulfur ligands with copper which, in the oxidized form of the center, allows a significant delocalization of unpaired spin density away from copper and into an antibonding sigma orbital between the two sulfurs. The oxidized Cu_A center in this model possesses substantial sulfur radical-Cu(I) character.

REFERENCES

1. Hoffman, B. M., Roberts, J. E., Swanson, M., Speck, S. H., and Margoliash, E. (1980) Proc. Natl. Acad. Sci., U.S.A. 77, 1452-1456.

2. Beinert, H., Griffiths, D. E., Wharton, D. C., and Sands, R. H. (1962) J. Biol. Chem. 237, 2337-2346.

3. Aasa, R., Albracht, S. P. J., Falk, K., Lanne, B., and Vanngard, T. (1976) Biochim. Biophys. Acta 422, 260-272.

4. Hu, V. W., and Chan, S. I. (1977) FEBS Lett. 84, 287-290.

5. Chan, S. I., Bocian, D. F., Brudvig, G. W., Morse, R. H., and Stevens, T. H. (1979) in Cytochrome Oxidase, King, T. E., Orii, Y., Chance, B., and Okunuki, K., eds., Elsevier/North Holland Biomedical Press, Amsterdam, 177-188.

6. Peisach, J., and Blumberg, W. E. (1974) Arch. Biochem. Biophys. 165, 691-708.

7. Blair, D. F., Martin, C. T., Gelles, J., Wang, H., Brudvig, G. W., Stevens, T. H., and Chan, S. I. (1983) Chemica Scripta 21, 43-53.

8. Solomon, E. I., Hare, J. W., and Gray, H. B. (1976) Proc. Natl. Acad. Sci., U.S.A. 73, 1389-1393.

9. Gray, H. B., and Malmstrom, B. G. (1983) Comments Inorg. Chem. 2, 203-209.

10. Roberts, J. E., Cline, J. F., Lum, V., Gray, H. B., Freeman, H., Peisach, J., Reinhammar, B., and Hoffman, B. M. (1984) J. Am. Chem. Soc., in press.

11. Van Camp, H. L., Wei, Y. H., Scholes, C. P., and King, T. E. (1978) Biochim. Biophys. Acta 537, 238-246.

12. Roberts, J. E., Brown, T. G., Hoffman, B. M., and Peisach, J. (1980) J. Am. Chem. Soc. 102, 825-829.

13. Stevens, T. H., and Chan, S. I. (1981) J. Biol. Chem. 256, 1069-1071.

14. Stevens, T. H., Martin, C. T., Wang, H., Brudvig, G. W., Scholes, C. P., and Chan, S. I. (1982) J. Biol. Chem. 257, 12106-12113.

15. Cruz-Halos, S. (1975) Ph.D. Thesis, University of California, Berkeley.

16. Sherman, F., Fink, G. R., and Lawrence, C. W. (1974) Methods in Yeast Genetics, Cold Spring Harbor Laboratory, New York.

17. Stevens, T. H. (1981) Ph.D. Thesis, California Institute of Technology, Pasadena.

18. George-Nascimento, C., and Poyton, R. O. (1981) J. Biol. Chem. 256, 9363-9370.

19. Yu, C., Yu, L., and King, T. E. (1975) J. Biol. Chem. 250, 1383-1392.

20. Hartzell, C. R., and Beinert, H. (1974) Biochim. Biophys. Acta 368, 318-338.

21. Pake, G. E., and Estle, T. L. (1973) The Physical Principles of Electron Paramagnetic Resonance, 2nd Ed., W. A. Benjamin, Inc., Reading.

22. Thomann, H., Dalton, L. R., and Pancake, C. (1984) Rev. Sci. Instrum. 55, 389-395.

23. Mims, W. B., Peisach, J., and Davis, J. L. (1977) J. Chem. Phys. 66, 5536-5550.

24. Van Ormondt, D., and Nederveen, K. (1981) Chem. Phys. Lett. 82, 443-446.

25. Narayana, M., and Kevan, L. (1983) Magn. Reson. Rev. 7, 239-242.

26. Whiffen, D. H. (1966) Mol. Physics 10, 595-596.

27. Van Camp, H., Sands, R. H., and Fee, J. A. (1981) J. Chem. Phys. 75, 2098-2107.

28. Brudvig, G. W., Stevens, T. H., Morse, R. H., and Chan, S. I. (1981) Biochemistry 20, 3912-3921.

29. Carrington, A., and McLachlan, A. D. (1967) Introduction to Magnetic Resonance, Chapman and Hall, New York.

30. Gordy, W. (1980) Theory and Applications of Electron Spin Resonance, John Wiley and Sons, New York.

31. Hadley, J. H., and Gordy, W. (1974) Proc. Natl. Acad. Sci., U.S.A. 71, 4409-4413.

32. Atherton, N. M. (1973) Electron Spin Resonance: Theory and Applications, John Wiley and Sons, New York.

33. Fessenden, R. W., and Schuler, R. H. (1965) J. Chem. Phys. 43, 2704-2712.

34. Greenaway, F. T., Chan, S. H. P., and Vincow, G. (1977) Biochim. Biophys. Acta 490, 62-78.

35. Brill, A. S., and Bryce, G. F. (1968) J. Chem. Phys. 48, 4398-4404.

36. Gray, H. B., and Solomon, E. I. (1981) in Metal Ions in Biology, Vol. 3, Spiro, T. G., ed., John Wiley and Sons, 1-39.

37. Sharnoff, M. (1965) J. Chem. Phys. 42, 3383-3395.

38. Kokoszka, G. F., Reimann, C. W., and Allen, H. C. J. (1967) J. Phys. Chem. 71, 121-126.

39. Hu, V. W., Chan, S. I., and Brown, G. S. (1977) Proc. Natl. Acad. Sci., U.S.A. 74, 3821-3825.

40. Blinn, E. L., Butler, K. M., Chapman, K. M., and Harris, S. (1977) Inorg. Chim. Acta 24, 139-143.

41. Scott, R. A., Cramer, S. P., Shaw, R. W., Beinert, H., and Gray, H. B. (1981) Proc. Natl. Acad. Sci., U.S.A. 78, 664-667.

42. Pauling, L. (1960) The Nature of the Chemical Bond, 3rd Edition, Cornell University Press.

43. Jones, D. D., Bernal, I., Frey, M. N., and Koetzle, T. F. (1974) Acta Cryst. B30, 1220-1227.

44. Mims, W. B., Peisach, J., Shaw, R. W., and Beinert, H. (1980) J. Biol. Chem. 255, 6843-6846.

45. Mims, W. B., and Peisach, J. (1978) J. Chem. Phys. 69, 4921-4930.

46. Mims, W. B., and Peisach, J. (1979) J. Biol. Chem. 254, 4321-4323.

47. Mims, W. B. (1976) in The Linear Electric Field Effect in Paramagnetic Resonance, Clarendon Press, Oxford.

48. Peisach, J., and Mims, W. B. (1978) Eur. J. Biochem. 84, 207-214.

49. Eglinton, D. G., Johnson, M. K., Thomson, A. J., Gooding, P. E., and Greenwood, C. (1980) Biochem. J. 191, 319-331.

50. Greenwood, C., Hill, B. C., Barber, D., Eglinton, D. G., and Thomson, A. J. (1983) Biochem. J. 215, 303-316.

51. Dooley, D. M., Rawlings, J., Dawson, J. H., Stephens, P. J., Andreasson, L., Malmstrom, B. G., and Gray, H. B. (1979) J. Am. Chem. Soc. 101, 5038-5046.

52. Babcock, G. T., Vickery, L. E., and Palmer, G. (1976) J. Biol. Chem. 251, 7907-7919.

53. Thomson, A. J., Brittain, T., Greenwood, C., and Springall, J. (1976) FEBS Lett. 67, 94-98.

54. Vallee, B. L., and Holmquist, B. (1980) Adv. Inorg. Biochem. 2, 27-74.

55. Stephens, P. J. (1976) Adv. Chem. Phys. 35, 197-264.

CHAPTER III

THE STRUCTURE OF CYTOCHROME a

INTRODUCTION

Cytochrome a is generally thought to be the primary acceptor of electrons from cytochrome c, acting as a one-electron mediator between cytochrome c and the other metal centers within cytochrome oxidase (1,2). Consistent with this function, the mid-point potential of cytochrome a is quite similar to that of cytochrome c (3,4), thereby allowing for a small loss in the total available redox energy at this first electron transfer. From cytochrome a, each electron is transferred to dioxygen coordinated at the oxygen binding site. The electrons are generally assumed to be transferred to the oxygen binding site via Cu_A, although recent evidence suggests that cytochrome a may also transfer electrons directly to the oxygen binding site (5). As discussed in chapter I of this thesis, the potential difference between cytochrome c and dioxygen is quite substantial (42 kcal per mole oxygen reduced), and it has been shown that cytochrome oxidase converts some of this potential energy into an electrochemical proton gradient across the mitochondrial inner membrane (6).

Cytochrome a has been proposed to be directly involved in proton pumping, coupling the electron transfer events at the site to the translocation of protons across the mitochondrial membrane (7). However, almost nothing is currently known about the mechanisms of electron transfer or, in particular, proton pumping in cytochrome oxidase. It is clear that a knowledge of the structures of the involved metal centers will be necessary before a complete understanding of both electron transfer and proton pumping can be achieved.

The cytochrome a site is known to consist of a low-spin iron coordinated by four in-plane nitrogen ligands from a heme a macrocycle, as shown in Fig. 1. No direct evidence exists as to the identity of the (endogenous) axial ligands, except that they do not exchange with exogenous ligands. Blumberg and Peisach (8) have

Figure 1

The heme a macrocycle found in cytochrome oxidase.

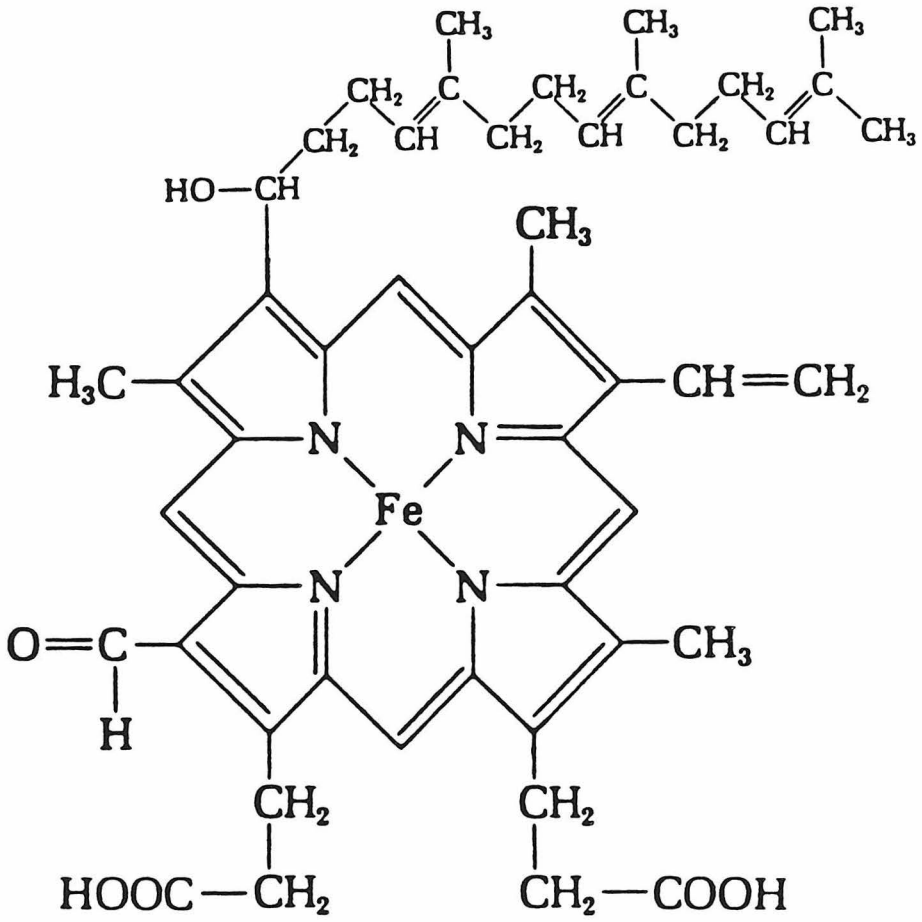
CH3
CH3
CH3
CH2
C
CH2
C
CH2
C
CH2
CH
CH2
CH
CH2
CH
CH3
HO—CH
CH3
H3C
CH=CH2
N
N
Fe
N
N
O=C
H
CH3
CH2
CH2
HOOC—CH2
CH2—COOH

compared the electron paramagnetic resonance (EPR) spectral g-values of a large variety of low-spin heme complexes, and on the basis of these comparisons have argued for bis-imidazole coordination in cytochrome a. Similar comparisons with optical and resonance Raman spectroscopies (9), and magnetic circular dichroism (MCD) spectroscopies (10,11) have led investigators to the same conclusion. However, none of these studies provides direct information on the axial ligands to cytochrome a, and other results have in fact shown that all of the spectral properties of cytochrome a site may not be satisfactorily simulated by model compounds (12,13). To date no definitive evidence for either mono- or bis-imidazole coordination of cytochrome a has been produced.

In this chapter, we have exploited the unique capabilities of electron nuclear double resonance (ENDOR) spectroscopy and the specific incorporation of isotopically substituted amino acids into the protein in order to identify axial ligands to cytochrome a. We present ENDOR studies of native and [1,3-$^{15}N_2$]histidine substituted yeast cytochrome oxidase which demonstrate conclusively the coordination of at least one histidine ligand to cytochrome a in cytochrome oxidase. Comparison of the observed ^{14}N and ^{15}N hyperfine couplings with those from various mono- and bis-imidazole porphyrin model compounds presents strong evidence for the coordination of a second histidine imidazole as well.

MATERIALS AND METHODS

All chemicals used in the enzyme purification were of enzyme grade when available; otherwise they were reagent grade. All the chemicals used in the growth of yeast such as vitamins, amino acids, and galactose were the highest grades available from Sigma. The [1,3-$^{15}N_2$]histidine·HCl was 95% enriched in ^{15}N at both histidine ring positions and was obtained from Veb Berlin-Chemie, Berlin-Adlershof. The percent enrichment was verified shortly before incorporation into the yeast by natural abundance ^{13}C NMR (see chapter II).

Preparation of Proteins and Model Compounds

Native and [^{15}N]His-substituted Yeast Cytochrome Oxidase. The preparations of native yeast cytochrome oxidase and protein substituted with [1,3-$^{15}N_2$]histidine are described in the previous chapter of this thesis.

Beef Heart Cytochrome Oxidase. Cytochrome oxidase from beef heart was prepared by the method of Yu et al. (14), and was a phospholipid "sufficient" sample. The protein concentration was 165 mg/ml (with 11 nmole heme a per mg protein). The protein was suspended in 1.0% sodium cholate, 50 mM potassium phosphate, pH 7.4.

Myoglobin-imidazole. Sperm whale metmyoglobin was purchased from Sigma and was suspended to a protein concentration of 5 mM in 1:1 (v/v) glycerol/water, 50 mM potassium phosphate, pH 7.4. Imidazole was added to a concentration of 40 mM to form metmyoglobin-imidazole. Unsubstituted imidazole was purchased from Sigma and crystallized from benzene-ethanol. The [^{15}N]imidazole (99% ^{15}N at both ring positions) was obtained from Stohler Isotopes.

bis-Imidazole Tetraphenyl Porphyrin. The bis-imidazole Fe(III)tetraphenyl porphyrin complexes were 3 mM in tetraphenyl porphyrin (Strem), 40 mM in imidazole (as above), and were suspended in 1:1 $CDCl_3/CD2Cl_2$.

EPR Spectroscopy

EPR spectra were recorded on a Varian E-Line Century Series X-band spectrometer equipped with an Air Products Heli-Trans low temperature controller. Data were collected and stored on a PDP8/A (Digital Equipment Corp.) microcomputer interfaced to the spectrometer. Instrumental conditions are given in the figures.

ENDOR Spectroscopy

ENDOR spectra were recorded at SUNY, Albany, on equipment and, except as noted in the figures, under the conditions described previously (15,16) and in chapter II of this thesis.

RESULTS

Characterization of Isotopically Substituted Yeast Cytochrome Oxidase

EPR spectroscopy. The EPR spectra of native (unsubstituted) yeast and [1,3-$^{15}N_2$]histidine-substituted yeast cytochrome oxidase are compared in Fig. 2. The spectra are virtually identical and, in particular, show very little high-spin heme or adventitious copper. Also indicated in Fig. 2 are the positions of ENDOR observation for the cytochrome *a* ($g = 2.24$) and Cu_A ($g = 2.04$) studies. Note that the position of ENDOR observation for the cytochrome *a* ENDOR studies is in a region of the EPR spectrum in which there should be little or no contribution from Cu_A.

ENDOR Spectroscopy. The ENDOR spectra observed at $g = 2.04$ arise almost completely from the Cu_A center in cytochrome oxidase. The spectra observed at $g = 2.04$ for native and [^{15}N]His-substituted yeast cytochrome oxidase are shown in Fig. 3. As discussed in the previous chapter, these data show conclusively that histidine is a ligand to Cu_A. They also serve to demonstrate that ^{15}N has been successfully incorporated into the [^{15}N]His-substituted sample.

ENDOR Spectral Analysis of Isotopically Substituted Model Compounds

Before presenting the ENDOR results for cytochrome *a* in [^{15}N]His-substituted cytochrome oxidase, it is instructive to compare the ENDOR spectra of two bis-imidazole porphyrin model compounds substituted with [1,3-$^{15}N_2$]imidazole. Native myoglobin contains a five-coordinate ferric heme center, with an endogenous histidyl imidazole providing an axial nitrogen ligand and a second axial site open to coordination of exogenous ligands. Addition of imidazole to metmyoglobin converts the center to a low-spin bis-imidazole heme

Figure 2

EPR spectra of native and [^{15}N]His-substituted yeast cytochrome oxidase showing both the Cu_A and cytochrome *a* signals. Conditions: temperature, 15 K; microwave power, 10 microwatts; field modulation, 16 G; microwave frequency, 9.179 GHz.

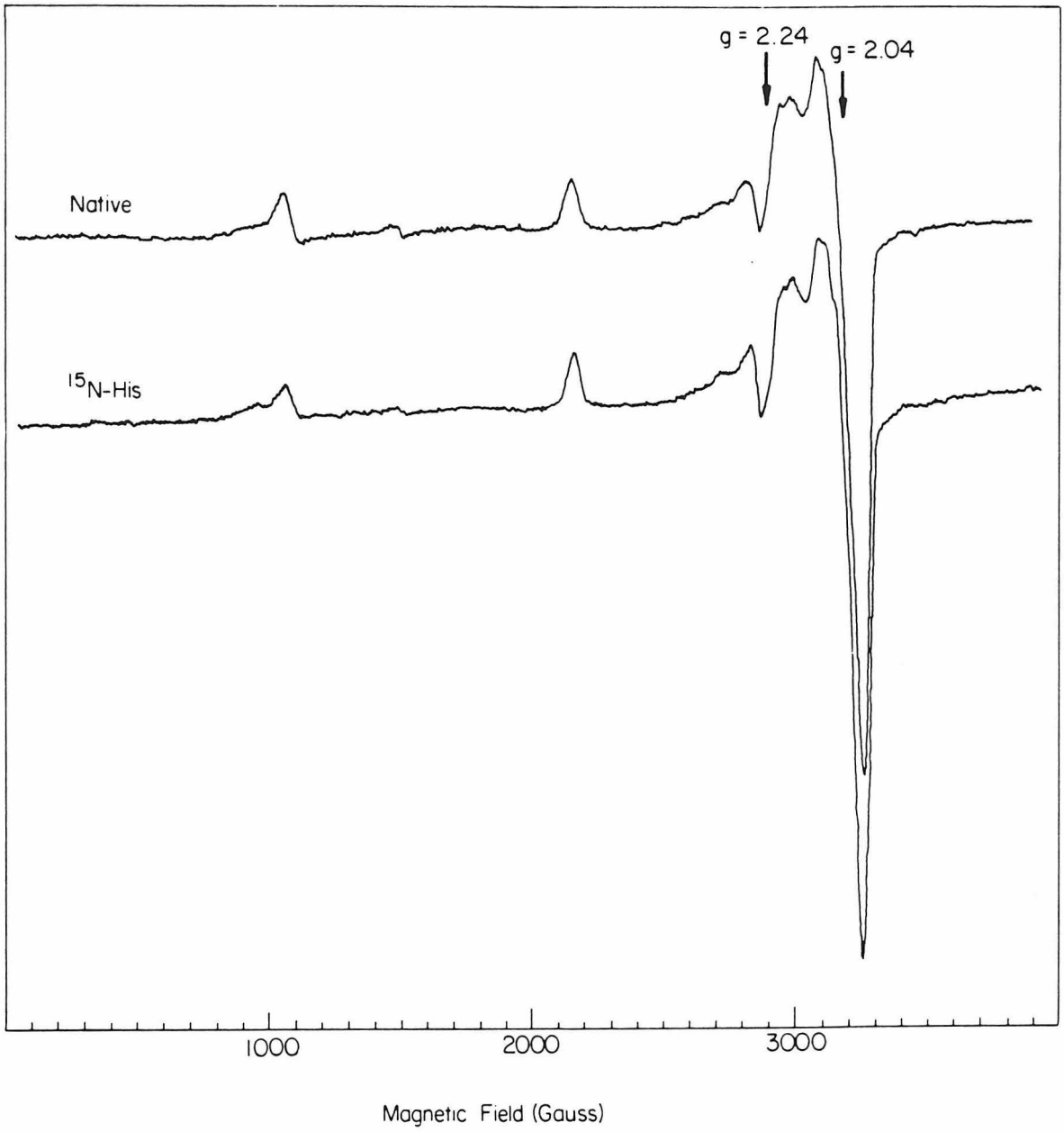
g = 2.24
g = 2.04
Native
^{15}N-His
1000
2000
3000
Magnetic Field (Gauss)

Figure 3

ENDOR spectra of Cu_A (observed at g = 2.04) in (A) native and (B) [^{15}N]His-substituted yeast cytochrome oxidase. Conditions: temperature, 2.1 K; microwave power, 10 microwatts; microwave frequency, (A) 9.03 GHz and (B) 9.08 GHz; field modulation, 4.0 G; sweep rate, 5.2 MHz/sec; instrumental time constant, 0.02 sec.

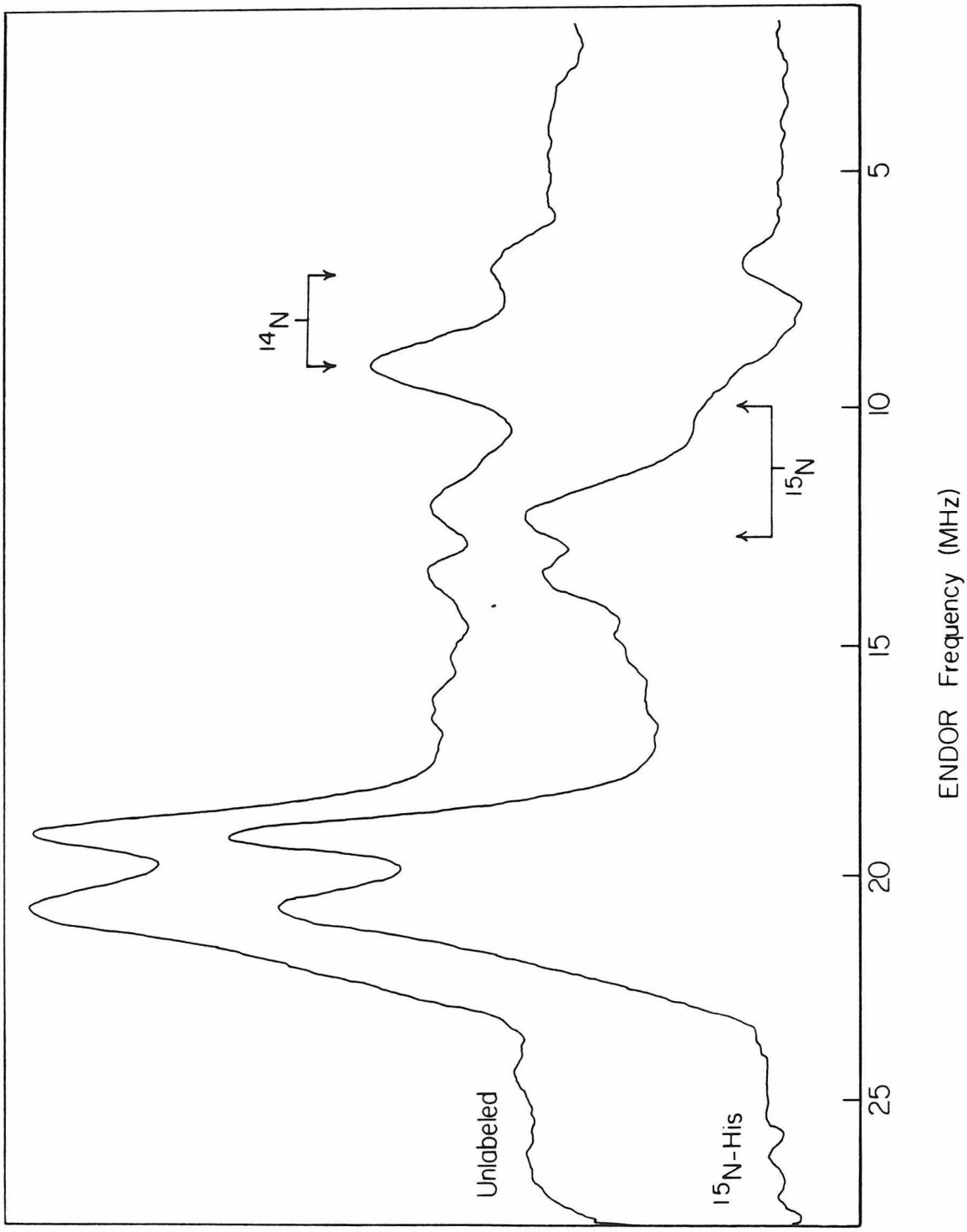
Unlabeled
^{15}N-His
^{14}N
^{15}N
5
10
15
20
25
ENDOR Frequency (MHz)

iron. This exogenous imidazole ligand can easily be replaced by [^{15}N]imidazole to yield a species in which one imidazole nitrogen ligand is ^{15}N and the other is (naturally abundant) ^{14}N. Another low-spin porphyrin model compound which has been extensively studied is bis-imidazole tetraphenyl porphyrin. This complex has been prepared with both axial imidazoles containing either (native) ^{14}N or (enriched) ^{15}N at the nitrogen position.

Myoglobin-imidazole. The ENDOR spectrum of metmyoglobin coordinated by exogenous native imidazole is shown in Fig. 4A. The ENDOR spectrum was recorded near the middle g-value (g = 2.26) in order to obtain optimal signal intensity. Spectra recorded near the g-value extrema (not shown), although less well resolved, demonstrate that the major signals in this area are reasonably isotropic. The spectrum in Fig. 4A contains several overlapping peaks in the low frequency region between 1 and 5 MHz. We note that for coupling to a single ^{14}N, two ENDOR signals should occur centered at one-half the hyperfine frequency and separated by twice the characteristic ^{14}N Zeeman frequency (under these conditions 2 (^{14}N) = 1.77 MHz). Since ^{14}N is an I=1 nucleus, each of these signals may be further split by twice the quadrupolar interaction; however, the quadrupole interaction is commonly quite small for low-spin hemes (17).

The ENDOR spectrum of an analogous species, different only in that [^{15}N]imidazole has been added as the exogenous ligand, is shown in Fig. 4B. A new signal is observed at 5.66 MHz and must be a result of the ^{15}N substitution in imidazole. Thus, although the ^{14}N ENDOR signals in the spectrum of the native enzyme are difficult to assign to individual coordinating atoms, the new signal observed in the ^{15}N-substituted sample can be assigned with certainty to an axial imidazole nitrogen. Spectra observed at different g-values (not shown) indicate that this new interaction is also isotropic in nature. From the known ^{15}N nuclear Zeeman frequency of 1.24 MHz, the Zeeman partner for this ^{15}N signal can be predicted to occur at either 8.15

Figure 4

ENDOR spectra of native and [^{15}N]imidazole-substituted metmyoglobin-imidazole (observed at g = 2.26). Conditions: temperature, 2.1 K; microwave power, 3.2 microwatts; microwave frequency, 9.09 GHz; field modulation, 2.0 G; sweep rate, 0.8 MHz/sec; instrumental time constant, 0.05 sec.

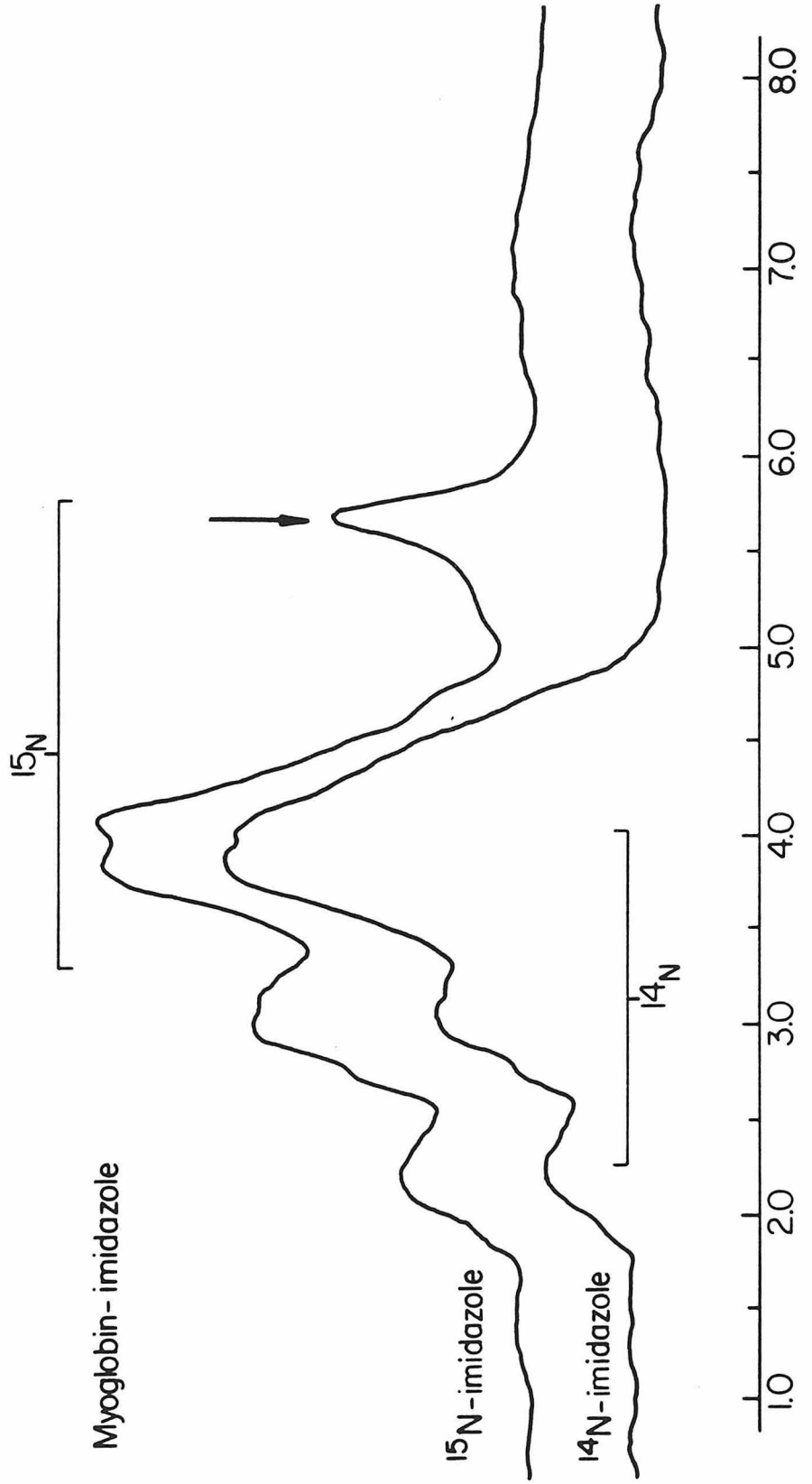
Myoglobin- imidazole
^{15}N-imidazole
^{14}N-imidazole
^{15}N
^{14}N
1.0
2.0
3.0
4.0
5.0
6.0
7.0
8.0
ENDOR Frequency (MHz)

or 3.17 MHz. Since no signals were found near 8 MHz in Fig. 4B, we conclude that the Zeeman partner for the ^{15}N signal must occur at 3.17 MHz, but is obscured by the other signals in this region of the spectrum. This assignment yields a ^{15}N hyperfine interaction of 8.8 MHz for this axial imidazole nitrogen ligand.

bis-Imidazole Tetraphenyl Porphyrin. A similar result is seen for native and ^{15}N-substituted bis-imidazole tetraphenyl porphyrin. The ENDOR spectra of the native ^{14}N and [^{15}N]imidazole-substituted forms are compared in Fig. 5. In the spectrum of the [^{15}N]imidazole-substituted sample, there is clearly a new signal at approximately 5.6 MHz attributable to coupling to an imidazole ring ^{15}N nitrogen. The other non-imidazole signals observed between 2 and 5 MHz most likely arise from porphyrin ring nitrogens and appear very similar to those seen for the bis-imidazole myoglobin samples.

ENDOR Comparison of Native and Isotopically Substituted Cytochrome a

The ENDOR spectrum of cytochrome a in native yeast cytochrome oxidase is shown in Fig. 6. At this g-value (g = 2.24), the cytochrome a contribution to the ENDOR absorption spectrum is maximized, whereas that from Cu_A is negligible. The general features of the spectrum are quite similar to those of unsubstituted myoglobin-imidazole and bis-imidazole tetraphenyl porphyrin. In particular there is a collection of unresolved signals in the low frequency region between 1 and 5 MHz, presumably arising from equatorially coordinated heme ring nitrogens.

The ENDOR spectra of native and [^{15}N]His-substituted yeast cytochrome oxidase are compared in Fig. 6. Analysis of these spectra reveals a signal near 5.6 MHz appearing only in the spectrum of the ^{15}N-substituted protein. This result is analogous to the results observed for the native and ^{15}N-substituted forms of bis-imidazole myoglobin and for bis-imidazole tetraphenyl porphyrin. The presence

Figure 5

ENDOR spectra of (A) native and (B) [^{15}N]imidazole-substituted bis-imidazole tetraphenyl porphyrin (observed at g = 2.28). Conditions: temperature, 2.1 K; microwave power, 3.2 microwatts; microwave frequency, (A) 9.13 and (B) 9.17 GHz; field modulation, 2.0 G; sweep rate, 0.8 MHz/sec; instrumental time constant, 0.05 sec.

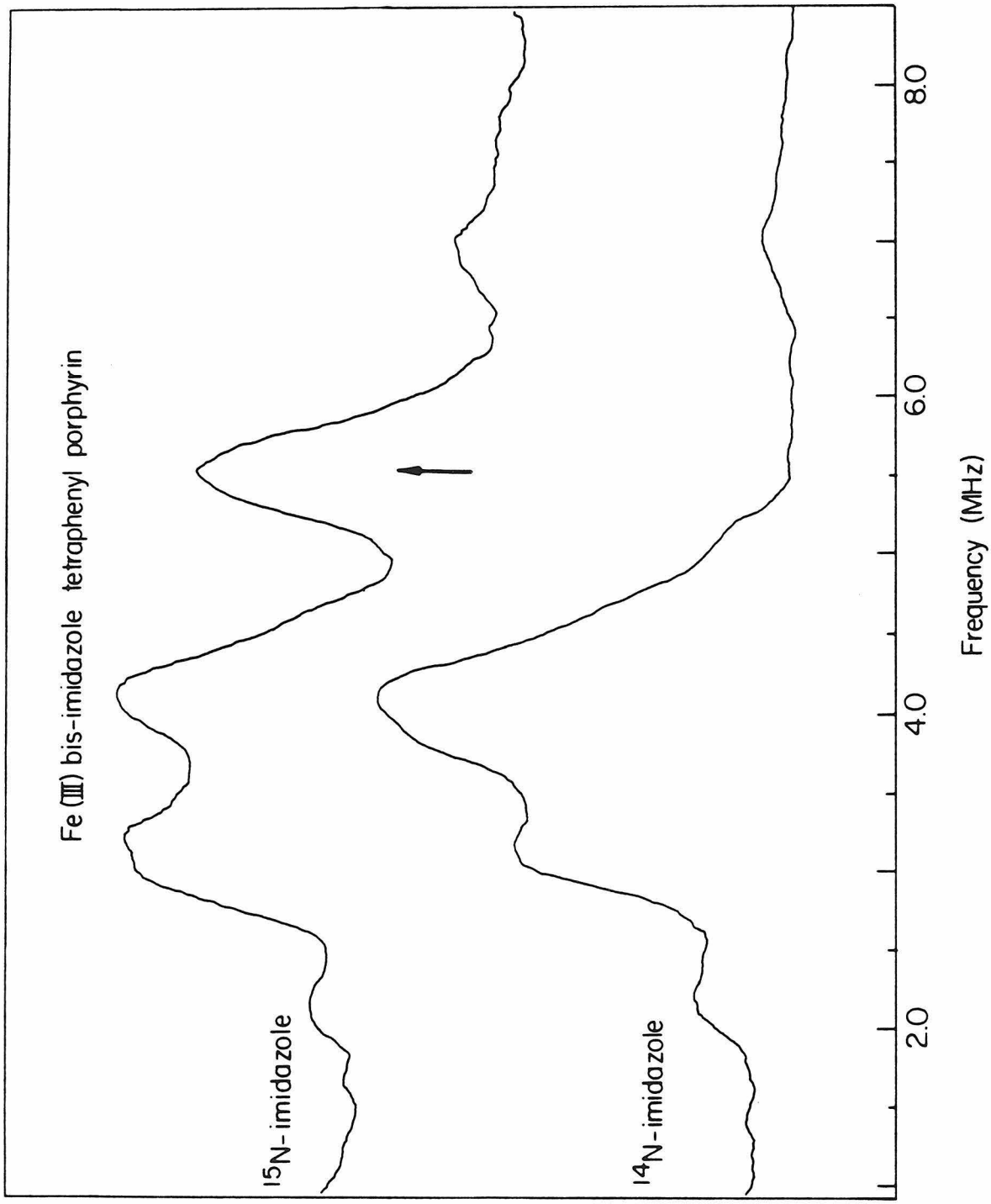
Fe (III) bis-imidazole tetraphenyl porphyrin
^{15}N-imidazole
^{14}N-imidazole
2.0
4.0
6.0
8.0
Frequency (MHz)

Figure 6

ENDOR spectra of cytochrome a in (A) native and (B) [^{15}N]His-substituted yeast cytochrome oxidase (observed at g = 2.24). Conditions: temperature, 2.1 K; microwave power, 3.2 microwatts; microwave frequency, (A) 9.03 and (B) 9.09 GHz; field modulation, 2.0 G; sweep rate, 1.6 MHz/sec; instrumental time constant, 0.05 sec.

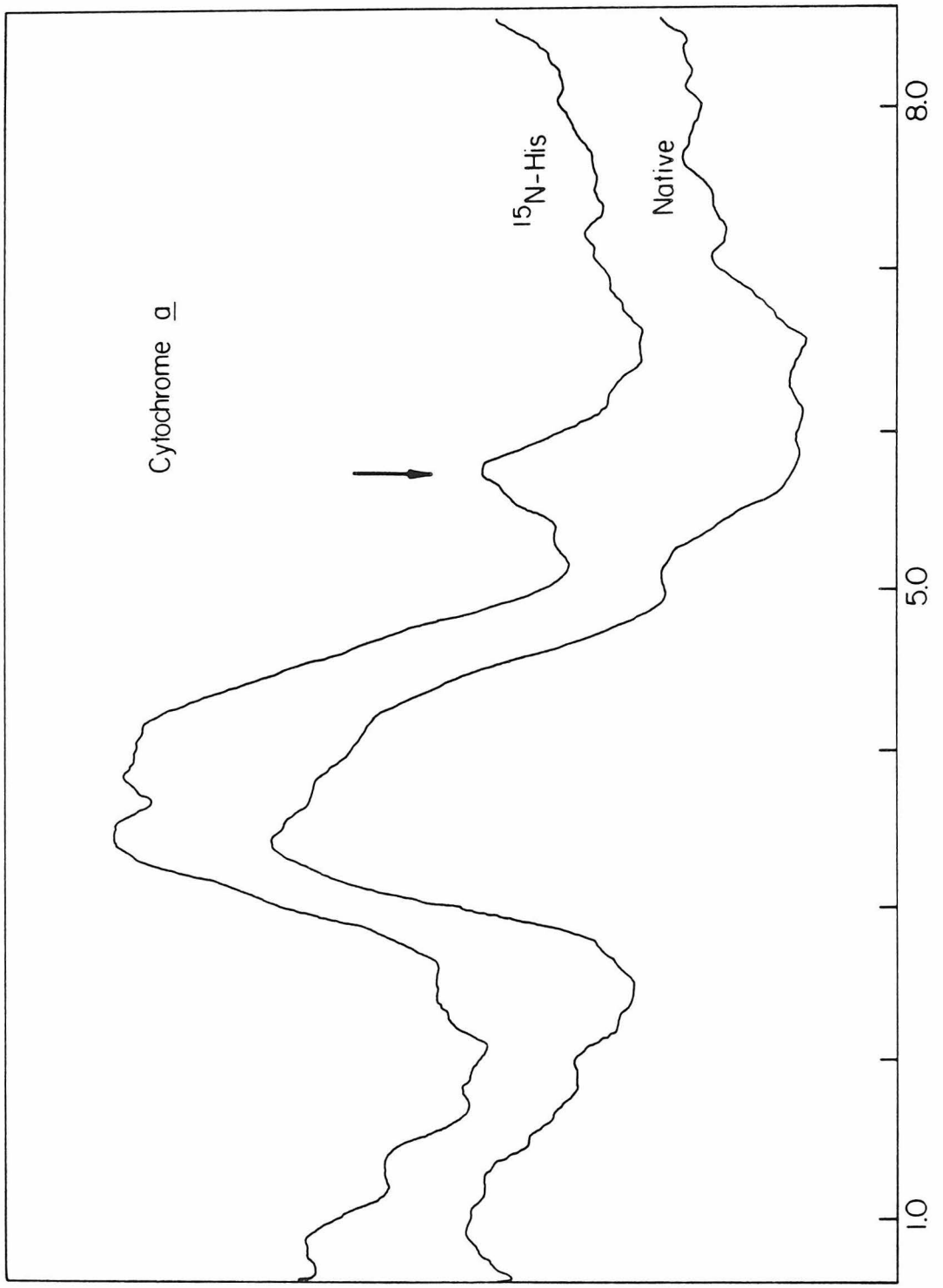
Cytochrome a
^{15}N-His
Native
1.0
5.0
8.0
ENDOR Frequency (MHz)

of this new signal clearly demonstrates the coordination of at least one histidyl imidazole nitrogen to cytochrome a. Moreover, the calculated ^{15}N hyperfine coupling to cytochrome a, assuming a ^{15}N ENDOR partner near 3.1 MHz, is approximately 8.8 MHz - the same as that observed in the myoglobin study and quite similar to that observed for bis-[^{15}N]imidazole tetraphenyl porphyrin.

Detailed ENDOR Analysis of Cytochrome a in the Beef Heart Protein

Due to the large g-value anisotropy in the EPR spectrum of cytochrome a, the EPR absorption intensity, and hence the ENDOR signal intensity, is an order of magnitude smaller for cytochrome a than for Cu_A. Consequently, it is difficult to obtain spectra with substantial signal to noise with the small amounts of yeast protein available. In an attempt to resolve some of the signals in the 1-5 MHz region of the ENDOR spectrum of cytochrome a, we examined a much larger (about five times greater) volume of cytochrome oxidase isolated from beef heart. The ENDOR spectrum of cytochrome a from the beef heart protein, shown in Fig. 7, is almost identical to that of the native yeast protein, although there is slightly better resolution in the former since we were able to use a smaller spectrometer time constant.

One (presumably heme ring) nitrogen coupling can be readily assigned in the beef heart spectrum: the signals at 3.3 and 5.0 MHz are split by twice the nuclear Zeeman frequency of ^{14}N and correspond to a ^{14}N hyperfine coupling of 8.3 MHz.

An important consideration to note is that the ENDOR enhancement effect (18,19) predicts that ENDOR signals from the same Zeeman pair will have relative signal intensities proportional to the square of their resonant frequencies. In general, this will cause resonances at lower ENDOR frequencies to be less intense than their partners at higher frequencies. For example, there appears to be a resonance centered at about 4.1 MHz in the spectrum of cytochrome a from the beef heart protein. Knowing the nuclear Zeeman frequency, we can

Figure 7

ENDOR spectrum of cytochrome a in beef heart cytochrome oxidase (observed at g = 2.26). Conditions: temperature, 2.1 K; microwave power, 3.2 microwatts; microwave frequency, 9.09 GHz; field modulation, 2.0 G; sweep rate, 1.6 MHz/sec; instrumental time constant, 0.02 sec.

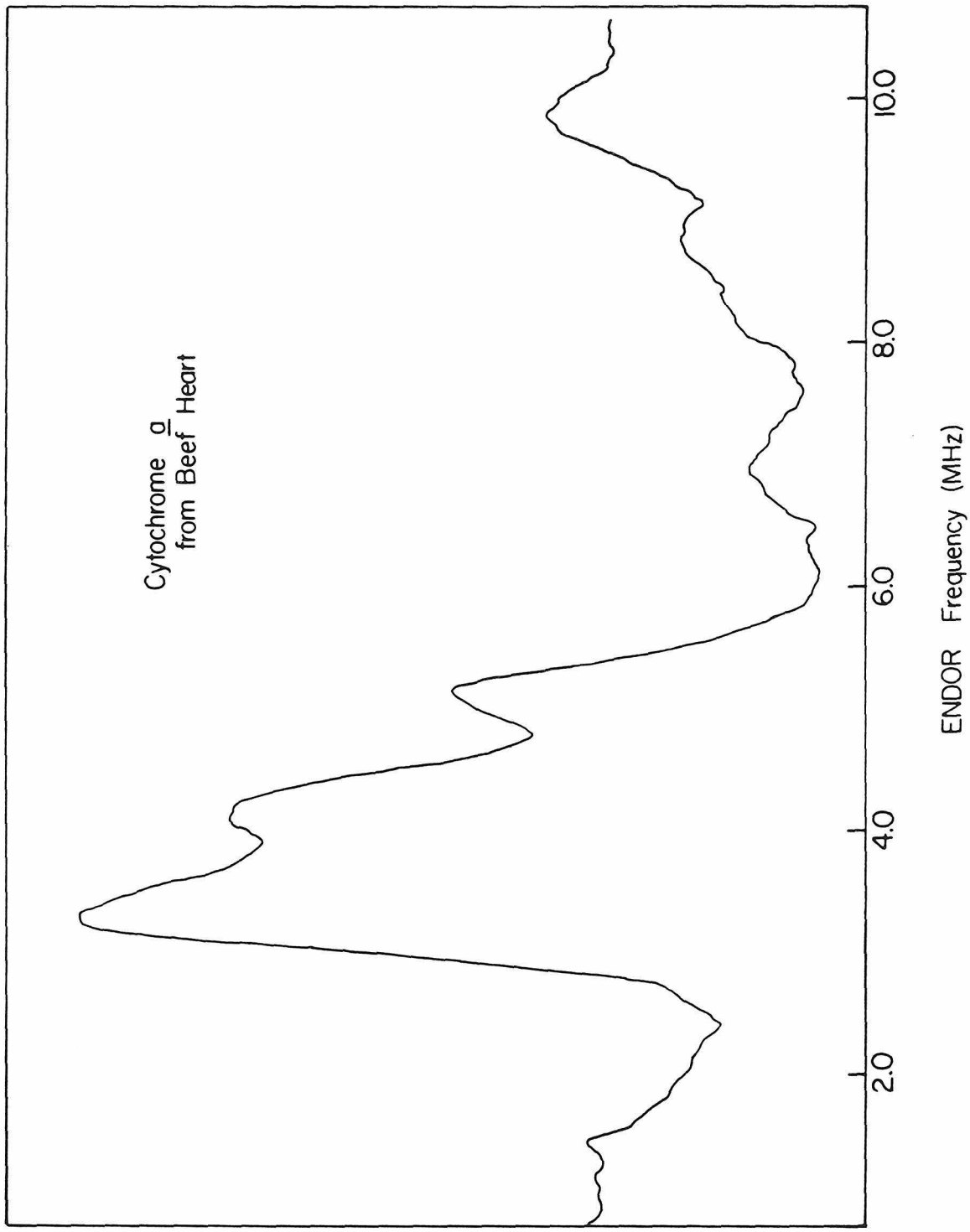
Cytochrome a
from Beef Heart
2.0
4.0
6.0
8.0
10.0
ENDOR Frequency (MHz)

predict this signal to have a Zeeman partner at either 2.3 or 5.8 MHz. The latter solution predicts the new signal at 5.8 MHz to be approximately twice as large as the signal seen at 4.1 MHz, whereas the former possibility predicts a new partner at 2.3 MHz which is one-third the size of the signal at 4.1 MHz. Since no signals are resolved at either position, we conclude that the Zeeman partner to the signal at 4.1 MHz must have a relatively low intensity. This leads to the (former) solution in which the Zeeman partner (predicted to occur at 2.3 MHz) has an intensity one-third that of the resolved transition. This interpretation results in a ^{14}N hyperfine coupling of 6.4 MHz for nitrogen ligand.

The remaining features of the spectrum are not resolved. They are most certainly not associated with hyperfine couplings to axial histidine nitrogens, and probably arise from couplings to equatorially coordinated heme nitrogens. In the absence of isotopic substitution data for these signals, we will forego attempts at further assignment and merely note the general shape of the spectrum for comparison with model compounds.

DISCUSSION

As discussed in the previous chapter, the coordination environment of the metal centers in cytochrome *c* oxidase is almost certainly the same in both the yeast and beef heart forms of the enzyme. The ENDOR results presented here for cytochrome *a* in native cytochrome oxidase from both species are indistinguishable within the resolution obtainable. The ability, in the yeast protein, to specifically incorporate histidine substituted with ^{15}N at the two imidazole ring nitrogen positions provides an opportunity to directly probe the axial coordination at cytochrome *a*, specifically to determine whether histidine is an axial ligand to this heme iron center in cytochrome oxidase.

The finding of an ENDOR resonance in the spectrum of cytochrome *a* in [1,3-$^{15}N_2$]histidine-substituted yeast cytochrome oxidase which is not present in the corresponding spectrum of the native enzyme is unambiguous proof that histidine provides at least one axial nitrogen ligand to cytochrome *a*. The strength of the hyperfine interaction for this ^{15}N coupling (A = 8.8 MHz) is identical to the ^{15}N-coupling observed for the ^{15}N-substituted myoglobin-imidazole complex (in which one of two axial imidazole ligands has ^{15}N replaced in place of the naturally abundant ^{14}N nitrogen. The coupling in cytochrome *a* is also very similar to the ^{15}N coupling observed for bis-[^{15}N]imidazole tetraphenyl porphyrin. These comparisons strongly suggest that cytochrome *a* is also bis-imidazole in coordination, and so quite likely has two axial histidine ligands.

It is important to point out that the observation of only one new resonance in the ENDOR spectrum of [^{15}N]His-substituted cytochrome *a*, relative to that of the unsubstituted center, does not preclude the existence of a second histidine ligand to cytochrome *a*. In fact, the corresponding spectra in native and ^{15}N substituted bis-imidazole tetraphenyl porphyrin also reveal only one new signal, despite the

symmetric substitution of the coordinating isotope. The possibility that the resonances of both axial ligands are coincident would reflect a degree of symmetry in the coordination environment near the axial ligands.

CONCLUSION

The incorporation of [^{15}N]His into yeast cytochrome oxidase has provided unambiguous proof of the coordination of at least one histidine imidazole nitrogen as an axial ligand to cytochrome *a*. The similarity of the ^{15}N hyperfine coupling reported here for [^{15}N]His-substituted cytochrome *a* to ^{15}N hyperfine couplings to axial imidazoles in two bis-imidazole porphyrin model compounds, provides strong evidence in support of the conclusion that cytochrome *a* is coordinated by two axial histidine nitrogens.

REFERENCES

1. Gibson, Q. H., Greenwood, C., Wharton, D. C., and Palmer, G. (1965) J. Biol. Chem. 240, 888-894.

2. Antalis, T. M., and Palmer, G. (1982) J. Biol. Chem. 257, 6194-6206.

3. Taniguchi, V. T., Ellis, W. R., Cammarata, V., Webb, J., Anson, F. C., and Gray, H. B. (1981) in Electrochemical and Spectrochemical Studies of Biological Redox Components, Kadish, K. M., ed., American Chemical Society, Washington, 51-68.

4. Anderson, J. L., Kuwana, T., and Hartzell, C. R. (1976) Biochemistry 15, 3847-3855.

5. Clore, G. M., Andreasson, L., Karlsson, B., Aasa, R., and Malmstrom, B. G. (1980) Biochem. J. 185, 139-154.

6. Wikstrom, M., Krab, K., and Saraste, M. (1981) Cytochrome Oxidase: A Synthesis, Academic Press, London.

7. Babcock, G. T., and Callahan, P. M. (1983) Biochemistry 22, 2314-2319.

8. Blumberg, W. E., and Peisach, J. (1971) in Probes of Structure and Function of Macromolecules and Membranes, Vol. 2, Chance, B., Yonetani, T., and Mildvan, A. S., eds., Academic Press, New York, 215-239.

9. Babcock, G. T., Callahan, P. M., Ondrias, M. R., and Salmeen, I. (1981) Biochemistry 20, 959-966.

10. Babcock, G. T., Vickery, L. E., and Palmer, G. (1976) J. Biol. Chem. 251, 7907-7919.

11. Eglinton, D. G., Hill, B. C., Greenwood, C., and Thomson, A. J. (1984) J. Inorg. Biochem. 21, 1-8.

12. Mims, W. B., Peisach, J., Shaw, R. W., and Beinert, H. (1980) J. Biol. Chem. 255, 6843-6846.

13. Peisach, J., and Mims, W. B. (1981) Israel J. Chem. 21, 59-60.

14. Yu, C., Yu, L., and King, T. E. (1975) J. Biol. Chem. 250, 1383-1392.

15. Van Camp, H. L., Scholes, C. P., and Mulks, C. F. (1976) J. Am. Chem. Soc. 98, 4094-4098.

16. Van Camp, H. L., Scholes, C. P., and Isaacson, R. A. (1976) Rev. Sci. Instrum. 47, 516-517.

17. Scholes, C. P., and Van Camp, H. L. (1976) Biochim. Biophys. Acta 434, 290-296.

18. Whiffen, D. H. (1966) Mol. Physics 10, 595-596.

19. Davies, E. R., and Reddy, T. R. (1970) Phys. Lett. 31A, 398-399.

CHAPTER IV

SEQUENCE ANALYSIS AND THE STRUCTURE OF CYTOCHROME OXIDASE

INTRODUCTION

The identification of specific amino acid ligands to the metal centers in cytochrome c oxidase not only provides specific information on the local environment of each of the active site metals, but also can aid in the determination of the location of the these sites within the overall protein structure. Armed with the knowledge of ligands to three of the metal centers in cytochrome oxidase, we now analyze the available protein sequence data in order to gain more insight into the overall structure of cytochrome oxidase.

The primary sequence of a protein contains valuable information regarding the tertiary structure of the functional protein. Although attempts at determining tertiary structure directly from primary sequence have met with little success, sequence information can be useful in determining some features of protein structure. An obvious example is information obtained from evolutionary comparisons of a given protein sequence from different species. Knowledge of which regions and residues are conserved as a protein sequence evolves from species to species can guide an investigator towards a better understanding of the relationship between structure and function. In general, active site regions are constrained to minor variations (ie., amino acid insertions, deletions, and substitutions), whereas regions with less specific function are allowed more variability. A knowledge of which regions in the primary sequence of a protein have remained constant can yield information on probable locations of important active sites.

A second technique which has recently been of some use in determining tertiary structure from primary sequence information is the analysis of a protein's sequence with respect to amino acid class. Amino acids can be grouped into different classes based on common chemical or biological properties. One of the first of these schemes to be proposed was that of Chou and Fasman (1). This scheme uses

empirical correlations between amino acid residue type and protein secondary structure (in this case, α-helix, β-sheet, and random coil regions of proteins and polypeptides). For globular proteins, particularly smaller ones, this analysis has enjoyed some success (2). Recently, Kyte and Doolittle (3) have proposed a technique for predicting membrane-spanning regions of integral membrane proteins. Based on both empirical correlations and physical properties of the amino acids, they have a proposed a "hydropathy" scale to determine regions of a primary sequence which display a high degree of hydrophobicity. They have further used this scale with a moving-segment analysis in which a given point in a sequence is assigned a hydropathy value based on the average hydropathy value of the individual residues in a segment centered at that point. Based on the observation that, on average, segments passing through the moderately hydrophobic interior of a protein are shorter than segments required to span a membrane bilayer, they chose a moving-segment length of 19 residues. This predictive tool, although certainly not infallible, has proven useful in the study of several proteins whose sequence, but not tertiary structure, is known.

In this study we combine the two techniques discussed above. Through the analysis of both sequence conservation and amino acid type localization, we are able to obtain some useful information on the structure of cytochrome oxidase and the possible locations of the various active site metals. The primary sequences of the major subunits of cytochrome c oxidase are known for several species of eukaryotes. Although some of the species compared in this study are separated by wide evolutionary spans and certain segments of their cytochrome oxidase protein sequences have diverged substantially, the basic biochemical and spectroscopic characteristics of the individual proteins have remained constant.

METHODS

The interactive computer program used in this study was written in Fortran for use on a Digital Equipment Corp. VAX computer. The segmental averaging function is taken directly from the technique proposed by Kyte and Doolittle (3). Additional features of this program allow averaging of sequence conservation information for any number of species. The standard deviation (between species) of the average hydropathy parameter can be calculated for the each point in the sequence. This measurement of structural conservation can then be subjected to segmental averaging in a manner analogous to the segmental averaging of the hydropathy parameter. Other predictive scales available are the Chou and Fasman α-helix, β-sheet, and random coil parameters (1), and a separate membrane-buried preference scale proposed by Argos, et al. (4). This latter scale gives qualitatively similar results to those of Kyte and Doolittle. Plots may be prepared for output on any standard lineprinter or for output using the Versaplot plotting routines with a Versatec plotter. The program will also search sequences for exact residue conservation and will search for particular amino acid residues. A provision is also included for a summary of the properties of each sequence, such as total molecular weight, average hydropathy, and the number of occurrences of each of the 21 standard amino acid residues.

Protein sequences can be entered manually or read in from a file, using the standard 1- or 3-letter codes. They are then stored in a separate file for subsequent use by the program.

The sequences from different species were aligned manually for optimum homology with a minimum of proposed insertions and deletions. Where available, the alignments of new species sequences relative to the beef heart or human protein sequences were as proposed by the original investigators.

RESULTS AND DISCUSSION

Subunit composition

Cytochrome *c* oxidase is a large multi-subunit enzyme. It is particularly unusual in that the three largest subunits are coded for by mitochondrial DNA, whereas the several smaller subunits are coded for by nuclear DNA. There has been considerable controversy over the exact subunit composition of the enzyme (see Wikstrom (5) for a review). The number of different subunits proposed has varied from six to as many as twelve, with varying stoichiometries for each of the subunits (although there seems general agreement that subunits I, II, and III exist as only one copy each per functional monomer). We will not attempt to make a judgement of the various proposals regarding the identity and composition of the smaller subunits, but will adopt the twelve subunit nomenclature presented in Table I, as proposed by Kadenbach and Merle (6). The only deviation from their scheme is the addition of a subunit which we call Va. The purpose of this chapter is to discuss sequence data with respect to possible metal active site locations. As will be discussed below, we have good evidence to believe that all four metals are located in the mitochondrially synthesized subunits I and II. For this reason, discussion will be centered on the three major subunits I, II, and III, with only a brief analysis of those smaller subunits which have been sequenced.

Various studies have been conducted to determine the biological and spectroscopic requirements for the proposed subunits of cytochrome oxidase. Subunits III, VIa, VIb, and VIIa have been removed in various studies (ref. 5 and references therein) with no major effect on the spectroscopic and electron transfer properties of the enzyme. Perhaps more importantly, a bacterial cytochrome aa_3 has been isolated from *Paracoccus denitrificans* which consists of only 2 subunits of molecular weights 45,000 and 28,000 daltons, respectively (7). The

Table I

The subunit composition of cytochrome oxidase, based on the nomenclature of Kadenbach and Merle (6). Except as noted, the molecular weights are predicted from the known primary structures of the beef heart subunits.

Beef Heart Cytochrome c Oxidase

Subunit Information From Sequence Data

Subunit	Molecular Weight (daltons)	Average Hydropathy*
I	56,789	+0.69
II	26,021	+0.25
III	29,918	+0.40
IV	17,024	-0.53
V	12,627	-0.61
Va	10,566	-0.90
VIa	9,500**	-
VIb	10,025	-0.90
VIc	7,500**	-
VIIa	5,441	-0.03
VIIb	4,900**	-
VIIc	4,700**	-
VIII	4,300**	-
Total	199,311	

*Hydropathy parameter from Kyte and Doolittle (3).

**Molecular weights determined by SDS-PAGE (6).

isolated protein is fully functional in electron transport and shows proton pumping activity (8,9). A similar bacterial cytochrome $\underline{aa_3}$ isolated from the thermophilic bacterium PS3 also shows proton pumping activity (10). Although the protein contains three subunits (with molecular weights of 56,000, 38,000, and 21,000 daltons), one of them presumably contains the tightly bound cytochrome $\underline{c}$ found in the complex. These results are consistent with theories that a bacterial symbiont was the evolutionary ancestor of eukaryotic mitochondria (11). From partial protein sequence data it has been determined that subunits I and II from the Paracoccus cytochrome oxidase bear substantial sequence homology with subunits I and II, respectively, from beef heart cytochrome oxidase. They have also been shown to be immunologically cross-reactive with antibodies to the beef heart subunits (12). Although it is possible that one or more of the smaller eukaryotic subunits might be contained within these two bacterial subunits, they not only would have had to dissociate into separate genetic regions during the evolution from bacteria to mitochondria, but also would have had to migrate from the mitochondrial to the nuclear genome, all the while retaining the capability of being incorportated into a functional oxidase protein. These arguments have been taken to imply that the four metal centers in the beef heart protein are contained completely within subunits I and II. Presumably, the smaller subunits (and possibly subunit III) have been added during evolution from bacterial symbiont to mitochondria for regulatory or other functions less intrinsic to oxygen reduction and proton pumping.

Analysis of the subunits coded by nuclear DNA

Sequence data are available for several of the smaller (nuclear) subunits of beef cytochrome oxidase. Figure 1 lists the known sequences of subunits IV (13), V (14,15), Va (16), VIb (17), and VIIa (18). In each case, the amino acid composition of these small

Figure 1

Amino acid sequences from some of the subunits of cytochrome oxidase coded for by the nuclear DNA. References are given in the text.

Beef Heart Subunit IV Protein Sequence

```
|  1                  | 21                  | 41                  | 61
AHGSVVKSEDYALPSYVDRRDYPLPDVAHVKNLSASQKALKEKEKASWSSLSIDEKVELYRLKFKESFAEMNRST
|  76                 | 96                  |116                  |136
NEWKTVVGAAMFFIGFTALLLIWEKHYVYGPIPHTFEEEWVARQTKRMLDMKVAPIQGFSAKWDYDKNEWK
```

Yeast Subunit V Protein Sequences
Beef Heart

```
|  1                  | 21                  | 41                  | 61
SDAHDEETFEEFTARYEKEFD.EAYDLFEVQRVLNNCFSYDLVPAPAVIEKALRAARRVNDLPTAIRVFEALKYK
SHGSH.ETDEEFDARWVTYFNKPDIDAWELRKGMNTLVGYDLVPEPKIIDAALRACRRLNDFASAVRILEVVKDK
|  76                 | 96
VENEDQYKAY.LDELKDVRQELGVPLKEELFPSSS
AGPHKEIYPYVIQELRPTLNELGISTPEELGLDKV
```

Beef Heart Subunit Va Protein Sequence

```
|  1                  | 21                  | 41                  | 61
ASGGGVPTDEEQATGLEREVMLAARKGQDPYNILAPKATSGTKEDPNLVPSITNKRIVGCIQEDNSTVIWFWLHK
|  76                 | 96
GEAQRCPSCGTHYKLVPHQLAH
```

Beef Heart Subunit VIb Protein Sequence

```
|  1                  | 21                  | 41                  | 61
AEDIQAKIKNYQTAPFDSRFPNQNQTRNCWQNYLDFHRCEKAMTAKGGDVSVCEWYRRVYKSLCPISWVSTWDDR
|  76
RAEGTFPGKI
```

Beef Heart Subunit VIIa Protein Sequence

```
|  1                  | 21                  | 41
SHYEEGPGKNIPFSVENKWRLLAMMTLFFGSGFAAPFFIVRHQLLKK
```

subunits is considerably more hydrophilic than the composition of the mitochondrially coded larger subunits. The average hydropathy values shown in Table I are all below zero, with all but VIIa below -0.5. Subunits IV and V are particularly unusual in having about 10% acidic Glu residues. From the highly charged and hydrophilic nature of these subunits, we conclude that they are not likely buried in the hydrophobic membrane interior.

Analysis of Subunit III

Subunit III has long been considered smaller than subunit II, but the sequence data shown in Fig. 2 predict a molecular weight in the beef heart protein of approximately 30,000 daltons for subunit III, as compared with only 26,000 daltons for subunit II. The sequences for subunit III from beef (19), human (20), mouse (21), Drosophila yakuba (fruit fly) (22), Aspergillus nidulans (a fungus) (23), Saccharomyces cerevisiae (yeast) (24), and Neurospora crassa (25) show that subunit III, like subunit I, has a fairly high average hydropathy parameter, ranging from 0.40 to 0.70 units. The moving segment hydropathy analysis shown in Fig. 3 reveals several hydrophobic regions. Using a moving segment length of 19 residues (sufficient to span the bilayer as an α-helix) three membrane spanning segments are found to have average segmental hydropathy values greater than +1.6. This hydropathy value is sufficient to confer a "high probability" of membrane spanning capability according to the empirical findings of Kyte and Doolittle (3). As many as three or four more segments have hydropathy parameters above +1.0.

The plot in Fig. 3 also shows the standard deviation in the hydropathy parameter of the various sequences, averaged in a moving-segment fashion analogous to that used for the hydropathy. A correlation that appears clear is that regions of relatively high sequence divergence tend to coincide with regions of greater hydrophilicity, that is, regions predicted to be at turning points of

Figure 2

Amino acid sequences of subunit III from various eukaryotic organisms. References are given in the text.

Subunit III Protein Sequences

```
Beef Heart
Human
Mouse
Drosophila
Aspergillus
Yeast
Neurospora

|  1                  | 21                  | 41                  | 61
MTHQT......HAYHMVNPSPWPLTGALSALLMTSGLTMWFH.FNSMTLLMIGLTTNMLT.MYQWWRDVIRESTF
MTHQS......HAYHHVKPSPWPLTGALSALLMTSGLAMWFH.FHSMTLLMLGLLTNTLT.MYQWWRDVTRESTY
MTHQT......HAYHMVNPSPWPLTGAFSALLLTSGLVMWFH.YNSITLLTLGLLTNILT.MYQWWRDVIREGTY
MSTHSN.....HPFHLVDYSPWPLTGAIGAMTTVSGMVKWFH.QYDISLFVLGNIITILT.VYQWWRDVSREGTY
MIYQSKRNFQLHPFHLVSESPWPLFTSISLFILTTATVLFMHGFEGFQYLVPVAVINVMYVMGLWFRDVISEGTY
MTHLERSRHQQHPFHMVMPSPWPIVVSFALLSLALSTALTMHGYIGNMNMVYLALFVLLTSSIIWFRDIVAEATY
MTNLIRSNFQDHPFHLVSPSPWPLNTSVCLLNLTTTGALSMHNFNNIHYLYYIALIGLVSAMFLWFRDIISEGTF

|  76                 | 96                  |116                  |136
QGHHTPAVQKGLRYGMILFIISEVLFFTGFFWAFYHSSLAPTPELGGCWPPTGIHPLNPLEVPLLNTSVLLASGV
QGHHTPPVQKGLRYGMILFITSEVFFFAGFFWAFYHSSLAPTPQLGGHWPRTGITPLNPLEVPLLNTSVLLASGV
QGHHTPIVQKGLRYGMILFIVSEVFFFAGFFWAFYHSSLVPTHDLGGCWPPTGISPLNPLEVPLLNTSVLLASGV
QGLHTYAVTIGLRWGMILFILSEVLFFVSFFWAFFHSSLSPAIELGASWPPMGIISFNPFQIPLLNTAILLASGV
LGNHTNAVQKGLNLGVGLFIISEVFFFLAIFWAFFHSAISPSVELGAQWPPLGIQGINPFELPLLNTIILLSSGV
LGDHTIAVRKGINLGFLMFVLSEVLIFAELFWAYFHSAMSPDVTLGACWPPVGIEAVQPTELPLLNTIILLSSEA
LGDHTLAVQRGLNLGIILFIVSEALFFLAIFWAFFHSALTPTVELGAQWPPIGIEPVNPFELPLLNTVILLSSGA

|151                 |171                  |191                  |211
SITWAHHSLMEGDRKHMLQALFITITLGVYFTLLQASEYYEAPFTISDGVYGSTFFVATGFHGLHVIIGSTFLIV
SITWAHHSLMENNRNQMIQALLITILLGLYFTLLQASEYFESPFTISDGIYGSTFFVATGFHGLHVIIGSTFLTI
SITWAHHSLMEGKRNHMNQALLITIMLGLYFTILQASEYFETSFSISDGIYGSTFFMATGFHGLHVIIGSTFLIV
TVTWAHHSLMENNHSQTTQGLFFTVLLGIYFTILQAYEYIEAPFTIADSVYGSTFYMATGFHGVHVLIGTTFLLV
TITYAHHSLIQGNRKGALYGTVVTILLAIVFTFFQGVEYTVSSFTISDSVYGSCFYFGTGFHGLHVIIGTAFLAV
TVTYSHHALIAGNRNKALSGLLITFWLIVIFVTCQYIEYTNAAFTISDGVYGSVFYAGTGLHFLHMVMLAAMLGV
TITYAHHALIKGEREGALYGSIATILLAIIFTGFQGVEYSVSSFTISDGAFGTCFFFSTGFHGIHVIIGTIFLAV

|226                 |246                  |266
CFFRQLKFHFTSNHHFGFEAGAWYWHFVDVVWLFLYVSIYWWGS
CFIRQLMFHFTSKHHFGFEAAAWYWHFVDVVWLFLYVSIYWWGS
CLLRQLKFHFTSKHHFGFEAAAWYWHFVDVIWLFLYVSIYWWGS
CLLRHLNNHFSKNHHFGFEAAAWYWHFVDVVWLFLYITIYWWGG
GLWRLAAYHLTDHHHLGYESGILQWHFVDVVWLFLYISVYYWGY
NYWRMRNYHLTAGHHVGYGTTIIYTHVLDVIWLFLYVTFYWWGV
ALWRIFAYHLTDNHHVGFEGGILYWHFVDVVWLFLYISVYYWES
```

Figure 3

Moving-segment hydropathy analysis of subunit III, averaged over the sequences of the organisms indicated and using a segment length of 19 residues. The lower curve represents the standard deviation of the moving-segment average at each residue with respect to evolutionary conservation among the indicated species.

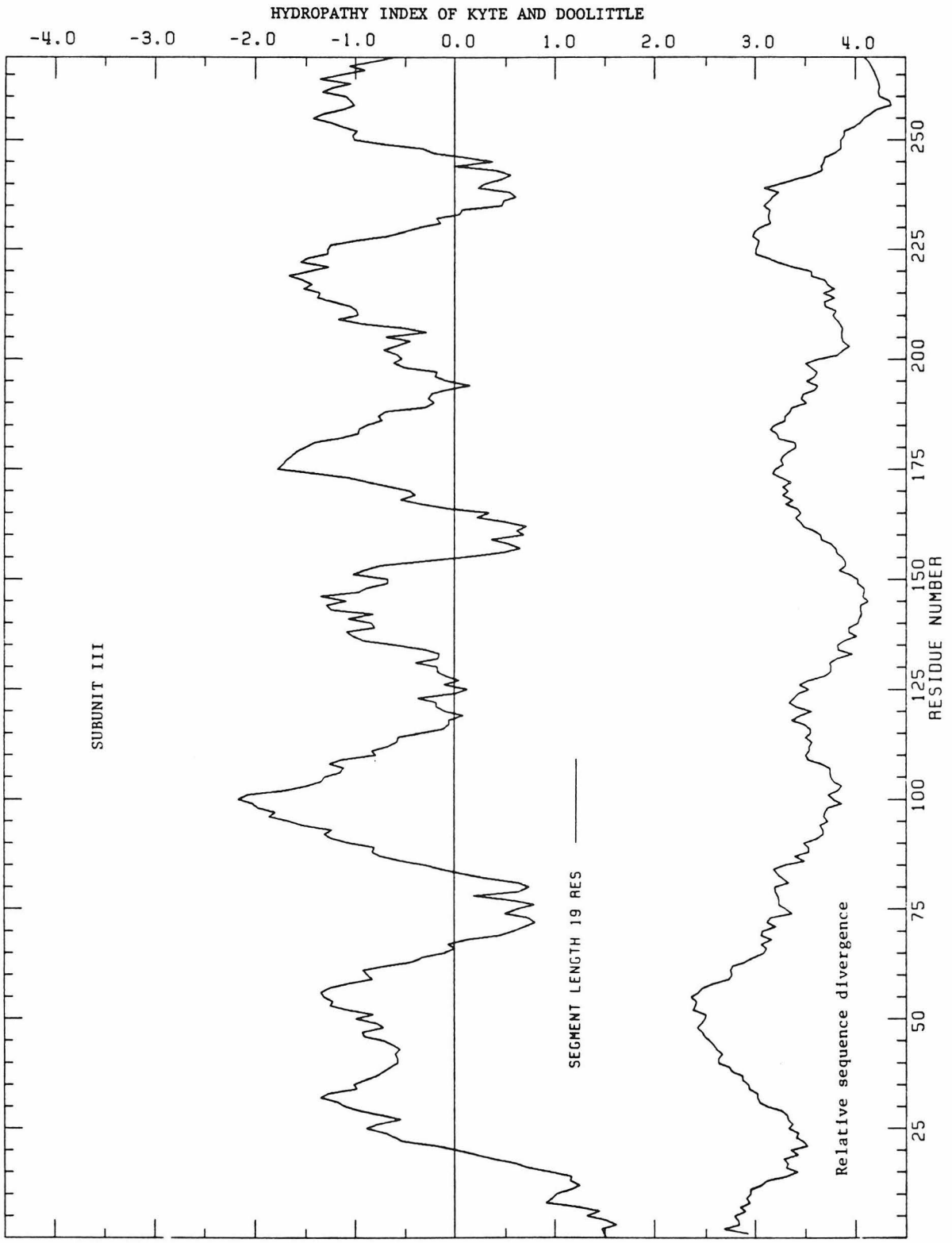
HYDROPATHY INDEX OF KYTE AND DOOLITTLE
-4.0
-3.0
-2.0
-1.0
0.0
1.0
2.0
3.0
4.0
SUBUNIT III
SEGMENT LENGTH 19 RES
Relative sequence divergence
25
50
75
100
125
150
175
200
225
250
RESIDUE NUMBER

the helices and therefore exposed to the aqueous layer. This might be expected since regions interior to the protein will likely contain more specific residue-residue interactions than regions exposed to the external aqueous phase and so are expected to be more sensitive to residue changes. It appears reasonable to predict that several of these segments are within the lipid bilayer.

The function of subunit III is difficult to ascertain. Although it seems likely to be associated at least partly with the lipid bilayer, it appears to be unnecessary for the electron transfer function of cytochrome oxidase (26). It has been reported that preparations of cytochrome oxidase depleted of subunit III lack proton pumping activity (27), and therefore that subunit III may contain a proton channel necessary for proton pumping. However, studies of the bacterial (two subunit) protein, which presumably lacks this subunit, demonstrate that is able to pump protons across the bacterial cell wall in which it resides (8-10). Subunit III may play some role in the regulation of cytochrome oxidase activity or in the determination of the structure and organization of the mitochondrial membrane and the other proteins in the electron transport chain.

Analysis of Subunit I

Subunit I is the largest of the subunits and also the most hydrophobic. The hydropathy value averaged over the entire subunit ranges from 0.68 for the human subunit to 0.80 for the subunit isolated from yeast (note that individual values in the Kyte and Doolittle hydropathy scale range from -4.5 for very hydrophilic residues to +4.5 for very hydrophobic ones). On this basis subunit I is similar in hydropathy to the known membrane spanning proteins bacteriorhodopsin and cytochrome b_5 (see these and other comparisons in ref. 3). The subunit I sequence is composed of over 50% non-polar (28) amino acids and contains only 10% charged residues. From these data we feel it is quite likely that a major portion of this subunit

lies within the lipid bilayer.

The aligned sequences for subunit I from six different species are compared in Fig. 4. They are the predicted protein sequences from the known gene sequences of subunit I from beef (19), human (20), mouse (21), Drosophila yakuba (fruit fly) (29), Saccharomyces cerevisiae (yeast) (24), and Neurospora crassa (30). With respect to the metal ligand identifications discussed in previous chapters, it is interesting to note that ten His residues are rigorously conserved in all the sequences for subunit I, but that no Cys residues are conserved (in fact, the sequence from Drosophila contains no Cys residues at all).

The moving-segment hydropathy analysis presented in Fig. 5 reveals a pronounced partitioning of the hydrophobic character of the primary sequence. Using a moving segment length of 19 residues, we note nine non-overlapping stretches with an average hydropathy greater than +1.6. Four other stretches are found with pronounced, but slightly less, hydrophobic character.

The ENDOR studies of isotopically substituted cytochrome oxidase presented in the previous chapters have proven the coordination of at least one Cys ligand to Cu_A and at least one His ligand to each of Cu_A and cytochrome a. A recent EPR study of isotopically substituted cytochrome oxidase has also proven the coordination of one His ligand to cytochrome a_3 (31). Although no specific information regarding the ligands to Cu_B is available, three different nitrogen hyperfine couplings have been reported for this site (32). Histidine is a common ligand in copper metalloproteins, and so it is likely that at least one of these couplings is due to a histidyl imidazole nitrogen.

It is inconceivable that the cysteine ligand to Cu_A is located in subunit I, since no Cys residues are conserved between the sequences of the subunit from beef and yeast even though very similar Cys β-proton couplings have been measured in the EPR spectra of Cu_A from both species. There are, however, several possible candidates for active site histidine ligands in this subunit. These rigorously

Figure 4

Amino acid sequences of subunit I from various eukaryotic organisms. References are given in the text.

```
Beef Heart          Subunit I Protein Sequences
Human
Mouse
Drosophila
Yeast
Neurospora

|  1                  | 21                  | 41                  | 61
.....MFINRWLFSTNHKDIGTLYLLFGAWAGMVGTALSLLIRAELGQPGTL.L.GDDQIYNVVVTAHAFVMIFF
.....MFADRWLFSTNHKDIGTLYLLFGAWAGVLGTALSLLIRAELGQPGNL.L.GNDHIYNVIVTAHAFVMIFF
.....MFINRWLFSTNHKDIGTLYLLFGAWAGMVGTALSILIRAELGQPGAL.L.GDDQIYNVIVTAHAFVMIFF
.....MSRQWLFSTNHKDIGTLYFIFGAWAGMVGTSLSILIRAELGHPGAL.I.GDDQIYNVIVTAHAFIMIFF
.....MVQRWLYSTNAKDIAVLYFMLAIFSGMAGTAMSLIIRLELAAPGSQYLHGNSQLFNGLVVGHAVLMCFC
MSSISIWTERWFLSTNAKDIGVLYLIFALFSGLLGTAFSVLIRMELSGPGVQYIADN.QLYNAIITAHAILMIFF

| 76                  | 96                  |116                  |136
MVMPIMIGGFGNWLVPLMIGAPDMAFPRMNNMSFWLLPPSFLLLLASSMVEAGAGTGWTVYPPLAGNLAHAGASV
MVMPIMIGGFGNWLVPLMIGAPDMAFPRMNNMSFWLLPPSLLLLLASAMVEAGAGTGWTVYPPLAGNYSHPGASV
MVMPMMIGGFGNWLVPLMIGAPDMAFPRMNNMSFWLLPPSFLLLLASSMVEAGAGTGWTVYPPLAGNPVHAGASV
MVMPIMIGGFGNWLVPLMLGAPDMAFPRMNNMSFWLLPPALSLLLVSSMVENGAGTGWTVYPPLSAGIAHGGASV
LVMPALIGGFGNYLLPLIIGATDTAFPRINNIAFWVLPMGLVCLVTSTLVESGAGTGWTVYPPLSSIQAHSGPSV
MVMPALIGGFGNFLLPLLVGGPDMAFPRLNNISFWLLPPSLLLLVFSACIEGGAGTGWTIYPPLSGVQSHSGPSV

|151                 |171                 |191                 |211
DLTIFSLHLAGVSSILGAINFITTIINMKPPAMSQYQTPLFVWSVMITAVLLLLSLPVLAAGITMLLTDRNLNTT
DLTIFSLHLAGVSSILGAINFITTIINMKPPAMTQYQTPLFVWSVLITAVLLLLSLPVLAAGITMLLTDRNLNTT
DLTIFSLHLAGVSSILGAINFITTIINMKPPAMTQYQTPLFVWSVLITAVLLLLSLPVLAAGITMLLTDRNLNTT
DLAIFSLHLAGISSILGAVNFITTVINMRSTGISLDRMPLFVWSVVITALLLLLSLPVLAGAITMLLTDRNLNTS
DLAIFALHLTSISSLLGAINFIVTTLNMRTNGMTMHKLPLFVWSIFITAFLLLLSLPVLSAGITMLLLDRNFNTS
DLAIFALHLSGVSSLLGSINFITTIVNMRTPGIRLHKLALFGWAVVITAVLLLLSLPVLAGAITMLLTDRNFNTS

|226                 |246                 |266                 |286
FFDPAGGGDPILYQHLFWFFGHPEVYILILPGFGMISHIVTYYSGKKEPFGYMGMVWAMMSIGFLGFIVWAHHMF
FFDPAGGGDPILYQHLFWFFGHPEVYILILPGFGMISHIVTYYSGKKEPFGYMGMVWAMMSIGFLGFIVWAHHMF
FFDPAGGGDPILYQHLFWFFGHPEVYILILPGFGIISHVVTYYSGKKEPFGYMGMVWAMMSIGFLGFIVWAHHMF
FFDPAGGGDPILYQHLFWFFGHPEVYILILPGFGMISHIISQESGKKETFGSLGMIYAMLAIGLLGFIVWAHHMF
FFEVAGGGDPILYEHLFWFFGHPEVYILIIPGFGIISHVVSTYS.KKPVFGEISMVYAMASIGLLGFLVWSHHMY
FFETAGGGDPILFQHLFWFFGHPEVYILIIPGFGIISTTISAYS.NKSVFGYIGMVYAMMSIGILGFIVWSHHMY

|301                 |321                 |341                 |361
TVGMDVDTRAYFTSATMIIAIPTGVKVFSWLATLHGGNIKWSPAMMWALGFIFLFTVGGLTGIVLANSSLDIVLH
TVGMDVDTRAYFTSATMIIAIPTGVKVFSWLATLHGSNMKWSAAVLWALGFIFLFTVGGLTGIVLANSSLDIVLH
TVGLDVDTRACFTSATMIIAIPTVGKVFSWLATLHGGNIKWSPAMLWALGFIFLFTVGGLTGIVLSNSSLDIVLH
TVGMDVDTRAYFTSATMIIAVPTGIKIFSWLATLHGTQLSYSPAILWALGFVFLFTVGGLTGVVLANSSVDIILH
IVGLDADTRAYFTSATMIIAIPTGIKIFSWLATIYGGSIRLATPMLYAIAFLFLFTMGGLTGVALANASLDVAFH
TVGLDVDTRAYFTAATLIIAVPTGIKIFSWLATCYGGSIRLTPSMLFALGFVFMFTIGGLSGVVLANASLDIAFH

|376                 |396                 |416                 |436
DTYYVVAHFHYVLSMGAVFAIMGGFVHWFPLFSGYTLNDTWAKIHFAIMFVGVNMTFFPQHFLGLSGMPRRYSDY
DTYYVVAHFHYVLSMGAVFAIMGGFIHWFPLFSGYTLDQTYAKIHFTIMFIGVNLTFFPQHFLGLSGMPRRYSDY
DTYYVVAHFHYVLSMGAVFAIMAGFVHWFPLFSGFTLDDTWAKAHFAIMFVGVNMTFFPQHFLGLSGMPRRYSDY
DTYYVVAHFHYVLSMGAVFAIMAGFIHWYPLFTGLTLNNKWLKSHFIIMFIGVNLTFFPQHFLGLAGMPRRYSDY
DTYYVVGHFYYVLSMGAIFSLFAGYYYWSPQILGLNYNEKLAQIQFWLIFIGANVIFFPMHFLGINGMPRRIPDY
DTYYVVAHFHYVLSMGAVFAMFSGWYHWVPKILGLNYNMVLSKAQFWLLFIGVNLTFFPQHFLGLQGMPRRISDY

|451                 |471                 |491                 |511
PDAYTMWNTISSMGSFISLTAVMLMVFIIWEAFASKREVLTVDLTTTNLEWLNGCPPPYHTFEEPTYVN..
PDAYTTWNILSSVGSFISLTAVMLMIFMIWEAFASKRKVLMVEEPSMNLEWLYGCPPPYHTFEEPVYMKS.
PDAYTTWNTVSSMGSFISLTAVLIMIFMIWEAFASKREVMSVSYASTNLEWLHGCPPPYHTFEEPTYVKVK
PDAYTTWNIVSTIGSTISLLGILFFFFIIWESLVSQRQVIYPIQLNSSIEWYQNTPPAEHSYSELPLLTN.
PDAFAGWNYVASIGSFIATLSLFLFIYILYDQLVNNKSVIYAKAPSSSIEPLLTSPPAVHSFNTPAVQS..
PDAFSGWNLISSFGSIVSVVASWLFLYIVYIQLVQGEYAGRYPWSIPQFYTDSLRALLNRSYPSLEWSISS
```

Figure 5

Moving-segment hydropathy analysis of subunit I, averaged over the sequences of the organisms indicated and using a segment length of 19 residues. The lower curve represents the standard deviation of the moving-segment average at each residue with respect to evolutionary conservation among the indicated species.

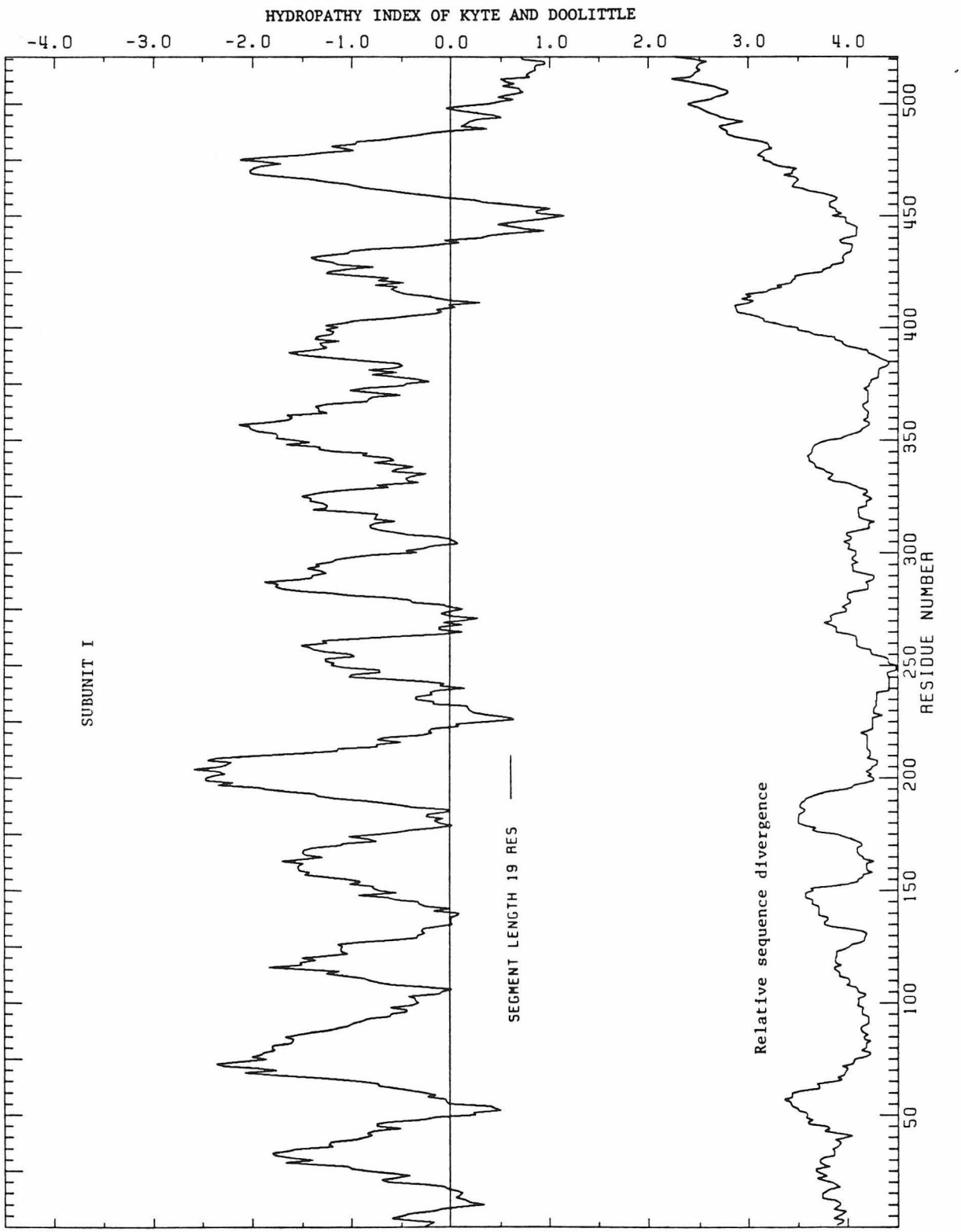
HYDROPATHY INDEX OF KYTE AND DOOLITTLE
-4.0
-3.0
-2.0
-1.0
0.0
1.0
2.0
3.0
4.0
SUBUNIT I
SEGMENT LENGTH 19 RES
Relative sequence divergence
50
100
150
200
250
300
350
400
450
500
RESIDUE NUMBER

conserved histidines are indicated in Fig. 5 by vertical arrows. Some qualitative assessments may be made regarding the suitability of these conserved residues as ligands to the metal centers in the protein. For example, His-68 and His-145 are near regions of quite high sequence divergence and so are unlikely to be ligands to active site metal centers. The metal centers in cytochrome oxidase have remained inaccessible to water-soluble labeling reagents and so are probably buried within the protein interior. Consequently, metal ligands are not expected to be in regions showing large hydrophilic character (low hydropathy values). Furthermore, amino acid ligands to the heme irons will have some neighboring residues in close proximity to the hydrophobic porphyrin surface and so are expected to be nonpolar. These considerations lead us to exclude His-436 and, to a lesser extent, His-297 and His-298 as possible metal ligand candidates. Of particular interest are His-240 and His-247 which are located in a region of moderate hydrophobicity. This region is also one of the most highly conserved regions of the protein. Not only does the plot of segmental hydropathy conservation show a very low value for the average standard deviation of this segment, but examination of the sequences in Fig. 4 shows that, in a 25 residue region surrounding these histidines, more than 90% of the residues are rigorously conserved between the 6 species. This observation provides good reason to suspect that at least one of these two histidine residues may be a metal ligand.

Analysis of Subunit II

Subunit II is less hydrophobic than subunit I and is also less evolutionarily conserved. Its average hydropathy values among the known species range from 0.11 to 0.46, placing it above the average value from a selection of water-soluble proteins (-0.4), but below the unusually high values for subunit I and other membrane spanning proteins (3).

The amino acid sequences of subunit II from beef (19,33), human (20), mouse (21), Drosophila yakuba (29), Zea mays (corn) (34), Saccharomyces cerevisiae (yeast) (24), and Neurospora crassa (35) are compared in Fig. 6. The fungi Saccharomyces and Neurospora have slightly larger predicted sequences due to the presence of exons in their gene sequences. Subunit II is unique among the major subunits of cytochrome oxidase in that two Cys residues are rigorously conserved in all organisms sequenced to date. These two cysteines are separated in the sequence by only three residues and are located in a highly conserved region. This region also contains a conserved histidine within three residues of one of the cysteines. Only two other histidines are conserved in this subunit, indicating that subunit II is almost certainly not the only metal-binding subunit; as discussed above, a minimum of three His residues (and likely more) are ligands to metals in the protein.

The moving-segment average hydropathy analysis of subunit II is shown in Fig. 7. Two potential membrane spanning segments are obvious from this plot. The maximum average hydropathy of each is well above the membrane-preference cutoff value of +1.6. Chemical labeling experiments confirm that subunit II is exposed to the cytoplasmic (aqueous) phase and also to the membrane interior (36-38). The bulk of the sequence, however, shows no clear preference for the hydrophobic bilayer, suggesting that a large amount of subunit II may lie within the globular protein region known to extend above the bilayer on the cytoplasmic side of the mitochondrial membrane (39-40). It is within this segment of the primary sequence that the two conserved Cys residues are located. A result which supports this conclusion is the chemical labeling of Glu-228 by a large water-soluble carbodiimide (41). This residue is located directly between Cys-226 and Cys-230 implying that these residues must be near the surface of the protein. This raises interesting possibilities regarding the location of Cu_A relative to the membrane bilayer. If Cu_A is the proton pump of cytochrome oxidase and it is located on the

Figure 6

Amino acid sequences of subunit II from various eukaryotic organisms. References are given in the text.

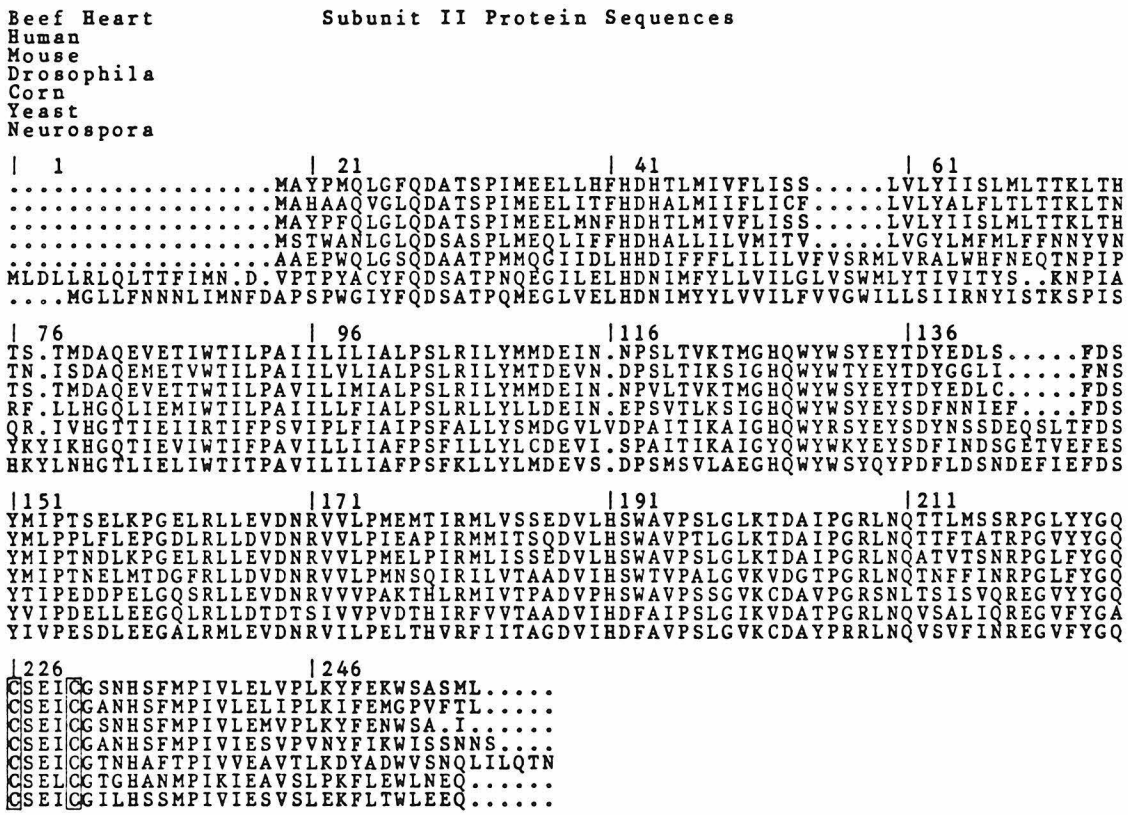
Beef Heart
Subunit II Protein Sequences
Human
Mouse
Drosophila
Corn
Yeast
Neurospora
| 1 | 21 | 41 | 61
.....MAYPMQLGFQDATSPIMEELLHFHDHTLMIVFLISS.....LVLYIISLMLTTKLTH
.....MAHAAQVGLQDATSPIMEELITFHDHALMIIFLICF.....LVLYALFLTLTTKLTN
.....MAYPFQLGLQDATSPIMEELMNFHDHTLMIVFLISS.....LVLYIISLMLTTKLTH
.....MSTWANLGLQDSASPLMEQLIFFHDHALLILVMITV.....LVGYLMFMLFFNNYVN
.....AAEPWQLGSQDAATPMMQGIIDLHHDIFFFLILILVFVSRMLVRALWHFNEQTNPIP
MLDLLRLQLTTFIMN.D.VPTPYACYFQDSATPNQEGILELHDNIMFYLLVILGLVSWMLYTIVITYS..KNPIA
....MGLLFNNNLIMNFDAPSPWGIYFQDSATPQMEGLVELHDNIMYYLVVILFVVGWILLSIIRNYISTKSPIS
| 76 | 96 |116 |136
TS.TMDAQEVETIWTILPAIILILIALPSLRILYMMDEIN.NPSLTVKTMGHQWYWSYEYTDYEDLS.....FDS
TN.ISDAQEMETVWTILPAIILVLIALPSLRILYMTDEVN.DPSLTIKSIGHQWYWTYEYTDYGGLI.....FNS
TS.TMDAQEVETTWTILPAVILIMIALPSLRILYMMDEIN.NPVLTVKTMGHQWYWSYEYTDYEDLC.....FDS
RF.LLHGQLIEMIWTILPAIILLFIALPSLRLLYLLDEIN.EPSVTLKSIGHQWYWSYEYSDFNNIEF....FDS
QR.IVHGTTIEIIRTIFPSVIPLFIAIPSFALLYSMDGVLVDPAITIKAIGHQWYRSYEYSDYNSSDEQSLTFDS
YKYIKHGQTIEVIWTIFPAVILLIIAFPSFILLYLCDEVI.SPAITIKAIGYQWYWKYEYSDFINDSGETVEFES
HKYLNHGTLIELIWTITPAVILILIAFPSFKLLYLMDEVS.DPSMSVLAEGHQWYWSYQYPDFLDSNDEFIEFDS
|151 |171 |191 |211
YMIPTSELKPGELRLLEVDNRVVLPMEMTIRMLVSSEDVLHSWAVPSLGLKTDAIPGRLNQTTLMSSRPGLYYGQ
YMLPPLFLEPGDLRLLDVDNRVVLPIEAPIRMMITSQDVLHSWAVPTLGLKTDAIPGRLNQTTFTATRPGVYYGQ
YMIPTNDLKPGELRLLEVDNRVVLPMELPIRMLISSEDVLHSWAVPSLGLKTDAIPGRLNQATVTSNRPGLFYGQ
YMIPTNELMTDGFRLLDVDNRVVLPMNSQIRILVTAADVIHSWTVPALGVKVDGTPGRLNQTNFFINRPGLFYGQ
YTIPEDDPELGQSRLLEVDNRVVVPAKTHLRMIVTPADVPHSWAVPSSGVKCDAVPGRSNLTSISVQREGVYYGQ
YVIPDELLEEGQLRLLDTDTSIVVPVDTHIRFVVTAADVIHDFAIPSLGIKVDATPGRLNQVSALIQREGVFYGA
YIVPESDLEEGALRMLEVDNRVILPELTHVRFIITAGDVIHDFAVPSLGVKCDAYPRRLNQVSVFINREGVFYGQ
|226 |246
CSEICGSNHSFMPIVLELVPLKYFEKWSASML.....
CSEICGANHSFMPIVLELIPLKIFEMGPVFTL.....
CSEICGSNHSFMPIVLEMVPLKYFENWSA.I.....
CSEICGANHSFMPIVIESVPVNYFIKWISSNNS....
CSEICGTNHAFTPIVVEAVTLKDYADWVSNQLILQTN
CSELCGTGHANMPIKIEAVSLPKFLEWLNEQ.....
CSEICGILHSSMPIVIESVSLEKFLTWLEEQ.....

Figure 7

Moving-segment hydropathy analysis of subunit II, averaged over the sequences of the organisms indicated and using a segment length of 19 residues. The lower curve represents the standard deviation of the moving-segment average at each residue with respect to evolutionary conservation among the indicated species.

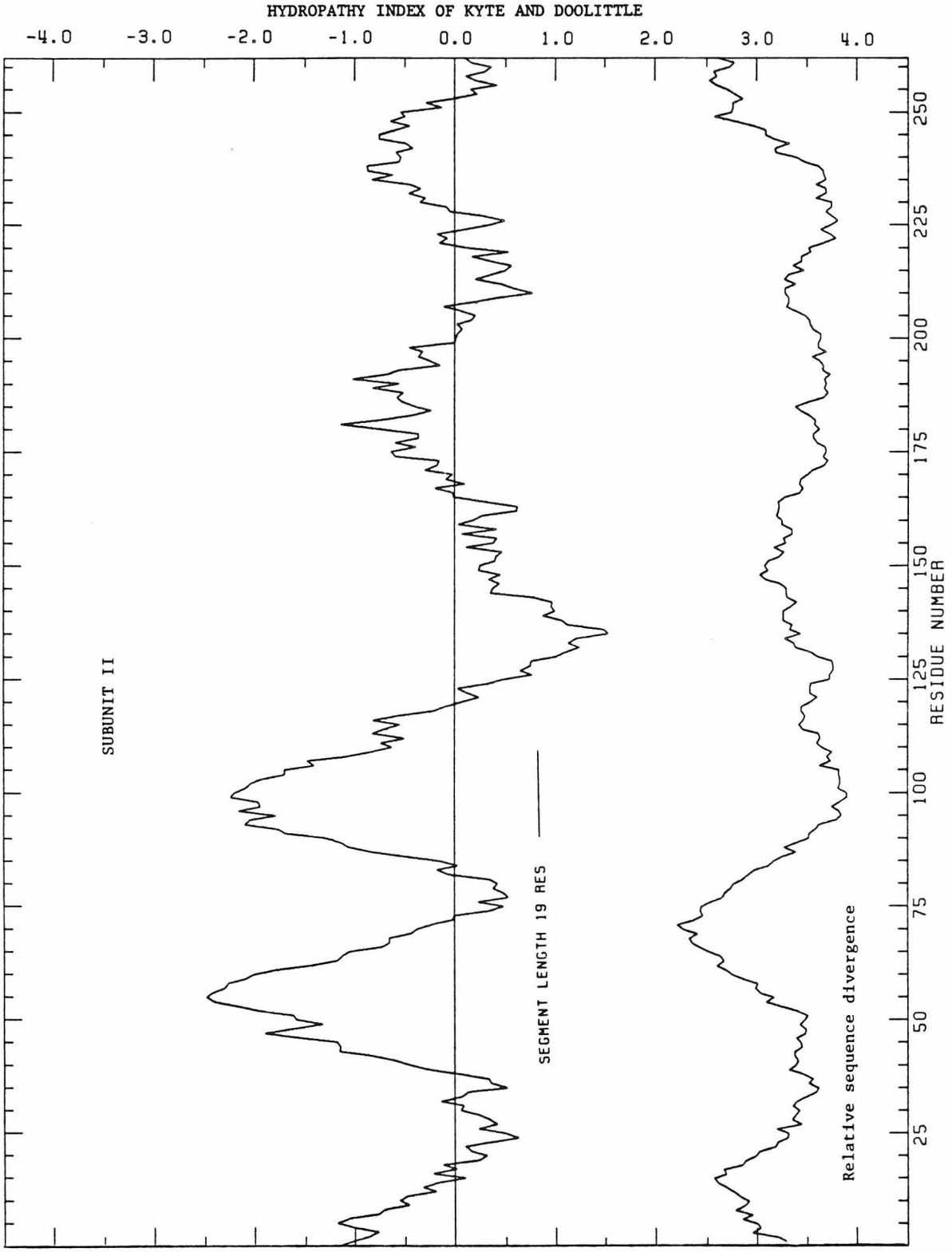
HYDROPATHY INDEX OF KYTE AND DOOLITTLE
-4.0
-3.0
-2.0
-1.0
0.0
1.0
2.0
3.0
4.0
SUBUNIT II
SEGMENT LENGTH 19 RES
Relative sequence divergence
25
50
75
100
125
150
175
200
225
250
RESIDUE NUMBER

cytoplasmic side of the membrane, a proton pumping mechanism must exist which allows for its location on the cytoplasmic side of the inner mitochondrial membrane.

A MODEL FOR Cu_A COORDINATION IN SUBUNIT II

The preceding discussion argues quite strongly that the cysteine ligand(s) to Cu_A are located in subunit II and, in fact, are Cys-226 and/or Cys-230. Based on this conclusion, we present a model for a possible mode of coordination at the Cu_A site which is consistent with the molecular orbital model proposed in Chapter III of this thesis. The main feature of the molecular orbital model is the coordination of copper by two cysteine sulfur ligands which are close enough to each other to form a partial bond between them. However, it is important that the two cysteine ligands not be able to approach too closely, as copper can be an efficient catalyst of the oxidation of cysteine to cystine (42). If the protein constrains the sulfur atoms to remain at a distance which is long relative to that of a stable disulfide bond, the complete conversion to cystine might be inhibited. We have noted that Cys-226 and Cys-230 are located four residues apart in the sequence. For a polypeptide folded into an α-helix, residues separated by this distance in the primary sequence occur adjacent to one another on the same face of the helix.

The CPK model illustrated in Fig. 8 shows a possible arrangement of two cysteine residues four amino acid residues apart on an α-helix. The utility of such a model is that it allows one to put upper and lower limits on the distance attainable between the two cysteine sulfurs. From this model, we estimate that the closest center-to-center distance available to these two sulfur atoms is approximately 3 Å. As discussed in Chapter III, this distance is too large for stable disulfide bond formation, since the disulfide bond length in cystine is 2.04 Å (43); however, this distance is probably close enough to allow a weak overlap of the sulfur atomic orbitals from different sulfur atoms as proposed in Chapter III.

Several consequences of this model for the protein coordination of Cu_A are immediately apparent. As mentioned in the previous

Figure 8

A model for cysteine coordination in the Cu_A site of cytochrome oxidase. Two cysteine residues, separated by three residues in the protein primary sequence, align almost above one another in an α-helical secondary structure, as shown in this CPK model.


3Å

section, a glutamic acid residue, Glu-228, has been shown to be labeled by a water-soluble carbodiimide (41). The helical model for Cu_A coordination places Glu-228 at the extreme opposite face of the α-helix relative to the copper binding site. This result explains how the two cysteine residues can both be coordinated to a well-buried copper site, while a residue between them appears to be exposed to the aqueous phase at the surface of the protein. The structure shown in Fig. 8, places the Cu_A center approximately 10 Å from the carboxyl group of Glu-228, and, presumably, from the surface of the protein.

A second consequence of this structure is that a rigorously conserved histidine residue, His-234, is predicted to lie on the same face of the α-helix as the copper site, directly adjacent to one of the sulfur ligands to the copper. This result and the fact that His-234 is conserved in all known sequences of subunit II, may indicate an important role for this aromatic group in the transfer of electrons and/or protons into or out of the Cu_A site.

A third consequence of this structure, and of the model for the electronic structure of the Cu_A site proposed in Chapter II, concerns the rigidity of the Cu_A coordination, in particular the rotational mobility of the cysteine sulfur ligands. The model for the electronic structure of oxidized Cu_A predicts some bonding character directly between the two sulfur atoms. For the optimization of this interaction, the two cysteine sulfur atoms must be able to approach as close as possible. As discussed above, the helix model for Cu_A coordination allows a closest approach of approximately 3 Å. To attain this minimal separation, however, the amino acid side chains must orient in a specific fashion. Significant rotation of the cysteine side chains about the α- or β-carbons would likely disrupt this interaction considerably. However, in the <u>reduced</u> Cu_A site, any bonding interaction between the sulfur atomic orbitals will be abolished and so this restriction will be lifted somewhat (presumably the interaction with copper will remain strong). This predicts that, in the reduced protein, the cysteine ligands to Cu_A may be able to

rotate somewhat to facilitate the donation of an electron to a nearby acceptor, or to allow the protonation of one of the cysteine sulfurs in an intermediate step of proton pumping.

Finally, we note that this proposed structure for the amino acid coordination structure of Cu_A places some restrictions on the placement of Cu_A with respect to the plane of the mitochondrial membrane. As mentioned above, the Cu_A site is expected to be approximately 10 Å from the surface of the protein and therefore cannot be buried very deeply within the lipid bilayer. As suggested in the previous section, Cu_A may well be located in the large section of the protein which extends above the lipid bilayer (40). This location would also place restrictions on the position of the oxygen binding site relative to the membrane surface. Although it may certainly be located below the surface of the membrane, the oxygen binding site is probably not located 40 Å from Cu_A at the extreme opposite surface of the bilayer. This positioning of the active site metals in cytochrome oxidase would require the existence of a proton channel which allows protons to be taken up from the matrix space to be consumed in the reduction of oxygen. The same channel, or a similar one, may also extend to Cu_A to provide protons to be pumped across the membrane.

CONCLUSION

The availability of protein sequence information for cytochrome oxidase from a large variety of organisms provides valuable information on the probable location of the active site metal centers in relation to the protein primary structure. In this respect, the identification of cysteine ligands to Cu_A, combined with the result that only two cysteine residues are evolutionarily conserved in the major subunits of cytochrome oxidase, provides convincing evidence that these two residues in subunit II provide the cysteine sulfur ligands to Cu_A. From the total number of conserved histidine residues in subunit II, and the predicted number of histidines involved in the coordination of the four metal centers in the protein, it can be concluded that some of the ligands to the four metal centers in the protein must come from other subunit(s) as well. The highly conserved nature of subunit I makes it a likely candidate to provide such ligands.

The amino acid composition of subunit I is quite hydrophobic on average. The moving-segment hydropathy analysis, combined with analysis of evolutionary sequence conservation, has provided some predictions of specific regions of the protein that might have particular functional significance. This analysis reveals that subunit I may contain numerous membrane-spanning α-helical regions. Assuming that these helices will align approximately perpendicular to the plane of the membrane and noting that the hemes in cytochrome oxidase have been shown to be oriented with the normal to the heme plane in the plane of the bilayer (44,45), it is tempting to suggest that one or both of the hemes in cytochrome oxidase may lie between two (or more) aligned α-helices within the lipid bilayer.

Finally, based on the assignment of specific cysteine residues as ligands to Cu_A, we have proposed a model for the Cu_A site in which the two cysteine residues are spatially adjacent on the face of an

α-helix. The physical restrictions placed on the closest approach of the two sulfur atoms explains the unusual resistance to oxidative crosslinking of two thiolate ligands coordinated to Cu(II), and is in complete agreement with the model for the electronic structure of Cu_A proposed in Chapter II. The helix containing this proposed copper binding site would presumably <u>not</u> be deeply buried within the bilayer, as evidenced by the solution reactivity of a nearby carboxyl group; however, the copper binding site could lie at least 10 Å from the surface of the protein. Electron transfer to and from copper may occur across the helix, or it may occur via a conserved histidine group located directly above the proposed copper binding site.

These proposals for the coordination structure of the metals in cytochrome oxidase, although somewhat speculative, provide an interesting framework from which to design future experiments aimed at further elucidating the overall structure and function of this complex protein.

REFERENCES

1. Chou, P. Y., and Fasman, G. D. (1974) Biochemistry 13, 211-222.
2. Chou, P. Y., and Fasman, G. D. (1978) Ann. Rev. Biochem. 47, 251-276.
3. Kyte, J., and Doolittle, R. F. (1982) J. Mol. Biol. 157, 105-132.
4. Argos, P., Rao, J. K. M., and Hargrave, P. A. (1982) Eur. J. Biochem. 128, 565-575.
5. Wikstrom, M., Krab, K., and Saraste, M. (1981) Cytochrome Oxidase: A Synthesis, Academic Press, London.
6. Kadenbach, B., and Merle, P. (1981) FEBS Lett. 135, 1-11.
7. Ludwig, B. (1980) Biochim. Biophys. Acta 594, 177-189.
8. Van Verseveld, H. W., Krab, K., and Stouthamer, A. H. (1981) Biochim. Biophys. Acta 635, 525-534.
9 Solioz, M., Carafoli, E., and Ludwig, B. (1982) J. Biol. Chem. 257, 1579-1582.
10. Sone, N., and Hinkle, P. C. (1982) J. Biol. Chem. 257, 12600-12604.
11. Gray, M. W., and Doolittle, W. F. (1982) Microbiol. Rev. 46, 1-42.
12. Ludwig, B., and Schatz, G. (1980) Proc. Natl. Acad. Sci., U.S.A. 77, 196-200.
13. Sacher, R., Steffens, G. J., and Buse, G. (1979) Hoppe-Seyler's Z. Physiol. Chem. 360, 1385-1392.
14. Tanaka, M., Haniu, M., Yasunobu, K. T., Yu, C., Yu, L., Wei, Y., and King, T. (1979) J. Biol. Chem. 254, 3879-3885.
15. Gregor, I., and Tsugita, A. (1982) J. Biol. Chem. 257, 13081-13087.
16. Biewald, R., and Buse, G. (1982) Hoppe-Seyler's Z. Physiol. Chem. 363, 1141-1153.
17. Steffens, G. C. M., Steffens, G. J., and Buse, G. (1979) Hoppe-Seyler's Z. Physiol. Chem. 360, 1641-1650.
18. Buse, G., and Steffens, G. J. (1978) Hoppe-Seyler's Z. Physiol. Chem. 359, 1005-1009.
19. Anderson, S., de Bruijn, M. H. L., Coulson, A. R., Eperon, I. C., Sanger, F., and Young, I. G. (1982) J. Mol. Biol. 156, 683-717.
20. Anderson, S., Bankier, A. T., Barrell, B. G., de Bruijn, M. H. L., Coulson, A. R., Drouin, J., Eperon, I. C., Nierlich, D. P., Roe, B. A., Sanger, F., Schreier, P. H., Smith, A. J. H., Staden, R., and Young, I. G. (1981) Nature (London) 290, 457-465.
21. Bibb, M. J., Van Etten, R. A., Wright, C. T., Walberg, M. W., and Clayton, D. A. (1981) Cell 26, 167-180.
22. Clary, D. O., and Wolstenholme, D. R. (1983) Nuc. Acids. Res. 11, 4211-4227.

23. Netzker, R., Kochel, H. G., Basak, N., and Kuntzel, H. (1982) Nuc. Acids. Res. 10, 4783-4794.

24. Bonitz, S. G., Coruzzi, G., Thalenfeld, B. E., Tzagoloff, A., and Macino, G. (1980) J. Biol. Chem. 255, 11927-11941.

25. Browning, K. S., and RajBhandary, U. L. (1982) J. Biol. Chem. 257, 5253-5256.

26. Saraste, M., Penttila, T., Coggins, J. R., and Wikstrom, M. (1980) FEBS Lett. 114, 35-38.

27. Saraste, M., Penttila, T., and Wikstrom, M. (1981) Eur. J. Biochem. 115, 261-268.

28. Lehninger, A. L. (1975) Biochemistry, Worth Publishers, New York.

29. de Bruijn, M. H. L. (1983) Nature (London) 304, 234-241.

30. de Jonge, J. C., and de Vries, H. (1983) Curr. Gen. 7, 21-28.

31. Stevens, T. H., and Chan, S. I. (1981) J. Biol. Chem. 256, 1069-1071.

32. Cline, J., Reinhammar, B., Jensen, P., Venters, R., and Hoffman, B. M. (1983) J. Biol. Chem. 258, 5124-5128.

33. Steffens, G. J., and Buse, G. (1979) Hoppe-Seyler's Z. Physiol. Chem. 360, 613-619.

34. Fox, T. D., and Leaver, C. J. (1981) Cell 26, 315-323.

35. Macino, G., and Morelli, G. (1983) J. Biol. Chem. 258, 13230-13235.

36. Eytan, G. D., Carroll, R. C., Schatz, G., and Racker, E. (1975) J. Biol. Chem. 250, 8598-8603.

37. Eytan, G. D., and Broza, R. (1978) J. Biol. Chem. 253, 3196-3202.

38. Chan, S. H. P., and Tracy, R. P. (1978) Eur. J. Biochem. 89, 595-605.

39. Ludwig, B., Downer, N. W., and Capaldi, R. A. (1979) Biochemistry 18, 1401-1407.

40. Fuller, S., Capaldi, R. A., and Henderson, R. (1979) J. Mol. Biol. 134, 305-327.

41. Millett, F., de Jong, C., Paulson, L., and Capaldi, R. A. (1983) Biochemistry 22, 546-552.

42. Klotz, I. M., Czerlinski, G. H., and Fiess, H. A. (1958) J. Am. Chem. Soc. 80, 2920-2923.

43. Jones, D. D., Bernal, I., Frey, M. N., and Koetzle, T. F. (1974) Acta Cryst. B30, 1220-1227.

44. Blasie, J. K., Erecinska, M., Samuels, S., and Leigh, J. S. (1978) Biochim. Biophys. Acta 501, 33-52.

45. Erecinska, M., Wilson, D. F., and Blasie, J. K. (1978) Biochim. Biophys. Acta 501, 53-62.

CHAPTER V

CONCLUSIONS

We have combined the unique capabilities of electron nuclear double resonance (ENDOR) spectroscopy and the direct incorporation of isotopically substituted amino acids into the yeast protein to identify ligands to the two low-potential metal centers in cytochrome c oxidase. The results prove conclusively that cytochrome a has at least one histidine ring nitrogen coordinated axially with respect to the heme plane. Comparison of the ENDOR spectrum of the isotopically substituted protein with those of appropriate model compounds provides strong evidence for a second axial nitrogen ligand from a second histidine ligand, resulting in a bis-imidazole heme a coordination structure for cytochrome a.

Isotopic substitution studies directed at the Cu_A center solidly identify at least one histidine and one cysteine as ligands to the copper, and the resolution of a third strongly coupled cysteine methylene proton provides strong evidence for two cysteine sulfur ligands to Cu_A. The coordination of oxidized copper by two thiolate sulfurs would make Cu_A unique among known metalloproteins, and may well explain its unusual spectroscopic properties.

We have proposed a model for the physical and electronic structure of the oxidized Cu_A site which successfully explains these spectroscopic properties. The unique feature of this model is the delocalization of a substantial amount of electron density out of an antibonding orbital between two coordinating sulfur atoms and into a half-empty 3d orbital on copper. This results in a system with a significant amount of Cu(I)-sulfur radical character; in this respect it is similar to previous models which involve localization of unpaired spin density on a single sulfur ligand to copper (1,2). The assignment of Cu(I) character to the oxidized center is consistent with the X-ray edge absorption data for the oxidized and reduced forms of Cu_A (3). The delocalization of unpaired spin onto sulfur explains the unusual nature of the EPR spectral features, in particular the

small and isotropic copper hyperfine interaction (4) and the finding of a g-value less than that of the free electron (5). Finally, the electronic structure predicted by this model explains the unusually intense features of the MCD spectrum of oxidized Cu_A (6).

Armed with the identification of ligands to several of the metal centers in cytochrome oxidase, we have examined the amino acid composition and evolutionary divergence of the sequences of cytochrome oxidase subunits from a wide variety of organisms in an attempt to gain insight into the overall structure of the protein. In particular, we present a strong argument for the localization of Cu_A in subunit II, and identify the specific cysteine residues involved in coordination of the copper. From this perspective, we propose a model for the coordination of Cu_A in which the two cysteine ligands are located adjacent to one another on the face of an α-helix within the protein. This model for the protein coordination of Cu_A is shown to be consistent with the model for the physical and electronic structure of Cu_A derived from spectroscopic considerations.

The incorporation of isotopically substituted amino acids into yeast cytochrome oxidase is a powerful tool for the determination of the coordination environment of the metal centers in the protein. In this and previous work, ligands to three of the four metal centers in cytochrome oxidase have been identified. Studies using the samples prepared here to identify ligands to ligands to the remaining metal center, Cu_B, are currently in progress. These structural assignments are essential to the determination of the overall structure of the protein and to a more complete understanding of the mechanisms of electron transfer, oxygen reduction, and proton pumping by this important respiratory enzyme.

REFERENCES

1. Chan, S. I., Bocian, D. F., Brudvig, G. W., Morse, R. H., and Stevens, T. H. (1979) in Cytochrome Oxidase, King, T. E., Orii, Yutaka, Chance, Britton, and Okunuki, Kazuo, eds., Elsevier/North Holland Biomedical Press, Amsterdam, 177-188.

2. Peisach, J., and Blumberg, W. E. (1974) Arch. Biochem. Biophys. 165, 691-708.

3. Hu, V. W., and Chan, S. I. (1977) FEBS Lett. 84, 287-290.

4. Hoffman, B. M., Roberts, J. E., Swanson, M., Speck, S. H., and Margoliash, E. (1980) Proc. Natl. Acad. Sci., U.S.A. 77, 1452-1456.

5. Aasa, R., Albracht, S. P. J., Falk, K., Lanne, B., and Vanngard, T. (1976) Biochim. Biophys. Acta 422, 260-272.

6. Eglinton, D. G., Johnson, M. K., Thomson, A. J., Gooding, P. E., and Greenwood, C. (1980) Biochem. J. 191, 319-331.